NATIONAL TECHNICAL UNIVERSITY OF ATHENS
SCHOOL OF NAVAL ARCHITECTURE AND MARINE ENGINEERING
DIVISION OF MARINE ENGINEERING

DIPLOMA THESIS

Waste Heat Recovery on a Liquefied Natural Gas Carrier with Tri-fuel Diesel Electric Propulsion using a Dual Loop Rankine Cycle

Eleni Lazaratou

Supervisor: Prof. Christos Frangopoulos, NTUA

Athens, October 2015

Acknowledgements

First and foremost, thank you to my advisor, Professor Christos Frangopoulos, for his cooperation, guidance, insight, incredible patience and attention to detail. The work he put into this text as well is into all his years of serving our university and the students at NTUA deserve a great deal of gratitude. With my best wishes for his happy and fruitful retirement, and my confidence that our school will continue to benefit from his contribution for a long time to come.

This project would not have been possible without the gracious assistance of Maran Gas Maritime in providing drawings and data. My heartfelt thanks Stavros Hatzigrigoris and Richard Gilmore for giving me the opportunity to join the LNG shipping industry and for being incredibly supportive of my continuing education. A special thanks is owed to Srdan Silic for continuously and generously sharing his wealth of experience on LNG and for his flexibility and unending encouragement in getting this thesis done. Thank you also to Spyros Gertsos and Nikos Grivas for their explanations on many technical details.

I would certainly not be where I am today without the support and the example of my parents, Niki Serakiotou and Spyros Lazaratos. I can only hope they know the gratitude I feel for the all they have provided me throughout my life. Thank you also to my sister Veni for always paving the way for my accomplishments and for being my most confident and unwavering fan. Finally, thank you to my grandparents, Eleni Parisi-Serakiotou and Kosmas Lazaratos, for always instilling in me the importance of my education.

Last but certainly not least, thank you to Vasilis, without whose help, humor, encouragement and patience this thesis and all my years at NTUA would not have been possible.

Διπλωματική Εργασία:
Εκμετάλλευση Απορριπτόμενης Θερμότητας σε Πλοίο Μεταφοράς Υγροποιημένου Φυσικού Αερίου Ντιζελοηλεκτρικής Πρόωσης με Χρήση Διπλού Κύκλου Rankine

Ελένη Λαζαράτου
Επιβλέπων Καθηγητής: Χρίστος Φραγκόπουλος

Σε συνήθεις βιομηχανικές εγκαταστάσεις, ένα μεγάλο ποσοστό της ενέργειας του καυσίμου, της τάξεως του 20-50%, χάνεται με τη μορφή απορριπτόμενης θερμότητας, με το μεγαλύτερο μέρος αυτής της θερμότητας να αποβάλλεται σε χαμηλές θερμοκρασίες. Το δεδομένο αυτό, σε συνδυασμό με το υψηλό κόστος καυσίμου και τις ολοένα αυξανόμενες ανησυχίες για την κατάσταση του περιβάλλοντος, επιβάλλουν την καλύτερη αξιοποίηση αυτής της διαθέσιμης ενέργειας.

Η παρούσα εργασία εξετάζει την ανάκτηση της απορριπτόμενης θερμότητας από ναυτικούς κινητήρες Diesel με την τεχνολογία του οργανικού κύκλου Rankine (OKR). Ο οργανικός κύκλος Rankine είναι ένας θερμοδυναμικός κύκλος που μετατρέπει διαθέσιμη θερμότητα σε χρήσιμη μηχανική ενέργεια. Στηρίζεται στον κλασικό κύκλο νερού-ατμού, αλλά προσαρμόζεται για την αξιοποίηση θερμότητας χαμηλών θερμοκρασιών μέσω της αντικατάστασης του νερού με κατάλληλο οργανικό ρευστό.

Τα οργανικά ρευστά, που αποτελούνται από ενώσεις άνθρακα με άλλα στοιχεία, έχουν ως βασικό πλεονέκτημα τα χαμηλά σημεία βρασμού τους, που επιτρέπουν την αξιοποίηση πηγών απορριπτόμενης ενέργειας σε θερμοκρασίες χαμηλότερες από το σημείο βρασμού του νερού, 100^{0}C. Από τα ποικίλα ρευστά που κρίνονται κατάλληλα για χρήση σε ναυτικές εφαρμογές, εδώ εξετάζονται το R-416a, η αμμωνία, το R-245fa, το νερό και το R-134a.

Η τεχνολογία OKR αρχικά εφαρμόστηκε τη δεκαετία του 1970, ωστόσο μόλις προσφάτως κέρδισε το ενδιαφέρον στον χώρο της Ναυτικής Μηχανολογίας, με το πρώτο σύστημα να εγκαθίσταται σε ένα οχηματαγωγό πλοίο το 2011.

Πεδίο εφαρμογής της τεχνολογίας αυτής στην παρούσα εργασία, είναι ένα πλοίο μεταφοράς υγροποιημένου φυσικού αερίου (Liquefied Natural Gas, LNG), μεταφορικής ικανότητας 158,000 m^3 με ντιζελοηλεκτρική πρόωση. Η απολυόμενη θερμότητα από τα καυσαέρια και από το ψυκτικό νερό ανακτάται με χρήση ενός διπλού κύκλου Rankine.

Οι καταλληλότερες τιμές παραμέτρων του διπλού κύκλου προσδιορίζονται για τέσσερις συνδυασμούς ρευστών με λύση προβλήματος βελτιστοποίησης, που έχει ως αντικειμενική συνάρτηση τη μεγιστοποίηση της αποδιδόμενης ισχύος. Τα αποτελέσματα καταδεικνύουν ικανή βελτίωση του βαθμού απόδοσης της προωστήριας εγκατάστασης κατά 2-7%, που εξαρτάται από την ταχύτητα του πλοίου, ενώ η κατανάλωση καυσίμου μπορεί να μειωθεί κατά 5-14.5%, αντίστοιχα.

Η τεχνοοικονομική θεώρηση του προτεινόμενου συστήματος έγινε με παραμετρική μελέτη όσον αφορά τόσο το κόστος του καυσίμου όσο και τον ονομαστικό ρυθμό φυσικής εξάτμισης του φορτίου. Η μελέτη δείχνει ότι, για τωρινές τιμές φυσικού αερίου (13-17 USD/mmBTU), το σύστημα έχει δείκτη καθαρής παρούσας αξίας γύρω στα 20 εκατομμύρια USD, ενώ η δυναμική περίοδος αποπληρωμής κυμαίνεται στο διάστημα 12-

14 έτη. Δεδομένου ότι η διάρκεια ζωής του υπό μελέτη πλοίου μπορεί να φτάσει τα 40 έτη, το σύστημα κρίνεται κατάλληλο για εφαρμογή.

Η εργασία κλείνει με προτάσεις για συνέχιση της ερευνητικής προσπάθειας, που περιλαμβάνουν πιθανές τροποποιήσεις στο προτεινόμενο σύστημα για βελτίωση της απόδοσης ή μείωση του κόστους του.

Contents

Acknowledgements 3
Figures 10
Tables 12
Symbols 14
1 Introduction 17
2 Thermodynamic Analysis of the Rankine Cycle 18
2.1 Increasing the thermal efficiency of the cycle 21
2.1.1 Superheating 21
2.1.2 Increasing pressure in the cycle – Reheating 21
2.1.3 Regenerative cycle 22
2.1.4 Dual loop cycle 24
2.2 Increasing the efficiency of heat recovery in the boiler 25
2.2.1 Subcritical vs Supercritical Rankine Cycles 26
2.2.2 Zeotropic mixtures of organic fluids 29
3 Organic Fluids 32
3.1 Categorization of organic fluids 32
3.1.1 Chemical categorization of organic fluids 32
3.1.2 Thermodynamic categorization of organic fluids 33
3.2 Important properties for selecting a working fluid 35
3.2.1 Water vs. organic working fluids 35
3.2.2 Crucial properties of organic fluids 36
3.2.3 Fluid selection strategies 44
4 Applications of Organic Rankine Cycles 47
4.1 Land-based ORC Applications 47
4.2 Marine ORC Applications 49
5 Analysis of the Existing Marine Propulsion System 53
5.1 Power production system and Main Generator Engines 53
5.2 Fuel consumption modes 54
5.2.1 Liquid fuel burning mode 54
5.2.2 Gas burning mode: Natural and forced boil-off gas 55
5.3 Fresh Water and Steam Systems 58
5.4 Operating Profile 59
5.4.1 Voyage and speed profile 59

5.4.2 Engine working profile 61
5.4.3 Consumption profile 63
5.4.4 Fresh water consumption profile 63
5.4.5 Steam consumption profile 64
5.5 Energy Balance and Quality of Rejected Heat 66
5.5.1 Energy Balance 66
5.5.2 Quality of Rejected Heat 70
6 Initial Design Parameters of the Studied Rankine System 78
6.1 ORC cycles for Exhaust Gas Recovery 79
6.2 Conclusions Based on Literature Review 82
7 Proposed Model, Analysis and Optimization 86
7.1 Analytical approach: Pinch analysis 86
7.2 Optimization problem 88
7.3 Simulation Algorithm 92
8 Simulation Results 94
8.1 Comparison of the Optimal Parameters for each Fluid Combination in the Dual Cycle 94
8.2 Parametric Analysis per Fluid Combination in the Dual Cycle 101
8.2.1 R416a-R134a Dual Cycle 101
8.2.2 Ammonia-R134a Dual Cycle 103
8.2.3 R245fa-R134a Dual Cycle 105
8.2.4 Water-R134a Dual Cycle 108
8.3 Final System Selection and Performance over the Vessel Operating Profile 111
8.3.1 Water-R134a Dual Cycle Performance over Vessel Operating Profile 112
8.3.2 R245fa-R134a Performance over Vessel Operating Profile 114
9 Thermo-economic and Environmental Analysis 116
9.1 Energy Savings 116
9.2 Economic Analysis 128
9.2.1 Savings from ORC System 128
9.2.2 Spending for ORC System 129
9.2.3 Economic Indices 133
9.3 Environmental Analysis 137
10 Conclusions and Suggestions for Further Study 139
Appendix: Calculation of the power production profile 141

Bibliography 144

Figures

Figure 2.1: Schematic diagram of the Rankine cycle 18
Figure 2.2: Temperature entropy (T-s) diagram of the Rankine cycle 18
Figure 2.3: Simple Rankine cycle with superheating 21
Figure 2.4: Effect of evaporation pressure on cycle output 22
Figure 2.5: Schematic of reheated Rankine cycle 22
Figure 2.6: Regenerative Rankine versus Carnot cycle 23
Figure 2.7: Schematic diagram of regenerative Rankine cycle 23
Figure 2.8: Schematic diagram of dual loop cycle 24
Figure 2.9: Temperature entropy diagram of dual loop cycle 24
Figure 2.10: Exergy destruction in heat transfer in a subcritical cycle 26
Figure 2.11: Subcritical vs. supercritical temperature entropy diagram 27
Figure 2.12: Exergy destruction in a supercritical cycle 28
Figure 2.13: Temperature entropy diagram of a zeotropic mixture 29
Figure 2.14: Evaporation process of a zeotropic mixture [13] 30
Figure 3.1: Saturation temperature entropy curves for (a) isentropic, (b) dry and (c) wet fluids [21] 34
Figure 3.2: Entropy difference between liquid and vapor for water vs. organic fluids 36
Figure 3.3: Reducing heat transfer irreversibility for a fixed source by employing a fluid with a higher critical point at or near critical condition [26] 38
Figure 4.1: ORC applications on the market [40] 47
Figure 4.2: ORC with existing internal combustion engines [20] 48
Figure 4.3: Potential savings from Opcon Marine's heat recovery system [45] 51
Figure 5.1: Propulsion system overview 53
Figure 5.2: Fuel oil feed system 55
Figure 5.3: Fuel gas burning with Natural Boil-off Gas 56
Figure 5.4: Fuel gas burning with Forced and Natural Boil-off Gas 57
Figure 5.5: Steam system of the studied vessel 59
Figure 5.6: Studied vessel operational profile 60
Figure 5.7: Speed profile of the studied vessel 60
Figure 5.8: Power distribution and engines used for laden condition 62
Figure 5.9: Power distribution and engines used for ballast condition 63
Figure 5.10: Forcing vaporizer characteristic curve [49] 65
Figure 5.11: Main generator engines and supporting systems 67
Figure 5.12: Main engines cooling water systems 68
Figure 5.13: Engine system power distribution vs. Engine load 70
Figure 6.1: Simplified schematic of propulsion system waste heat streams 78
Figure 6.2: Proposed dual cycle system by Zhang et al. [60] 80
Figure 6.3: Dual Cycle System proposed by Zhang et al. [62] 81
Figure 6.4: Dual ORC cycle for containership propulsion proposed by Choi and Kim [63] 82
Figure 6.5: Schematic of proposed system 83
Figure 7.1: Proposed layout of dual cycle system 86
Figure 7.2: Pinch analysis [67] 87

Figure 7.3: Using the composite curves to determine energy targets [67] 87
Figure 8.1: Optimum Dual Cycle Power Output 97
Figure 8.2: Optimum Dual Cycle Power Output with Maximum Pressure 50 bar 98
Figure 8.3: Power Output for R416a-R134a Dual Cycle 102
Figure 8.4: Optimal Independent Variables for R416a-R134a Dual Cycle 102
Figure 8.5: Efficiency for R416a-R134a Dual Cycle 103
Figure 8.6: HT Cycle Sizing Parameters for R416a-R134a Dual Cycle 103
Figure 8.7: Power Output for Ammonia-R134a Dual Cycle 104
Figure 8.8: Optimal Independent Variables for Ammonia-R134a Dual Cycle 104
Figure 8.9: Efficiency for Ammonia-R134a Dual Cycle 105
Figure 8.10: HT Cycle Sizing Parameters for Ammonia-134a Dual Cycle 105
Figure 8.11: Power Output for R245fa-R134a Dual Cycle 106
Figure 8.12: Efficiency for R245fa -R134a Dual Cycle 106
Figure 8.13: Optimal Independent Variables for R245fa-R134a Dual Cycle 107
Figure 8.14: HT Cycle Sizing Parameters for R245fa –R134a Dual Cycle 107
Figure 8.15: Power Output and Turbine Outlet Dryness for Water-R134a Dual Cycle ... 108
Figure 8.16: Optimal Independent Variables for Water-R134a Dual Cycle 109
Figure 8.17: Efficiency for Water-R134a Dual Cycle 109
Figure 8.18: HT Cycle Sizing Parameters for Water-R134a Dual Cycle 110
Figure 9.1: Change in BOG mass flow and LHV through a voyage [71] 117
Figure 9.2: Graphical method of finding NBOG speed for laden voyage 120
Figure 9.3: Graphical method of finding NBOG speed for ballast voyage 120
Figure 9.4: Laden Power Production with Water-R134a Dual Rankine Cycle 123
Figure 9.5: Ballast Power Production with Water-R134a Dual Rankine Cycle 124
Figure 9.6: Laden Power Production with R245fa-R134a Dual Rankine Cycle 124
Figure 9.7: Ballast Power Production with R245fa-R134a Dual Rankine Cycle 125
Figure 9.8: Historic LNG prices in USD/mmBTU since 1997 in different areas [77] 135
Figure 9.9: NPV for Water-R134a Dual Cycle 135
Figure 9.10: DPB for Water-R134a Dual Cycle 136
Figure 9.11: IRR for Water-R134a Dual Cycle 136
Figure 9.12: NPV for R245fa-R134a Dual Cycle 136
Figure 9.13: DPB for R245fa-R134a Dual Cycle 137
Figure 9.14: IRR for R245fa-R134a Dual Cycle 137

Tables

Table 3.1: Calculated ξ Value vs. Actual Thermodynamic Data 35
Table 3.2: Common Greenhouse Gases 41
Table 3.3: Substances banned under EU Regulation 1005 (2009) 42
Table 3.4: Refrigerants suitable for 'R' character associated with Environmental Protection Notation 43
Table 3.5: ASHRAE Safety Designation of Refrigerants [39] 43
Table 3.6: Organic and other fluids proposed for ORC in Relevant Literature 45
Table 3.7: Organic and other fluids proposed for ORC in Relevant Literature Continued 46
Table 4.1: Qualitative comparison of land-based ORC applications [41] 49
Table 5.1: Propulsion system efficiency 53
Table 5.2: Main Generator Engines and coupled Alternators 54
Table 5.3: Electric Propulsion Motors 54
Table 5.4: Reduction Gearbox 54
Table 5.5: Atmospheric boiling points of natural gas components 58
Table 5.6: Fresh Water Generators 58
Table 5.7: Average speed per voyage mode 60
Table 5.8: Power distribution - Laden voyages 61
Table 5.9: Power distribution - Ballast voyages 62
Table 5.10: Consumption by fuel type in examined period 63
Table 5.11: Forcing vaporizer design curve 65
Table 5.12: Vessel steam requirements 66
Table 5.13: Heat Balance - Gas Mode 69
Table 5.14: Quality of waste heat streams 75
Table 6.1: Thermal degradation of various refrigerants 79
Table 6.2: Environmental and Safety Characteristics of Examined Fluids 84
Table 6.3: Thermodynamic Characteristics of Examined Fluids 84
Table 7.1: Dual cycle constant parameters 88
Table 8.1: Dual Cycle Optimization Results 94
Table 8.2: HT Cycle Optimization Results 95
Table 8.3: LT Cycle Optimization Results 95
Table 8.4: Extensive and Intensive Properties for Optimal R416a-R134a Dual Cycle 96
Table 8.5: Extensive and Intensive Properties for Optimal Ammonia-R134a Dual Cycle. 96
Table 8.6: Extensive and Intensive Properties for Optimal R245fa-R134a Dual Cycle 96
Table 8.7: Extensive and Intensive Properties for Optimal Water-R134a Dual Cycle 97
Table 8.8: Dual Cycle Optimization Results with Maximum Pressure 50 bar 99
Table 8.9: HT Cycle Optimization Results with Maximum Pressure 50 bar 99
Table 8.10: LT Cycle Optimization Results with Maximum Pressure 50 bar 100
Table 8.11: Extensive and Intensive Properties for Optimal R416a-R134a Dual Cycle with Maximum Pressure 50 bar 100
Table 8.12: Extensive and Intensive Properties for Optimal R245a-R134a Dual Cycle with Maximum Pressure 50 bar 101
Table 8.13: Example of Finding the Equilibrium Point of Water-R134a Dual Cycle and Engines 112

Table 8.14: Water-R134a Dual Cycle Operating Point - Laden 112
Table 8.15: Water-R134a Dual Cycle Operating Point - Ballast 112
Table 8.16:Water-R134a Dual Cycle Sizing Case 113
Table 8.17: R245fa-R134a Dual Cycle Operating Point - Laden 114
Table 8.18: Water-R245fa Dual Cycle Operating Point - Ballast 114
Table 8.19: R245fa-R134a Dual Cycle Sizing Case 115
Table 9.1: Natural Boil-off Rates 118
Table 9.2: Relevant LNG properties 118
Table 9.3: NBOG energy release as a function of nominal BOR 119
Table 9.4: Calculated NBOG Speed 119
Table 9.5: Power Production with Water-R134a Dual Cycle - Laden Voyage 121
Table 9.6: Power Production with Water-R134a Dual Cycle - Ballast Voyage 121
Table 9.7: Power Production with R245fa- R134a Dual Cycle - Laden Voyage 122
Table 9.8: Power Production with R245fa -R134a Dual Cycle - Ballast Voyage 122
Table 9.9: Potential Performance Improvements with Water-R134a Dual Cycle 122
Table 9.10: Potential Performance Improvements with R245fa-R134a Dual Cycle 123
Table 9.11: Energy Saved per Year with Water-R134a Dual Cycle - Laden Voyage 126
Table 9.12: Energy Saved per Year with Water-R134a Dual Cycle - Ballast Voyage 126
Table 9.13: Energy Saved per Year with Water-R134a Dual Cycle – Overall (MWh) 126
Table 9.14: Energy Saved per Year with R245fa-R134a Dual Cycle - Laden Voyage 127
Table 9.15: Energy Saved per Year with R245fa-R134a Dual Cycle - Ballast Voyage ... 127
Table 9.16: Energy Saved per Year with R245fa-R134a Dual Cycle – Overall (MWh) .. 127
Table 9.17: Fuel Saved per Year with Water-R134a Dual Cycle – Overall (Metric Tonnes) 127
Table 9.18: Fuel Saved per Year with R245fa-R134a Dual Cycle – Overall (Metric Tonnes) 128
Table 9.19: Assumed heat transfer coefficients 130
Table 9.20: Normal speed of fluid within piping and length of piping in ORC system 131
Table 9.21: Constant values for components cost estimation 132
Table 9.22: Comparison of Capital Costs for Proposed Systems 133
Table 9.23: Emissions reductions in Metric Tonnes for Water-R134a Dual Cycle 137
Table 9.24: Emissions reductions in Metric Tonnes for R245fa-R134a Dual Cycle 138

Symbols

Latin symbols

Ab_x	The fraction of a substance x remaining in the atmosphere
ALT	Atmospheric lifetime
c_p	Isobaric specific heat capacity of a fluid
E_{NBOG}	Thermal energy released by burning of natural boil-off gas per day
f_L	Load factor of the MGE as a percentage of the MCR
h	Specific enthalpy
Δh_{vap}	Latent heat of vaporization can be symbolized as
$\dot{m}$	Mass flow
p	Pressure
PP	Pinch point
$\dot{Q}$	Work per unit time (thermal power)
$\dot{q}_f$	Specific fuel energy consumption
RSP	Rotational speed parameter
R_x	Radiative efficiency of a substance x or the radiative forcing per unit mass increase in atmospheric abundance of the substance x
RF_x	Radiative forcing due to a pulse emission of a gas X
s	Specific entropy
SP	Size parameter
T	Temperature
U	Coefficient of heat transfer in a heat exchanger (kW/m^{2}K)
VFR	Isentropic Volume Ratio
$\dot{W}$	Work per unit time (mechanical power)
z	Altitude

Greek symbols

ε	Exergy efficiency
η	Efficiency
θ	Latidude
λ	Thermal conductivity
χ	Dryness of a non-saturated vapor-fluid mixture.
ξ	Inverse slope of the temperature entropy curve
∇_{CARGO}	Cargo capacity in cubic meters

Subscripts

$Crit$	Refers to critical properties of a fluid
e	Refers to an electrical property (i.e. electrical energy or efficiency)
is	Refers to an isentropic property (i.e. isentropic efficiency)
m	Refers to a mechanical property (i.e. mechanical energy or efficiency)

Red	Refers to a thermodynamic property given as a ratio to the corresponding critical value

Abbreviations

BOG	Boil-off Gas
BWR	Back work ratio
CFC	Chloro-Fluoro-Carbon
EGB	Exhaust Gas Boiler
FBOG	Forced Boil-off Gas
FWG	Fresh Water Generator
GWP	Global Warming Potential
GVU	Gas Valve Unit
HCFC	Hydro-Chloro-Fluoro-Carbon
HFC	Hydro-Fluoro-Carbon
HFO	Heavy fuel-oil
HT	High temperature
IGC	International Code for the Construction and Equipment of Ships Carrying Liquefied Gases in Bulk (IGC Code)
LD	Low-duty
LNG	Liquid natural gas
LT	Low Temperature
MARPOL	International Convention for the Prevention of Pollution from Ships
MCR	Maximum Continuous Rating
MGE	Main Generator Engine
NBOG	Natural Boil-off Gas
NCR	Normal Continuous Rating
ODP	Ozone Depleting Potential
ORC	Organic Rankine Cycle
PFC	Per-Fluoro-Carbon
SOLAS	International Regulation for the Safety of Life at Sea

1 Introduction

An estimated 20-50% of fuel energy in industrial processes is lost as waste heat. The large majority of this heat is rejected at low temperatures with an approximate 60% of industrial waste heat having a temperature below 230^0C and an impressive 90% having a temperature below 316^0C [13]. The high cost of fuel and growing concerns about the environment demand better utilization of this energy source.

The present study examines waste heat recovery using an organic Rankine cycle (ORC), a thermodynamic cycle based on the classic steam-water Rankine cycle but adapted for exploitation of low-grade heat by replacing water with an organic compound.

The class of organic compounds encompasses a large number of molecules, which contain atoms of carbon linked to other elements. The main benefit of using organic compounds is that their lower boiling points and critical properties allow for evaporation at lower temperatures than water, meaning lower temperature heat sources can be exploited.

The goal of the present work is to apply ORC waste heat recovery technology to a marine propulsion system in order to improve the propulsion efficiency and reduce fuel consumption.

ORC technology for waste heat recovery is not new with the first applications having been examined in the 1970s. However, it has only gained ground for marine applications in the past few years with the first system installed on a 75,000 GT large car/truck carrier in 2011 [1], [2].

The vessel to be examined in the present work is a 159,000 m^3 liquefied natural gas (LNG) carrier with a triple-fuel diesel-electric propulsion system. The waste heat from the exhaust gas and the engine cooling water will be recovered using a dual loop Rankine system. Ultimately, it will be shown that the propulsion system efficiency can be improved by 2-7% while the fuel energy consumption to maintain a given speed can be reduced by 5-14.5%, depending on the speed.

The analysis will begin with a review of the theoretical concepts behind the proposed system, which includes an overview of Rankine cycle basics in Chapter 2 and an analysis on organic fluids and their relevant properties in Chapter 3. Existing applications of ORC technology will be presented in Chapter 4.

The propulsion system to be examined in the present work is described in detail in Chapter 5. The initial design parameters for the Rankine cycle application will be reviewed in Chapter 6. The simulation model, analytical approach and optimization problem to be used for the final system design will be presented in Chapter 7 and the results of the simulation will be included in Chapter 8. The results will be assessed from a techno-economic viewpoint in Chapter 9 and the final conclusions and suggestions for further research will be presented in Chapter 10.

2 Thermodynamic Analysis of the Rankine Cycle

Equipment based on the Rankine Cycle is used for 80% of the world's electricity production [3]. It is among the most well-known and widely used thermodynamic cycles.

In the classic Rankine Cycle, the working fluid is water/steam. The organic Rankine cycle replaces water with an organic fluid, the advantages of which will be examined in the next section. The working principle of the cycle, however, remains unchanged.

The four basic steps of the cycle are, as in Figure 2.1, (1→2) adiabatic compression, (2→3) isobaric heating, (3→4) adiabatic expansion and (4→1) isobaric cooling. The steps take place in a feed pump, boiler, turbine and condenser, respectively [4].

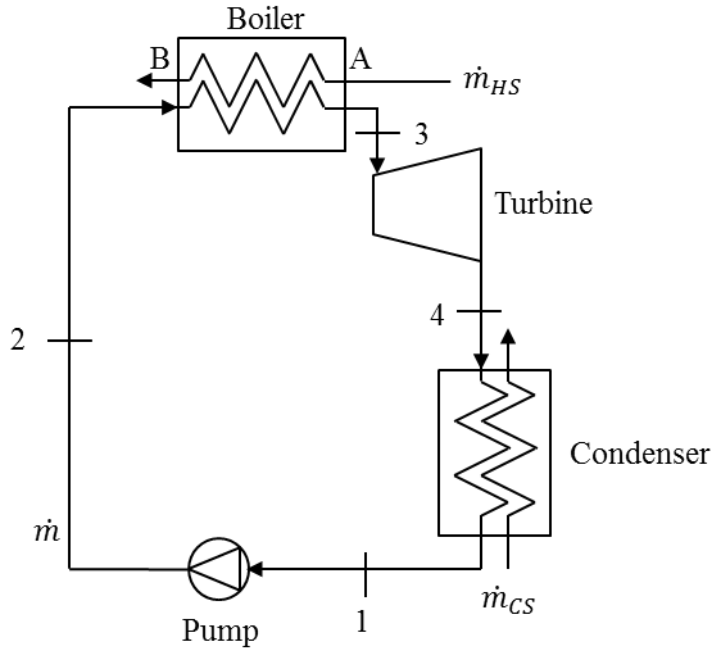

Figure 2.1: Schematic diagram of the Rankine cycle

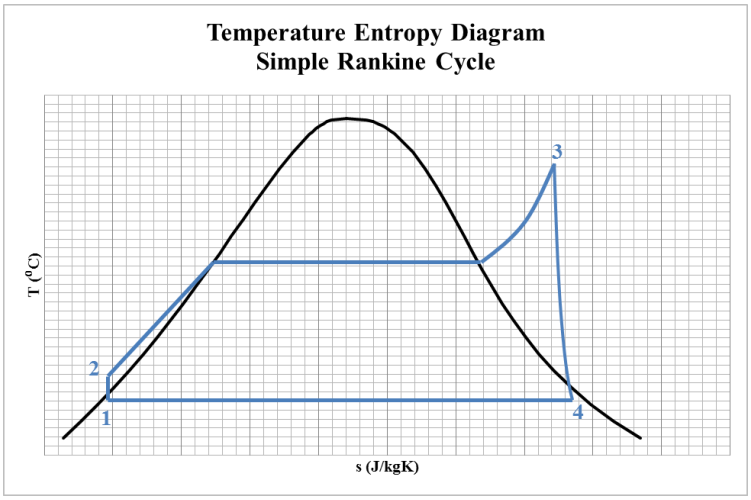

Figure 2.2: Temperature entropy (T-s) diagram of the Rankine cycle

1→2 Adiabatic compression

The working fluid is pumped from the condenser and fed to the boiler. The mechanical work[1] consumed is:

$$\dot{W}_P = \dot{m}(h_2 - h_1)/\eta_{mP} \tag{2.1}$$

where

$\dot{m}$ the mass flow of the working fluid
h_i the fluid specific enthalpy at point i
η_{mP} the mechanical efficiency of the pump.

In reality, the process is not isentropic. Therefore the specific enthalpy at the outlet of the pump is found using the isentropic efficiency η_{isP} and the theoretical enthalpy h_{2is} where $s_{2is} = s_1, p_{2is} = p_2$:

$$\eta_{isP} = \frac{h_{2is} - h_1}{h_2 - h_1} \leftrightarrow h_2 = h_1 + \frac{h_{2is} - h_1}{\eta_{isP}} \tag{2.2}$$

2→3 Isobaric heating

Heat is input in the system in the boiler through three separate heat exchangers: the preheater, which increases the liquid temperature, the evaporator, in which the saturated liquid is evaporated, and the superheater, which further increases the temperature of the steam. This heat is symbolized with $\dot{Q}_H$.

$$\dot{Q}_H = \dot{m}(h_3 - h_2) \tag{2.3}$$

Here, the heat source is considered to be a waste heat stream, the available heat of which can be expressed as follows:

$$\dot{Q}_{HS} = \dot{m}_{HS}(h_A - h_B) \tag{2.4}$$

It is noted that not all of the available heat from the waste heat stream can be absorbed by the working fluid. The efficiency of the heat recovery is therefore:

$$\eta_Q = \frac{\dot{Q}_H}{\dot{Q}_{HS}} \tag{2.5}$$

3→4 Adiabatic expansion

The useful work of the cycle is produced in the turbine where the expansion and subsequent enthalpy loss of the working fluid is converted to mechanical work:

[1] In the equations in this section, heat and work are given per unit time. In other words, the thermal or mechanical power is used.

$$\dot{W}_T = \dot{m}(h_3 - h_4)\eta_{mT} \tag{2.6}$$

As was true for compression, the expansion process is not isentropic. Therefore the specific enthalpy at the outlet of the expander is found using the isentropic efficiency η_{isT} and the theoretical enthalpy h_{4is} where $s_{4is} = s_3, p_{4is} = p_4$:

$$\eta_{isT} = \frac{h_3 - h_4}{h_3 - h_{4is}} \leftrightarrow h_4 = h_3 - (h_3 - h_{4is}) \cdot \eta_{isT} \tag{2.7}$$

4→1 Isobaric cooling

Heat is lost in the condenser, a surface heat exchanger which collects and condenses the vapor at the outlet of the turbine, rejecting heat to the environment. The heat rejected is:

$$\dot{Q}_C = \dot{m}(h_4 - h_1) \tag{2.8}$$

Cycle efficiency

The net work produced by the system is the difference between the mechanical work produced in the turbine and the mechanical work consumed in the pump:

$$\dot{W}_{net} = \dot{W}_T - \dot{W}_P = \dot{m} \cdot [\eta_{mT}(h_3 - h_4) - (h_2 - h_1)/\eta_{mP}] \tag{2.9}$$

The heat input to produce this work is $\dot{Q}_H$ as defined in Equation (2.3). Therefore the thermal efficiency of the cycle is:

$$\eta_R = \frac{\dot{W}_{net}}{\dot{Q}_H} = \frac{\eta_{mT}(h_3 - h_4) - (h_2 - h_1)/\eta_{mP}}{h_3 - h_2} \tag{2.10}$$

Keeping in mind that the available heat from the source is not completely absorbed by the working fluid, the overall efficiency of the system can then be expressed as:

$$\eta_{TOT} = \eta_R \cdot \eta_Q \tag{2.11}$$

From Equation (2.11), it is clear that there are two ways to increase the efficiency of the system:

(1) Increase the thermal efficiency of the cycle.

(2) Increase the efficiency of the heat recovery in the boiler.

In the following sections, various methods are examined for doing just that.

It is noted that in this type of waste heat recovery system, from the point of view of thermodynamics, the goal is not to increase the Rankine cycle thermal efficiency or the heat recovery efficiency individually, but to maximize their product, the total efficiency.

When economic considerations are eventually taken into account, the goal is to maximize the financial benefit of the Rankine cycle system. Ultimately, the thermodynamically optimal and financially optimal systems may not coincide, since the

thermodynamically optimal system may require large and costly equipment offsetting the economic benefits of increased power output [5].

2.1 Increasing the thermal efficiency of the cycle

As is known from the first law of thermodynamics, energy cannot be created or destroyed so that an increase in the internal energy of a closed system is equal to the heat supplied to the system minus the work done by it. The thermal or first-law efficiency of the system is a measure of the work that can be produced for a given heat input. Different Rankine cycle arrangements can be used to improve thermal efficiency.

2.1.1 Superheating

One basic method for increasing the thermal efficiency of a Rankine cycle is superheating. Superheating involves heating the working fluid to a temperature beyond its vapor saturation curve for the system evaporation pressure. As can be seen in Figure 2.3, this increases the work of the cycle by 33'4'43 while the added heat is increased by 33'b'b3. Since the ratio of these areas is larger than the corresponding ratio for the cycle, the thermal efficiency is increased. As an added benefit, the vapor at the turbine outlet is drier, reducing the risk of droplet formation and turbine blade erosion.

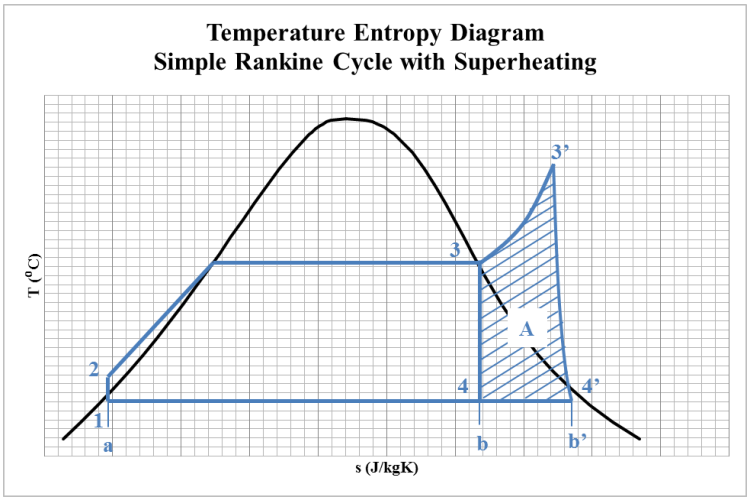

Figure 2.3: Simple Rankine cycle with superheating

2.1.2 Increasing pressure in the cycle – Reheating

Aside from increasing the superheating temperature, another method of increasing the thermal efficiency is by increasing the evaporation pressure. As can be seen in Figure 2.4, an increase of the evaporation pressure from P_3, to P_3 does not have a significant impact on the net work, which is increased by the area A compared to the original cycle, but decreased by the similarly sized area B. However, the rejected heat to the cold stream is decreased by the area b44'b'b resulting in a higher efficiency [4].

The amount by which the thermal efficiency can be improved with increased pressure is limited by the turbine outlet conditions. As pressure is increased for the same maximum temperature, the outlet vapor becomes more wet while normally a dryness of χ = 0.9 is considered the minimum acceptable to avoid turbine blade erosion. This problem can be overcome by using reheating. In a reheated cycle, as shown in Figure 2.5, the working fluid is only partially expanded in the turbine when it is sent back to the boiler for

reheating before returning to the turbine for the rest of expansion. The reheated cycle efficiency is slightly higher than the simple Rankine cycle, though the main benefit of reheating remains the increased dryness at the turbine outlet [4].

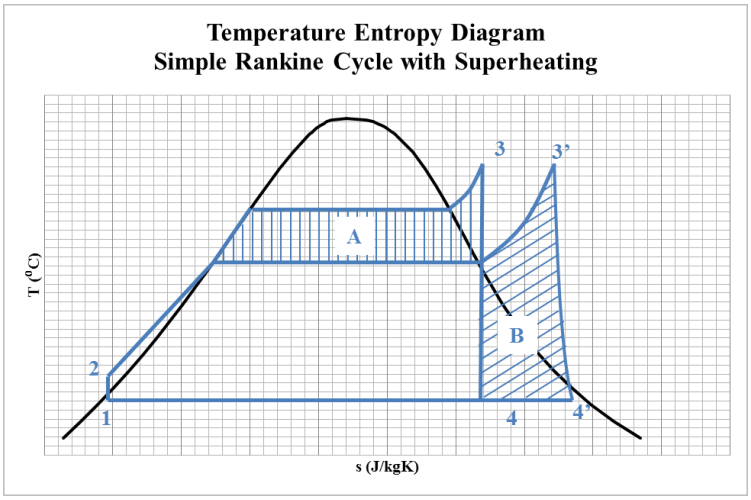

Figure 2.4: Effect of evaporation pressure on cycle output

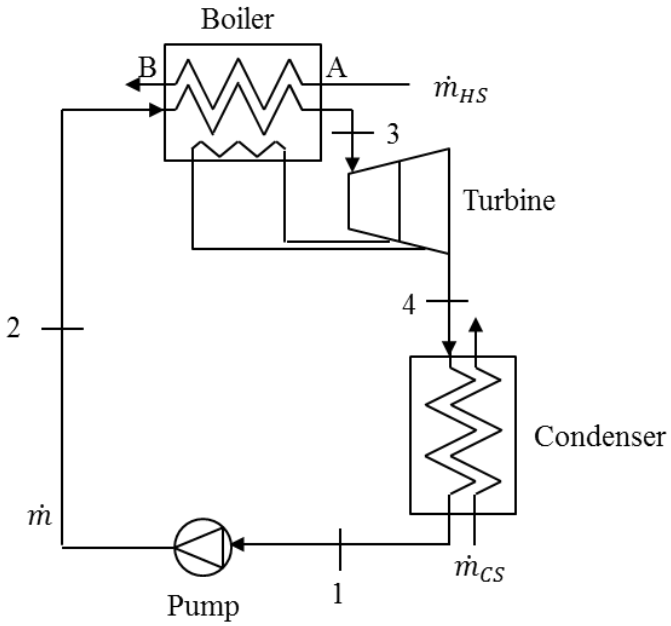

Figure 2.5: Schematic of reheated Rankine cycle

2.1.3 Regenerative cycle

A well-known conclusion of thermodynamics is that the maximum thermal cycle efficiency is that of the Carnot cycle which is bounded by the line 1'345' in Figure 2.6:

$$\eta_{Carnot} = 1 - \frac{T_L}{T_H} \tag{2.12}$$

where T_H is the heating temperature and T_L the condensing temperature. The simple Rankine cycle (12345'1), shown in Figure 2.6 without superheating, has of course a lower efficiency.

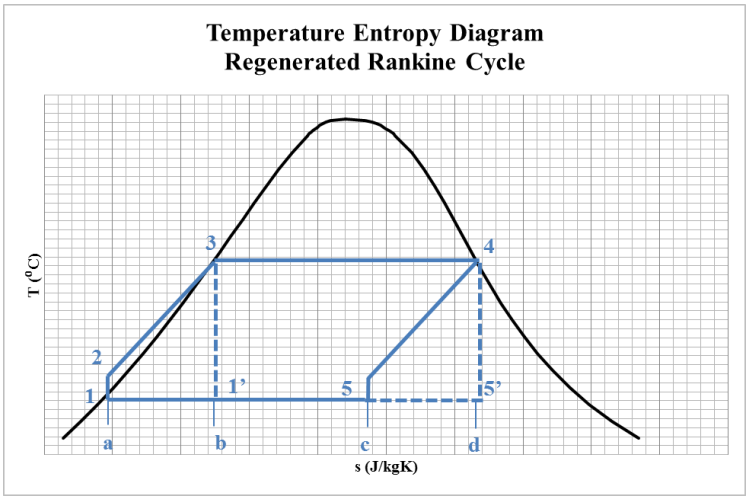

Figure 2.6: Regenerative Rankine versus Carnot cycle

In the regenerative cycle, the stream of warm vapor in the turbine is used to preheat the stream of water after the pump and before the boiler. In the ideal regenerative cycle, this heat transfer takes place within the turbine and is completely reversible. The lines 4-5 and 1-2-3 are then parallel and the corresponding areas 123ba and 54dc are equal. The efficiency of the ideal regenerative Rankine cycle is therefore equal to that of the Carnot cycle [4].

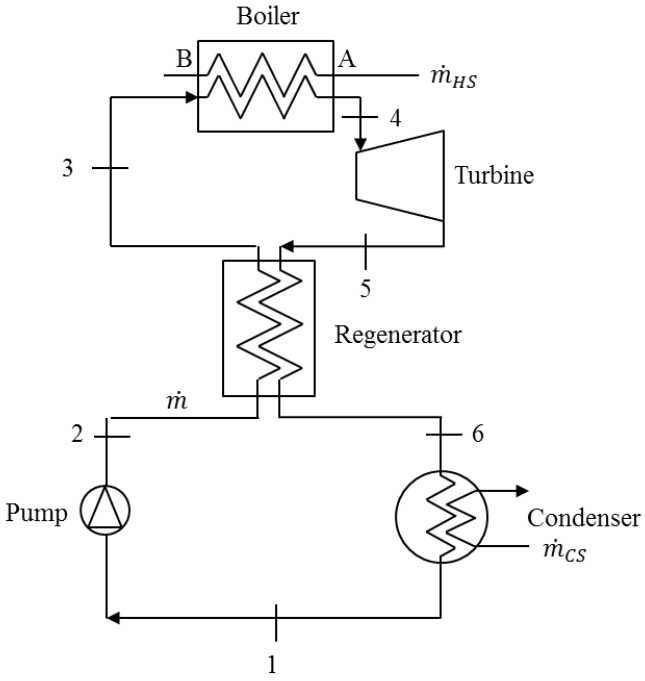

Figure 2.7: Schematic diagram of regenerative Rankine cycle

Of course, real regenerative cycles cannot achieve reversible heat transfer while for practical reasons heat transfer takes place using extraction steam or the entire turbine outlet

steam outside the expander rather than in the turbine shell itself. Nevertheless, the use of recuperating preheaters is an effective way to increase cycle efficiency [4].

2.1.4 Dual loop cycle

Another cycle which aims to improve cycle efficiency while compromising on cycle simplicity is the dual loop cycle: a combined system of two cycles HT and LT. The cycles are connected in a heat exchanger which serves as the condenser for the HT loop and the evaporator for the LT loop. Each loop can use a different working fluid [6].

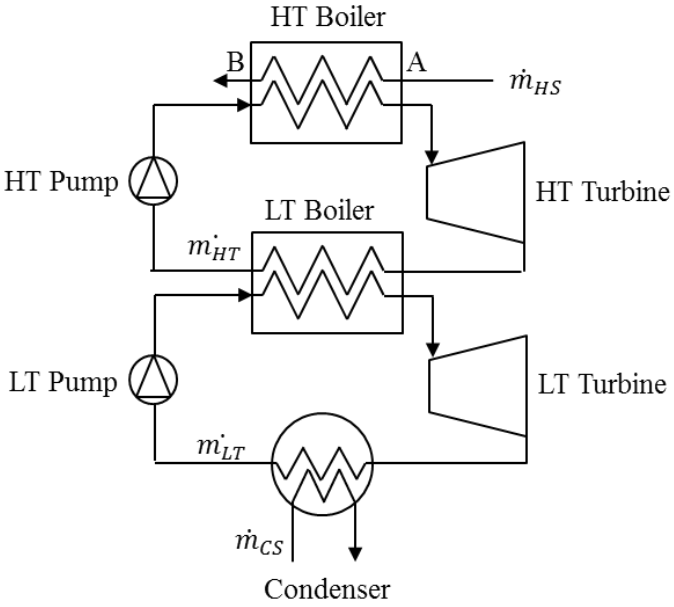

Figure 2.8: Schematic diagram of dual loop cycle

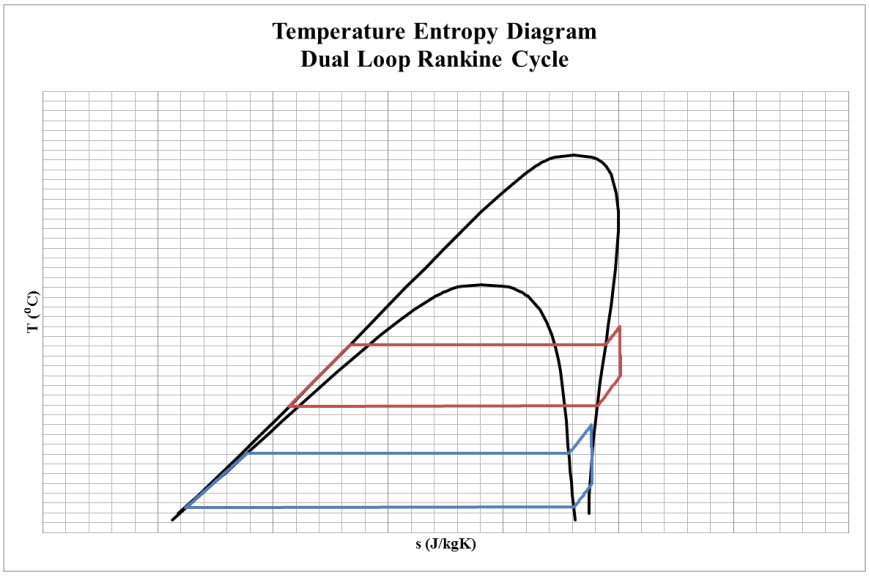

Figure 2.9: Temperature entropy diagram of dual loop cycle

2.2 Increasing the efficiency of heat recovery in the boiler

As has been noted in the previous section, while many methods can be used in an effort to improve the thermal efficiency of a Rankine cycle, this improvement alone cannot achieve the best overall efficiency of the installed waste heat recovery system. The efficiency of heat recovery must be simultaneously optimized for the best overall system performance.

As noted in the second law of thermodynamics, in real thermodynamic systems, the available energy from the heat source cannot be completely absorbed because real energy conversion processes are irreversible [7]. Effects such as chemical reactions, heat transfer through finite temperature differences, mixing components at different states, unrestrained expansion and friction are responsible for these irreversibilities which can be quantified using the concept of exergy [8].

Exergy is the maximum useful work which could be produced by a system through a process which brings the system into equilibrium with its environment, defined by the thermal reference state T_0, p_0. In contrast to energy, which is conserved, exergy is destroyed during heat transfer. As a result, exergy balances must contain a term for exergy destruction ($\dot{E}_D$) and exergy loss ($\dot{E}_L$) to the environment, as shown in Equation (2.13).

$$\dot{E}_{in} = \dot{E}_{out} + \dot{E}_D + \dot{E}_L \tag{2.13}$$

By quantifying these terms, the exergy or second law efficiency can be determined.

$$\zeta = \frac{\dot{E}_{out}}{\dot{E}_{in}} = 1 - \frac{\dot{E}_D + \dot{E}_L}{\dot{E}_{in}} \tag{2.14}$$

For heat transfer processes, exergy destruction can be defined using the thermodynamic average temperatures[2] of the hot and cold streams, symbolized T_{ha} and T_{ca} respectively, as well as the heat transfer rate $\dot{Q}$.

$$\dot{E}_D = \left(1 - \frac{T_0}{T_{ha}}\right)\dot{Q} - \left(1 - \frac{T_0}{T_{ca}}\right)\dot{Q} \tag{2.15}$$

Since the heat transfer rate is proportional to the temperature difference between two streams, $\dot{Q} \propto T_{ha} - T_{ca}$, Equation (2.15) can be simplified to:

$$\dot{E}_D \propto T_0 \cdot \frac{(T_{ha} - T_{ca})^2}{T_{ha} T_{ca}} \tag{2.16}$$

[2] The thermodynamic average temperature of a a heat stream is defined by:

$$T_a = \frac{\int_{in}^{out} T ds}{s_{out} - s_{in}} = \frac{(h_{out} - h_{in}) - \int_{in}^{out} v dp}{s_{out} - s_{in}}$$

When ignoring pressure losses:

$$T_a = \frac{h_{out} - h_{in}}{s_{out} - s_{in}}$$

Therefore exergy destruction is reduced and second law efficiency increased when the thermodynamic average temperatures of the two streams are close.

This can be represented graphically as in Figure 2.10. The area between the heat source and working fluid curves represents the exergy destruction for the heat transfer. The smaller this area, the more efficient the heat transfer.

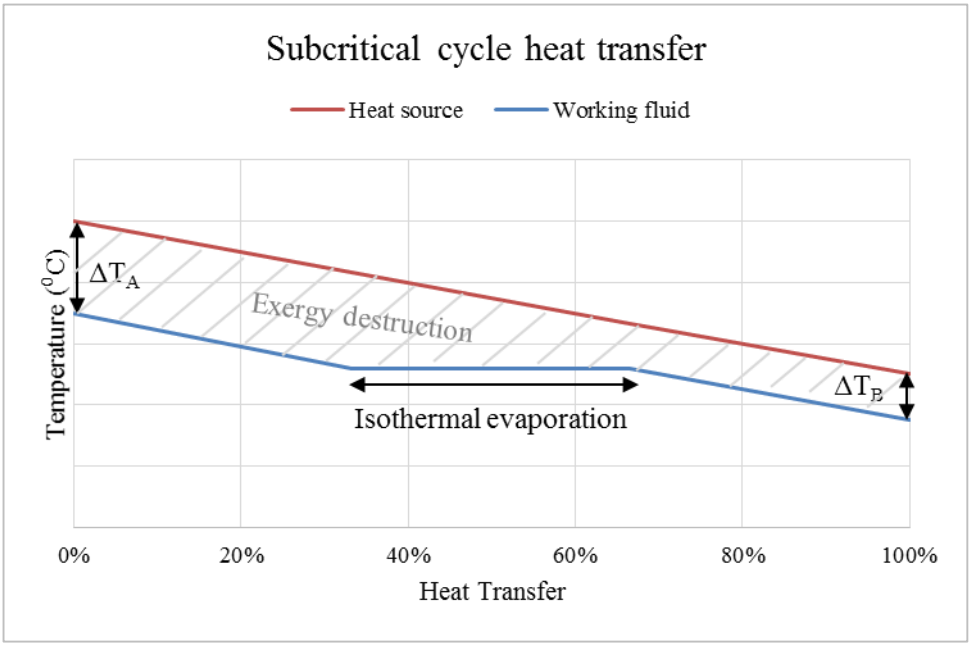

Figure 2.10: Exergy destruction in heat transfer in a subcritical cycle

2.2.1 Subcritical vs Supercritical Rankine Cycles

One method to increase the efficiency of heat transfer in the Rankine cycle is by using fluids above their critical point.

The critical point of a fluid is the peak of its saturation line. It is defined by two parameters: the critical temperature (T_{Crit}) and critical pressure (p_{Crit}). The critical temperature is the maximum temperature at which a substance can exist as a liquid. Above this temperature it will be in gaseous phase and cannot be liquefied, no matter how high pressure is applied. At the critical temperature, the pressure required to liquefy the gas is called the critical pressure.

In the classic water-steam Rankine cycle, evaporation occurs at a temperature well below water's critical point (374°C, 220.64 bar). The cycle is therefore called subcritical.

By contrast, if the evaporation in a Rankine cycle is above the working fluid's critical temperature, the cycle is called supercritical. A supercritical cycle is fairly easy to achieve with organic working fluids, as their critical point generally occurs at lower pressures and temperatures than water.

In Figure 2.11, a subcritical and a supercritical cycle are shown. The advantage of the supercritical cycle can be easily seen. Due to the absence of an isothermal evaporation zone, the supercritical fluid is better matched with the sensible heat source meaning the exergy destruction of the heat exchange is reduced and the second law efficiency correspondingly increased.

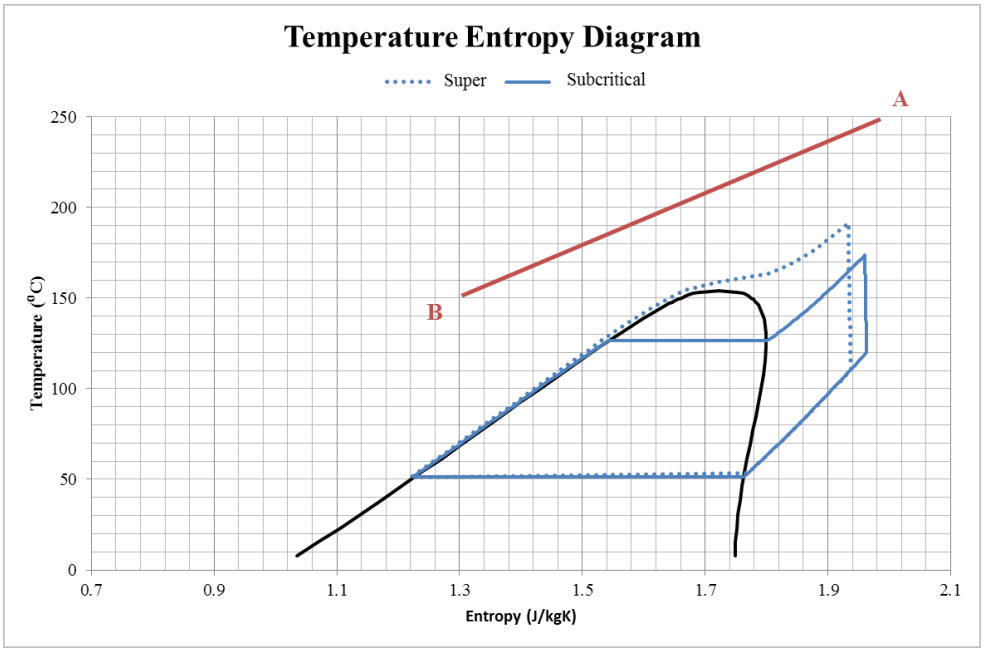

Figure 2.11: Subcritical vs. supercritical temperature entropy diagram

It should be noted, however, that supercritical cycles are not without their disadvantages. One major drawback is the larger heat exchangers needed for supercritical cycles. This need can easily be understood by examining Equation (2.17) for heat exchange:

$$\dot{Q} = U \cdot A_r \cdot \Delta T_{lm} \tag{2.17}$$

where

U the coefficient of heat transfer

A_r the heat transfer area and

ΔT_{lm} the logarithmic mean temperature difference calculated as:

$$\Delta T_{lm} = \frac{\Delta T_A - \Delta T_B}{\ln\left(\frac{\Delta T_A}{\Delta T_B}\right)} \tag{2.18}$$

which is smaller for the supercritical cycle as shown in Figure 2.12, as compared to the subcritical cycle, represented in Figure 2.10, meaning the heat transfer area for the supercritical cycle must be larger.

Furthermore, supercritical cycles require higher pressures, which call for equipment with higher strength and more expensive materials [9].

The use of supercritical cycles for Rankine power systems has been examined by many researchers. Chen et al. [9] examined 35 different working fluids in subcritical and supercritical cycles. Their results suggest that the type of cycle most suited to an application depends both on the heat source temperature as well as on the used fluid (i.e. wet, dry or isentropic, properties explained in Subsection 3.1.2). Karellas and Schuster [10] examined the potential of supercritical cycles with various heat source types (including

internal combustion waste heat and geothermal energy) at various supercritical pressures ranging from $1.01 \cdot p_{crit}$ to $1.1 \cdot p_{crit}$. They found that the use of supercritical cycles could increase both thermal and total system efficiency, however the heat source temperature and pressure had to be appropriate. Even in cases when the supercritical cycle resulted in reduced thermodynamic efficiency, the higher heat recovery efficiency led to increased system efficiency overall, especially for higher heat source temperatures. Braimakis et al. [5] examined pure and binary mixtures of natural refrigerants (i.e. hydrocarbons such as butane, pentane and hexane) in sub and supercritical cycles. They found that supercritical cycles showed benefits for higher temperatures (above 200-250^{0}C) for pure fluids while for mixtures supercritical cycles showed benefits for even medium range heat sources. However, they noted that the supercritical cycles were characterized by high rotational speeds, system sizes, volume flow ratios and required heat transfer areas meaning a techno-economic analysis would be needed before drawing any final conclusions about the use of such system.

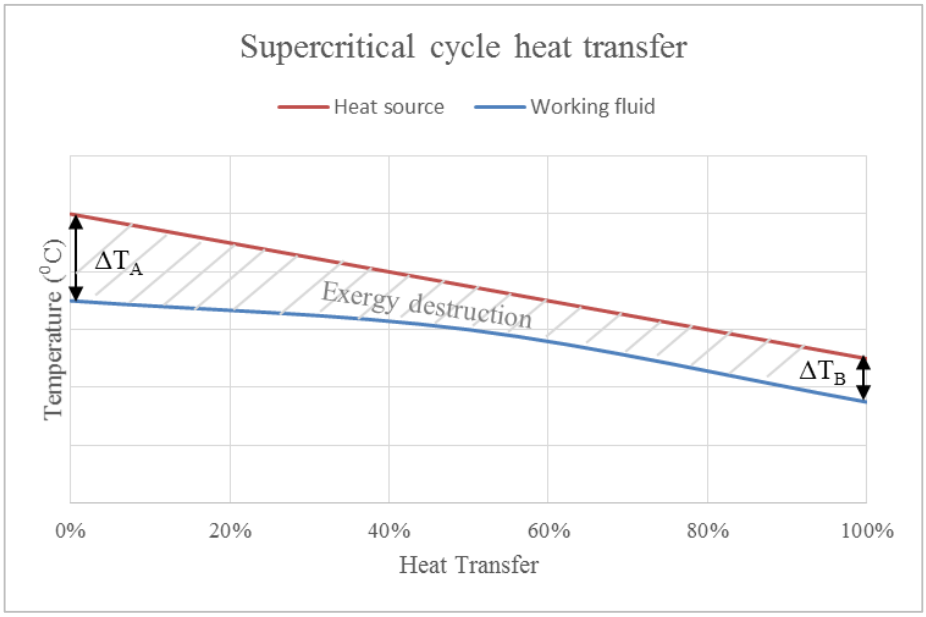

Figure 2.12: Exergy destruction in a supercritical cycle

Finally, Pan et al. in [11] examined the performance of subcritical cycles used at pressures close to their critical points. They found that fluids thermal properties undergo strong variations at near critical pressures. While the thermal efficiency of the cycles they examined varied continuously for increased pressure, reaching a maximum for pressures around $1.15 \cdot p_{crit}$, other properties showed strong discontinuities near the critical point. Most interestingly, the mass flow rate of the organic compound and the net power output of the cycle were markedly increased for pressures near the critical point around $P_{Red} = 0.95 - 1$. In fact, the researchers showed that subcritical cycles at near critical conditions can achieve power outputs near to or even better than supercritical cycles for the same fluid.

2.2.2 Zeotropic mixtures of organic fluids

While supercritical cycles reduce irreversibility by providing better temperature matching for evaporation, they do not improve the temperature matching for condensation which still takes place isothermally. This restriction can be overcome with the use of zeotropic mixtures, which change phase at constant pressure but not at constant temperature as shown in Figure 2.13 [12], [6]. A zeotropic mixture is a mixture whose components have different mass fractions in the vapor and liquid phase at equilibrium condition. By contrast, azeotropic mixtures have identical compositions in both phases and behave similarly to pure fluids [13].

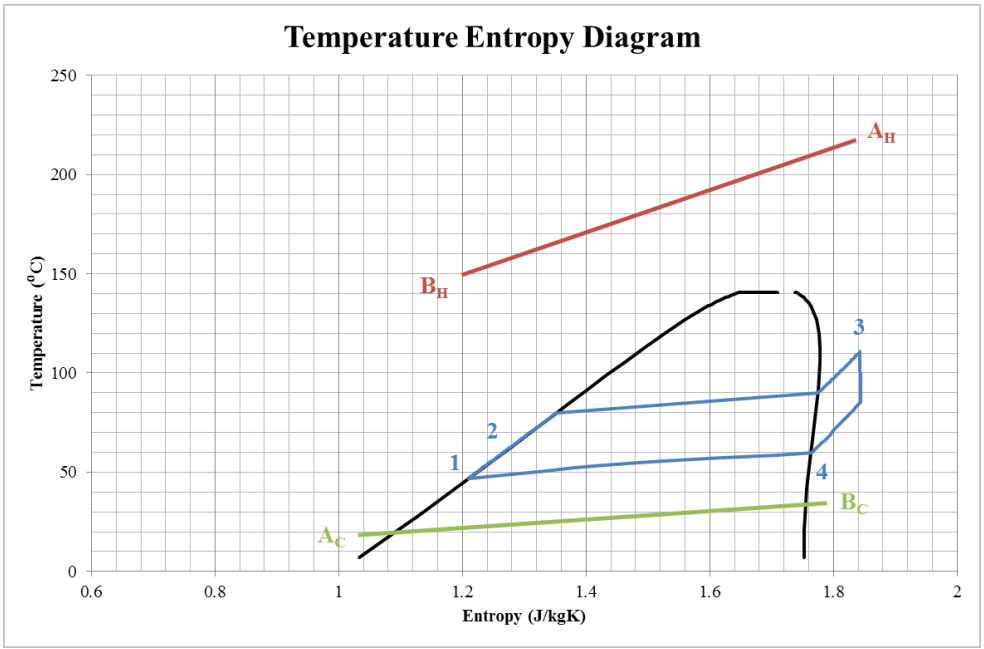

Figure 2.13: Temperature entropy diagram of a zeotropic mixture

An explanation of this phenomenon can be seen in Figure 2.14, the upper portion of which shows a typical phase equilibrium diagram of a binary zeotropic mixture. The x-axis represents the mole fraction of each component while the y-axis represents temperature. The two characteristic curves in the diagram are the dew point line and the bubble point line. The dew point represents the temperature at which a gas of given composition will begin to condense when cooled and the first liquid droplets will form. The bubble point represents the temperature at which a liquid of given composition will begin to boil when heated and the first vapor bubbles will form. The temperature difference between the the dew point and bubble point of the given mixture is called the boiling range (BR) or temperature glide for the mixture. Point A represents the boiling/dew point of the pure, less volatile component (i.e. the component with a higher boiling temperature) while Point B represents the boiling/dew point of the pure, more volatile component (i.e. the component with a lower boiling temperature).

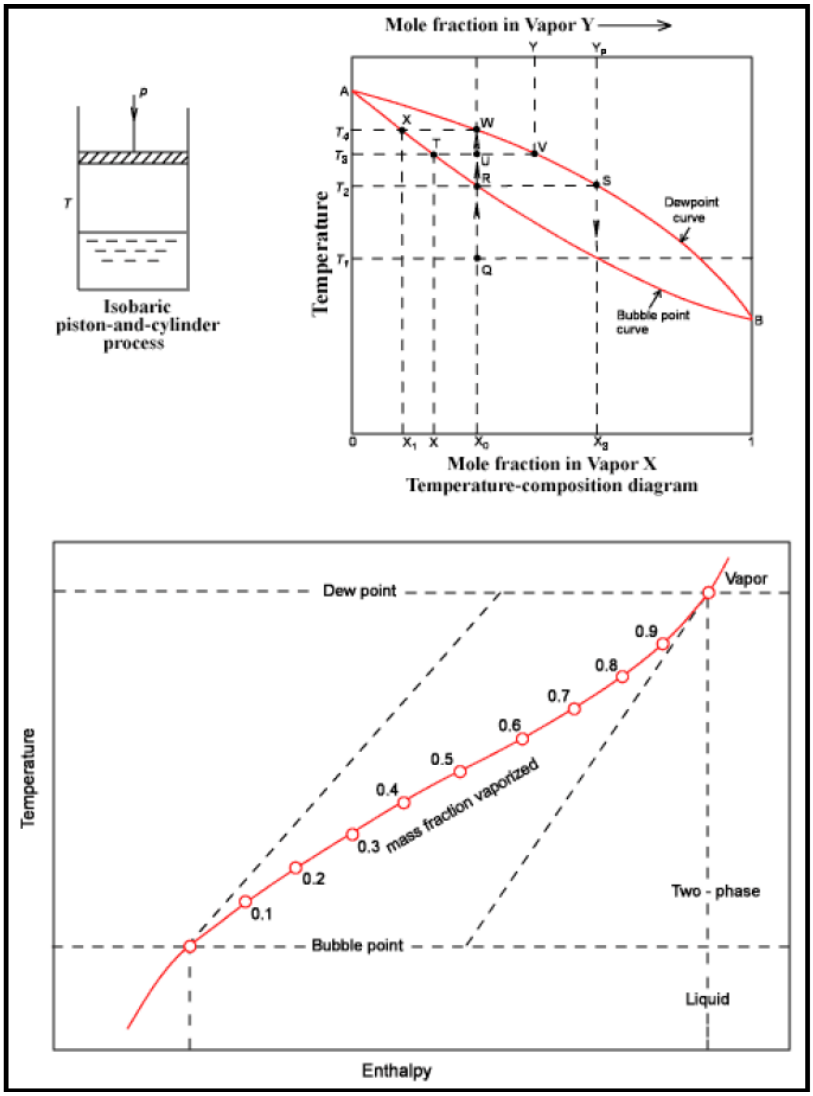

Figure 2.14: Evaporation process of a zeotropic mixture [13]

A better understanding of the process can be found by examining the isobaric heating of a zeotropic mixture of composition X_0 from an initial liquid temperature of T_1 to a fully vaporous state at temperature T_4, respectively points Q and W in Figure 2.14. At the temperature T_2, the fluid will begin to evaporate and the produced vapor will have a composition of Y_0 as at point S, rich in the volatile fluid. With further increase in temperature to T_3, both components will continue to evaporate. The composition of the liquid will now be X as at point T and the composition of the vapor will now be Y as at point V. Finally, at the temperature T_4 the fluid will be fully evaporated. The vapor will have the initial composition of X_0. The final droplet of liquid to evaporate will have a composition of X_1, rich in the less volatile fluid.

The temperature enthalpy curve resulting from this process is shown in the lower portion of Figure 2.14. It is clear that this curve will provide much better matching with a sensible heat source than a pure mixture with an isothermal evaporation zone.

As a result of their favorable evaporation profile, zeotropic mixtures for Rankine power systems have been the topic of many studies, most of which examine exergy

efficiency since the main benefit of zeotropic mixtures is reduced exergy destruction in heat transfer.

Lecompte et al. [14] follow this trend and investigate the potential of zeotropic mixtures performance measured by second law efficiency. They found that it can be increased around 7-14% compared to pure working fluids due to the higher heat input and heat conversion efficiency. The improvement is based primarily on the improved behavior in the condenser, where a better match with the glide slope of the sensible heat sink (cooling fluid) reduces the heat transfer irreversibilities of cooling.

Le at al. [15] note that this thermodynamic benefit of zeotropic fluids is not their only advantage. As they are produced by mixing different pure fluids, the base components can be chosen so as to improve practical characteristics of the fluid such as flammability, toxicity or environmental impact.

Nevertheless, studies suggest that the benefits of zeotropic mixtures depend greatly on the application and performance criteria examined. Zhao and Bao in [16] examined the criteria of thermal efficiency, output work and exergy efficiency of zeotropic ORC cycles. They found that for lower heat source temperatures, zeotropic mixtures outperformed pure fluids. However, as heat source temperatures increased, pure working fluids performed better than mixtures.

The work of Le at al. [15] again emphasized the importance of performance criteria selection based on the application. Their examination of R245fa and n-pentane individually and in various mixtures showed that the total irreversibility of the cycle components was lower for the mixtures. However, if the exergy flow rate lost to the cooling water was included in the total irreversibility rate, then the ratio of exergy loss to net power output was higher for the mixtures. This suggests that when the ORC heat sink medium can be further recovered, for example in combined heat and power (CHP) plants, then zeotropic mixtures should be preferred, whereas pure fluids should be chosen in applications where the heat sink is not further utilized. Nevertheless, in the work of Le et al. when economic rather than purely thermodynamic factors were used for cycle optimization, certain zeotropic mixtures proved more profitable even in cases where exergy flow to the cooling water is not recovered.

3 Organic Fluids

Of the estimated 20-50% of fuel energy in industrial processes which is lost as waste heat, the large majority is rejected at low temperatures with an approximate 60% of industrial waste heat having a temperature below 230^0C and an impressive 90% having a temperature below 316^0C [13]. At such low temperatures, classic steam-water Rankine cycles become less profitable because low-pressure steam also has low density requiring large and costly equipment. The organic Rankine cycle addresses this problem by replacing steam with an organic compound.

The class of organic compounds encompasses a large number of molecules, which contain atoms of carbon linked to other elements, most commonly hydrogen, oxygen or nitrogen. However, certain carbon containing compounds, such as carbon oxides (CO_x), carbonic acid (H_2CO_3) and carbonic salts like calcium carbonate ($CaCO_3$), are traditionally not classified as organic. At the same time, some non-organic compounds such as ammonia (NH_3) are commonly considered as working fluids for ORC systems without any differentiation made to the cycle name [17].

3.1 Categorization of organic fluids

Organic compounds can be classified based on their chemical structure or their thermodynamic properties.

3.1.1 Chemical categorization of organic fluids

Based on their chemical structure, organic fluids can be classed under the following groups [12], [18]:

(1) *Halocarbons* are organic compounds in which carbon is linked to one or more halogen atoms, which comprise group 17 of the periodic table, like fluorine, chlorine, bromine or iodine. Subgroups of halocarbons include:

a. Chloro-Fluoro-Carbons (CFCs): These once very common refrigerants have been banned since 2010, because of their high ozone depletion potential[3] (ODP up to 1) [19].
b. Hydro-Chloro-Fluoro-Carbons (HCFCs): These substances were initially used to replace CFCs. Their ozone depleting potential is much lower than that of CFCs, ranging from 0.01 to 0.1, however it is still high enough to be a cause of environmental concern. HCFCs are in the process of being phased out of use and will be completely banned by 2030 [19].
c. Hydro-Fluoro-Carbons (HFCs): These substances are the most common substitutes for banned HCFCs. Because they do not contain chlorine or bromine, they have an ODP of zero. Furthermore, they have good thermodynamic properties, though some

[3] Ozone depleting substances are compounds which degrade under ultraviolet light in the stratosphere releasing chlorine or bromide which deplete the ozone layer responsible for protecting earth from UVB radiation. The impact of a chemical on the ozone is quantified with its Ozone Depletion Potential, the ratio of the ozone impact of the chemical compared to a similar mass of CFC-11 [79].

have high Global Warming Potential[4] (GWP). The compound known as R245fa, used in many practical applications like [20] belongs to this group.

d. Per-Fluoro-Carbons (PFCs): These substances have a very high GWP. They can also be corrosive, toxic or highly flammable and are generally not favorable for ORC applications.

(2) Hydrocarbons are compounds of carbon and hydrogen. Examples include methane, ethane, propane, butane and toluene, among others. They have favorable thermodynamic properties, zero ozone depleting potential, and low toxicity, and, with the exception of methane, low global warming potential. However, they are largely flammable.

(3) Alcohols, for example methanol or ethanol, are organic compounds in which carbon is bonded with a hydroxyl group (OH). They are also difficult to use because of their high flammability, corrosiveness and possible toxic vapors.

(4) Though not chemically classified as organic compounds, certain *inorganic fluids* should be mentioned here due to their potential for use in ORC systems. These include ammonia, water and carbon dioxide.

3.1.2 Thermodynamic categorization of organic fluids

While a chemical categorization of organic fluids is useful for understanding the types of compounds which are being examined, a more practical classification is based on their thermodynamic behavior. Thermodynamically, organic fluids can be classified based on the slope of the saturation vapor curve in their temperature-entropy diagram [12].

(1) Wet fluids have a saturation vapor curve with a negative slope $\left(\frac{\partial T}{\partial S} < 0\right)$ as can be seen in Figure 3.1. The primary concern with wet fluids is that at the end of expansion, the fluid is within the vapor dome meaning liquid droplets can form posing a risk of erosion and damage to turbine blades. This problem can be countered with the use of superheating, though the process adds complexity to the cycle. A minimum dryness fraction of 85%-90% is generally considered acceptable. The primary example of a wet fluid is water, while other examples include ethanol and ammonia.

(2) Dry fluids have a saturation vapor curve with a positive slope $\left(\frac{\partial T}{\partial S} > 0\right)$. Droplet formation is not a concern for these fluids, so superheating is not needed. In fact, if the fluid is "too dry", it may still be superheated at the end of expansion. To avoid wasting this energy and increasing the cooling load, regeneration is often used with dry fluids, which increases performance but adds complexity to the system. Examples of dry fluids include n-pentane, iso-pentane, toluene and the common refrigerant R245fa.

[4] The Global Warming Potential (GWP) of a substance, refers to the amount of global warming caused by the substance compared to the warming caused by a similar mass of CO_2 [79].

(3) Isentropic fluids have a saturation vapor curve with infinite slope $\left(\frac{\partial T}{\partial S} \to \infty\right)$. These fluids remain at saturation during expansion, eliminating both the risk of condensation and the need for regeneration. This makes these the ideal working fluid. Examples of isentropic fluids include R11, R123 and benzene.

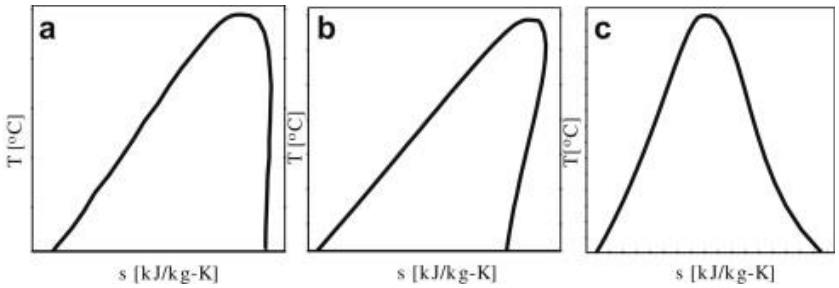

Figure 3.1: Saturation temperature entropy curves for (a) isentropic, (b) dry and (c) wet fluids [21]

Liu et al. [22] suggested an equation for estimating the inverse of the slope of the temperature-entropy curve (and therefore predicting the thermodynamic behavior of the fluid as wet, dry or isentropic):

$$\xi = \frac{\partial S}{\partial T} = \frac{c_p}{T_{ev}} - \frac{\frac{n \cdot T_{ev,red}}{1 - T_{ev,red}} + 1}{{T_{ev}}^2} \cdot \Delta h_{vap} \tag{3.1}$$

where

c_p the specific heat capacity of the fluid

T_{ev} the fluid evaporation temperature

$T_{ev,red} = T_{ev}/T_{Crit}$ the reduced evaporation temperature

T_{crit} the critical temperature of the fluid

Δh_{vap} the latent heat of evaporation of the fluid

n a constant suggested by Liu et al [22] to be 0.375 or 0.38.

Of course, $\xi < 0$ will represent a wet fluid, $\xi = 0$ an isentropic fluid and $\xi > 0$ a dry fluid. Table 3.1 shows the results of the application of Equation (3.1) for several fluids as well as their categorization based on the slope of their T-s curve as produced from experimental data. It can be seen that the equation gives a good indication of a fluid's characteristics, however is not completely accurate due to the simplifications required to develop it. For this reason, Chen et al. [9] suggest when possible to use measured thermodynamic data (i.e. the slope of the temperature-entropy curve) in order to categorize a fluid as wet, dry or isentropic.

Table 3.1: Calculated ξ Value vs. Actual Thermodynamic Data		
Examined fluid	***Calculated ξ as per Equation (3.1)***	***Fluid type from actual thermodynamic data***
Water	-13.1818	Wet
Ethanol	-5.4299	Wet
R11	-0.3903	Isentropic
R123	0.1202	Isentropic
Benzene	0.3316	Isentropic
HFE7100	1.8252	Dry
n-Pentane	1.2835	Dry
Iso-pentane	1.1801	Dry
Toluene	1.060	Dry
p-Xylene	1.539	Dry

3.2 Important properties for selecting a working fluid

It is clear from the Section 3.1 that working fluids composition and properties can vary significantly so that a crucial point in Rankine system design is selecting the correct one. The working fluid affects the efficiency and output of the system, the system size and design, its stability and safety, as well as the impact of the system on the environment [12].

The first selection in designing the system is whether a traditional steam Rankine cycle or an ORC cycle will be used.

3.2.1 Water vs. organic working fluids

Water as a working fluid has several advantages [23]: it is cost effective and readily available, it is non-toxic, non-flammable, environmentally-friendly and chemically stable and it has low viscosity, which reduces friction losses and pump work.

However, water carries with it all the disadvantages of a wet fluid, including the need for superheating and risk of blade erosion and damage. The boiler consists of three stages (preheating, evaporating and superheating) which increase the related cost and complexity of the system. Turbines for steam Rankine systems are generally complex and expensive, since the pressure ratio and enthalpy drop are high and several expansion stages are needed [12], [23]. The chief drawback of water, however, remains that it is inappropriate for heat recovery from low-temperature sources [15].

The chief advantages of organic working fluids are their lower boiling and freezing points, lower critical properties and lower condensation entropy, all of which allow for heat recovery from lower temperature sources [24]. Organic fluids also have a higher density than water, allowing for lower volumetric flows and more compact systems. Furthermore, the layout of the ORC system is simpler, since all three phases of evaporation (preheating, vaporization and superheating) can take place in one heat exchanger and there is no need for a drum to separate vapor from liquid. Dry and isentropic organic fluids eliminate the risk of condensation in the turbine, reducing erosion and increasing turbine lifetime up to 30 years (as opposed to 15-20 years for steam turbines). Furthermore, the pressure ratio and enthalpy drop are usually lower in such cycles, meaning single or two-stage turbines

can be used with much lower cost than the multi-stage steam turbines. Rotating speeds are reduced, reducing blade tip speed and the related mechanical stresses as well as allowing for direct generator drive without reduction components [23].

Organic working fluids, however, are not without their own disadvantages and difficulties. Cost of fluids, toxicity, flammability and environmental impact are among the basic difficulties to be overcome [15]. Organic fluids also tend to have higher Back Work Ratios (BWR), which means that the fraction of work produced by the turbine which is consumed in the pump is higher than for water-steam. Condensation cannot be done in a vacuum, as for water, as infiltration is an issue. Finally, as can be seen from Figure 3.2, the entropy difference between the saturated liquid curve and saturated vapor curve is much smaller for organic fluids than for water. This means that the enthalpy of vaporization is reduced. In other words, to produce the same thermal power in the evaporator, the mass flow rate of an organic fluid must be much higher than the same rate for water [25].

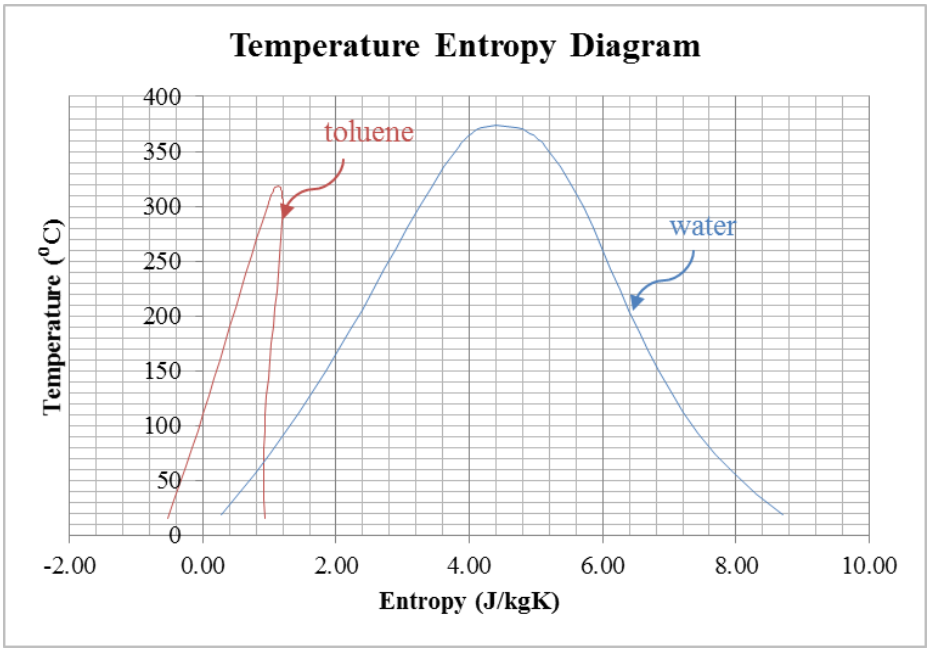

Figure 3.2: Entropy difference between liquid and vapor for water vs. organic fluids

Overall the above trade-offs mean that ORC systems are more profitable for low to medium power range cycles or low temperature heat sources while for higher power range cycles and temperature heat sources, steam cycles are preferred [23].

3.2.2 Crucial properties of organic fluids

Assuming an organic fluid is selected over water for a Rankine power production system, the selection of which organic fluid to use is then key. Many factors should be weighed when selecting between possible organic fluids. These can be classified as (1) thermodynamic factors, which affect the efficiency and net work of the system, (2) legislative or environmental factors, which quantify the environmental effect of used fluids, and (3) safety factors, which address issues of toxicity and flammability [18]. The classification of fluid characteristics into the above categories is not always unique, since

some properties affect both thermodynamic and practical aspects of the cycle design. Nevertheless, one such classification is proposed below.

3.2.2.1 *Thermodynamic factors*

Thermodynamic factors affect the total efficiency of the system: either the thermodynamic efficiency of the cycle or the efficiency of heat recovery.

(1) Latent heat of vaporization:

A high latent heat of vaporization has been shown to increase cycle efficiency [7], the theoretical maximum of which can be calculated as below for a sensible[5] heat source [26]:

$$\eta_{max} = 1 - \frac{T_L}{T_{in} - T_{out}} \ln\left(\frac{T_{in}}{T_{out}}\right) \qquad \textit{(Eq. 1)}$$

where

T_L the heat rejection absolute temperature
T_{in} the inlet temperature of the evaporator
T_{out} the outlet temperature of the evaporator.

A high latent heat means that most of the heat exchange will be at constant temperature and the inlet and outlet temperatures of the evaporator will be close, with positive effects on η_{max} [26].

However for waste heat applications, a high cycle efficiency is not the most important concern. Rather the objective is to maximize the total system efficiency, which includes heat recovery. In that case, a lower latent heat of vaporization means that the heat transfer process occurs mostly at variable temperature. This allows for better matching between the heat source and working fluid, decreasing irreversibility. For this reason, in ORC applications, the ratio of vaporization latent heat and sensible heat greatly influences thermal and exergy efficiency.

The latent heat of vaporization can be symbolized as Δh_{vap} while its units are kJ/kg.

(2) Thermal conductivity

Thermal conductivity should be high to increase heat transfer and reduce irreversibilities. Thermal conductivity can be symbolized as λ while its units are W/mK.

(3) Specific heat capacity

A high specific heat value for the working fluid means more external heat is required to change its temperature by a specific amount. Hung et al in [7] suggest that a fluid with a low specific heat value should be used to lighten the load on the condenser.

Isobaric specific heat capacity can be symbolized as c_p while its units are kJ/kgK.

[5] Sensible heat refers to heat exchange which results in a temperature change. The term is used in contrast to latent heat which is exchanged during a phase change and occurs without a change of temperature. $\dot{Q}_{Sensible} = \dot{m} c_p \Delta T$

(4) Critical temperature

As previously mentioned, the critical temperature is the maximum temperature at which a substance can exist as a liquid, symbolized as T_{crit}. Above this temperature it will be in gaseous phase and cannot be liquefied no matter how high pressure is applied.

Fluids with very low critical temperatures can be problematic for Rankine applications as they require very low condensing temperatures which are not always possible to achieve [27].

Furthermore, thermal efficiency has been shown to increase for fluids with high critical temperatures [12], [18]. For the same heat source stream, a fluid with a higher critical temperature provides better matching with the source as shown in Figure 3.3, reducing the heat transfer irreversibility and improving thermal efficiency. This assumes, of course, that the cycle employs both fluids at or near their critical point.

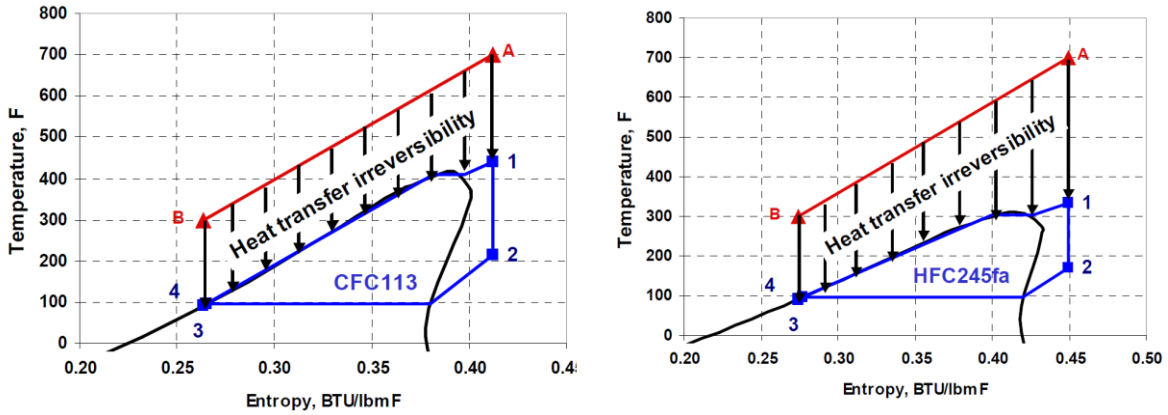

Figure 3.3: Reducing heat transfer irreversibility for a fixed source by employing a fluid with a higher critical point at or near critical condition [26]

However, using fluids with a high critical temperature in sub-critical configurations means working at specific vapor densities much lower than the critical density.

(5) Density

The working fluid density has an immediate effect on the system size with higher densities leading to smaller and cheaper systems. This is because low density means the size of the turbine must be increased as the volumetric flow will be increased for the same mass flow.

Furthermore, as the volumetric flow is increased for the same pipe diameter, fluid velocities are increased resulting in higher pressure losses. To combat this effect, the hydraulic diameter of pipes and heat exchangers must be enlarged as well [25].

In addition, two parameters directly related to density, the size parameter and isentropic volume flow ratio, are crucial for determining the isentropic efficiency of the turbine. In fact, neglecting the influence of the Reynolds number, the isentropic efficiency can be determined as a function of these two parameters alone [12].

The size parameter is a direct indicator if the magnitude of the turbine can be calculated as [12], [5]:

$$SP = \frac{\sqrt{\dot{V}_{T,out}}}{\sqrt[4]{\Delta h_{T,is}}} = \frac{\sqrt{\dot{m}_{T,out}/\rho_{T,out}}}{\sqrt[4]{\Delta h_{T,is}}} \tag{3.2}$$

where the subscript T indicates that the symbols refer to the turbine

$\dot{V}_{T,out}$ represents the volume flow at the outlet of the turbine

$\Delta h_{T,is}$ the isentropic enthalpy drop in the turbine.

The second important parameter derived from density, the isentropic volume ratio, can be defined as [12], [5]:

$$VFR = \frac{\dot{V}_{T,out}}{\dot{V}_{T,in}} = \frac{\rho_{T,in}}{\rho_{T,out}} \tag{3.3}$$

Lower values of VFR mean smaller, simpler turbines but also higher turbine efficiency with certain researchers maintaining that the value should be less than 50 for a turbine efficiency above 80% [12], [5].

While not related to the isentropic efficiency of the turbine, the rotational speed parameter defined in [5] is also related to density and can be quite important, as very high turbine speeds are achieved with more expensive turbines. The rotational speed parameter can be defined as:

$$RSP = \frac{\Delta h_{T,is}^{0.75}}{10\sqrt{\dot{V}_{T,out}}} = \frac{\Delta h_{T,is}^{0.75}}{10\sqrt{\dot{m}_{T,out}/\dot{\rho}_{T,out}}} \tag{3.4}$$

(6) Molecular weight

The efficiency of a turbine is strongly correlated to its aerodynamic performance. When flow in the turbine reaches the speed of sound (Mach number 1), shock effects reduce turbine performance. In fluids with low molecular weight, like water, the speed of sound is low, so shock effects occur at lower turbine speeds. As a result, turbines for heavy fluids like organic compounds (with high molecular weight) have a higher overall efficiency.

(7) Freezing point

The freezing point of the used fluid must be lower than the minimum cycle temperature to ensure that the fluid will remain in liquid state [28]. Vlaskos et al. [18] recommend a freezing point above -50°C.

(8) Atmospheric boiling temperature

The boiling temperature of the fluid in atmospheric conditions should be high enough to avoid evaporation at high ambient temperatures, especially if the cycle condensing pressure is near atmospheric. Vlaskos et al. [18] recommend at least 50°C.

(9) Viscosity

The viscosity should be kept low to reduce friction and pressure losses.

(10) Chemical stability

Chemical stability should be high especially at the temperature ranges of the cycle. As certain organic compounds can be degraded if they are topically overheated, thermal oil cycles can be used to transfer heat from the source to the working fluid [27].

3.2.2.2 ***Legislative or environmental factors***

Legislative factors deal with the environmental impact of a potential working fluid.

(11) Global Warming Potential

As has been mentioned, the Global Warming Potential (GWP) of a substance refers to the amount of global warming caused by the substance compared to the warming caused by a similar mass of carbon dioxide. It is calculated as the ratio of the time integrated radiative forcing[6] due to a pulse emission of 1 kg of a substance compared to the same measure for a reference gas, generally carbon dioxide [29]:

$$GWP_x = \frac{\int_0^\tau RF_x(t)dt}{\int_0^\tau RF_{CO_2}(t)dt} \tag{3.5}$$

where τ is the time horizon of the calculation, normally 20, 50 or 100 years. The choice of time horizon is subjective, but 100 years is often used following the precedent set by the Kyoto Protocol in 1997 [30]. RF_x is the radiative forcing due to a pulse emission of a gas X and can be calculated as [29]:

$$RF_x(t) = Ab_x R_x(t) \tag{3.6}$$

where

- R_x the radiative efficiency of a substance x or the radiative forcing per unit mass increase in atmospheric abundance of the substance x
- Ab_x the the fraction of the substance remaining in the atmosphere after a pulse emission.

The GWP of various compounds are regularly calculated by the Intergovernmental Panel on Climate Change [31]. Compounds with a high GWP are called greenhouse gasses,

[6] A basic concept of global warming is the process of radiative forcing. Energy from sunlight which reaches the atmosphere is either absorbed or reflected. At the same time, the earth and atmosphere, as a warm body in cold space, is constantly radiating energy in the form of infrared radiation. In equilibrium, this lost energy to space should be equal to the absorbed energy from the sun. Substances with a high global warming potential, when released to the atmosphere, change its composition so that more energy is absorbed from the sun than is lost to space, resulting in the heating of the atmosphere known as global warming. Radiative forcing is a measure of the excess energy flow to the atmosphere with units of W/m^2 [34].

because of their contribution to the greenhouse effect. The most common greenhouse gases are shown in Table 3.2 [32].

Table 3.2: Common Greenhouse Gases

Compound	***Symbol***	***Description***	***GWP***
Carbon Dioxide	CO_2	The greenhouse gas used as a reference for the GWP of other gases	1
Methane	CH_4	A common by-product of the production and transport of hydrocarbons	28-36
Nitrous oxide	N_2O	Emitted from agricultural and industrial activities	298
Fluorinated gases	Hydrofluorocarbons (HFCs), perfluorocarbons (PFCs), nitrogen trifluoride (NF3), and sulfur hexafluoride (SF6)	Synthetic gases with often high GWP	HFCs: 12-14,800 PFCs: 7,390-12,200 NF3: 17,200 SF6: 22,800

Due to their high GWP, fluorinated gases are regulated in Europe, most recently by the EU Regulation 517 (2014) which establishes rules for containment, use, recovery and destruction of fluorinated gases or products and equipment which contain them, as well as sets quantitative limits for the use of hydrofluorocarbons which will be gradually reduced by 79% over the next fifteen years [33], [34].

(12) Ozone Depletion Potential

Also mentioned above, the Ozone Depletion Potential of a substance is the ratio of its impact on the ozone compared to a similar mass of CFC-11. It can be calculated as [17]:

$$ODP_x = \frac{\sum_z \sum_\theta \sum_t \Delta O_3(z,\theta,ALT)_x \cdot cos\theta}{\sum_z \sum_\theta \sum_t \Delta O_3(z,\theta,ALT)_{CFC-11} \cdot cos\theta} \tag{3.7}$$

where

- z altitude
- θ latitude
- ALT the atmospheric lifetime of a substance
- ΔO_3 the change in the ozone at steady state per unit mass emission rate of the substance.

Substances with ODPs around or above 1 have already been banned (like CFCs), while others with ODPs even as low as 0.01 (HCFCs) are in the process being phased out.

The first major regulation of ozone-depleting substances was achieved by the Montreal Protocol of 1987 [35]. However since then, newer and stricter regulations have been enforced.

Specifically for the maritime community, the International Convention for the Prevention of Pollution from Ships, MARPOL 73/78, Annex VI, Regulation 12 prohibits installations which contain ozone-depleting substances other than HCFCs on ships constructed after 19 May 2005 and installations which contain HCFCs on ships constructed after 1 January 2020 [19]. While the regulation does not apply to permanently sealed equipment with no refrigerant charging connections (such as domestic refrigerators, water coolers and self-contained air-conditioners), it does apply to refrigeration equipment such as compressors, condensers and evaporators in larger systems.

For ships with a European flag, EU Regulation 1005 (2009) is even more restrictive, banning the production of controlled ozone depleting substances or the production of systems which use them since 2010 [36]. The banned substances fall under several groups listed in Table 3.3.

Table 3.3: Substances banned under EU Regulation 1005 (2009)

Group	***Substance***		***ODP***
Group I	$C_xF_xCl_x$	CFC-11, 12, 113, 114, 115	0.6-1
Group II	$C_xF_xCl_x$	CFC-13, 111, 112, 211, 212, 213, 21, 215, 216, 217	1
Group III	$C_xF_xBr_xCl_x$	Halons	3-10
Group IV	CCl_4	CTC	1.1
Group V	$C_2H_3Cl_3$	1,1,1-TCA	0.1
Group VI	CH_3Br	Methyl bromide	0.6
Group VII	$C_xH_xF_xBr_x$	HBFCs	0.7-7.5
Group VIII	$C_xH_xF_xCl_x$	HCFCs	0.01-0.52
Group IX	CH_2BrCl	BCM	0.12

The currently available refrigerants that have zero ODP and a GWP_{100} value below 1950 are listed in Table 3.4. Refrigerants considered by MARPOL to be “mainline” and suitable for use in marine applications are marked with an asterix. The list is not exhaustive, and other substances which meet appropriate ODP and GWP limits can also be used [37].

3.2.2.3 *Safety factors*

Safety factors are characteristics of a potential working fluid which directly affect its safe use.

(13) Toxicity

For obvious reasons, any working fluid should have low toxicity [7].

(14) Flammability

Flammability should also be kept to a minimum.

Table 3.4: Refrigerants suitable for 'R' character associated with Environmental Protection Notation				
Regrigerant No.	***Name***	***Formula***	***ODP***	***GWP_{100}***
R134a *	1,1,1,2-Tetrafluoroethane	CF_3CH_2F	0	1300
R718	Water	H_2O	0	0
R744	Carbon dioxide	CO_2	0	1
R407A *	Blend of R32/125/134a	CH_2F_2 CF_3CHF_2 CF_3CHF_2F	0	1770
R407C *	Blend of R32/125/134a	CH_2F_2 CF_3CHF_2 CF_3CHF_2F	0	1526
R410A *	Blend of R32/125	CH_2F_2 CF_3CHF_2	0	1725
R32	Difluoromethane	CH_2F_2	0	580
R50	Methane	CH_4	0	24.5
R152a	1,1-Difluoroethane	CHF_2CH_3	0	140
R30	Methylene chloride	CH_2Cl_2	0	15
R717*	Ammonia	NH_3	0	0
R170	Ethane	CH_3CH_3	0	3
R290 *	Propane	$CH_3CH_2CH_3$	0	3
R600 *	Butane	C_4H_{10}	0	3
R600a *	Isobutane	$CH(CH_3)_3$	0	3

These two qualities are summarized by the safety designation of the fluid according the American Society for Refrigeration Engineers, as shown in Table 3.5. Class A refrigerants do not display evidence toxicity at concentrations less than or equal to 400 ppm while Class B refrigerants do. Class 1 refrigerants do not show flame propagation at atmospheric conditions, while Class 2 refrigerants do, having a lower flammability limit of more than 0.1 kg/m3 at atmospheric conditions and a heat of combustion less than 19 kJ/kg. Finally, Class 3 refrigerants are highly flammable with a lower flammability limit less than or equal to 0.1 kg/m3 at atmospheric conditions and a heat of combustion greater than or equal to 19 kJ/kg [38]

Table 3.5: ASHRAE Safety Designation of Refrigerants [39]		
	Lower toxicity	***Higher toxicity***
Higher flammability	A3	B3
Lower flammability	A2	B2
	A2L*	B2L*
No flame propagation	A1	B1
**The designation L indicates lower flammability refrigerants with a maximum burning velocity of ≤ 10 cm/s*		

3.2.3 Fluid selection strategies

Generally, no single fluid can be deemed the optimal fluid, because the number of available fluids is very large and only subsets of these have been tested. Furthermore, the possible fields for ORC applications are so many that the desirable traits of fluids as well as the criteria on which they are judged can vary widely [12].

In most academic ORC studies, researchers choose working fluids from an available data set, based on the required characteristics detailed above. Papadopoulos et al. [28] are notable in this respect as they use computer aided molecular design (CAMD) in conjunction with process optimization methods to theoretically synthesize mixtures which could be used as working fluids and which meet the set criteria.

However, as this study seeks to find solutions for an ORC system that could be easily and readily installed on the studied ship, the fluid selection will be based on an initial list of candidates which meet the above thermodynamic, legislative and safety criteria and are readily available for use. Finally, fluids will be selected based on their recommended status by MARPOL or based on their use in other similar ORC studies. An initial pool of fluids can be seen in Table 3.6.

Table 3.6: Organic and other fluids proposed for ORC in Relevant Literature					
Name	***ODP***	***GWP***	***Safety***	***Molar Mass***	***Critical temp.***
				(kg/kmol)	***(°C)***
R50	0	21	A3	16.04	-82.59
R744	0	1	B1	44.01	30.98
R170	0	6	A3	30.07	32.17
R41	0	97	A1	34.03	44.13
R125	-	-	A1	120.02	66.02
R410a	-	-	A1	86.02	69.27
R218	0	8600	A1	188.02	71.87
R143a	0	4300		84.04	72.71
R32	-	-	A2	52.02	78.11
R421a	-	-	-	112.47	81.36
R407a	-	-	A1	99.23	82.39
R407c	-	-	A1	99.19	83.53
R417a	0	2346	-	108.92	85.26
R407d	-	-	A1	97.23	92.60
R413a	-	-	A2	108.45	94.57
R32-30%/R134a-70%	-	-	-	87.03	95.00
R290	0	3.3	A3	44.10	96.74
R134a	0	1430	A1	102.03	101.06
R227ea	0	3220	-	170.03	101.75
R152a	0	124	A2	66.05	113.26
RC318	0	10300	-	200.04	115.23
R124	0.022	620	A1	136.48	122.28
R236fa	0	9810	A1	152.04	124.92
R717	0	0	B2	17.03	132.25
R600a	0	3	A3	58.12	134.66
R236ea	0	1370	-	152.04	139.29
R245fa-65%/R152a-55%	-	-	-	110.25	139.75
R114	1	9800	A1	170.92	145.68
R245fa-45%/R152a-10%	-	-	-	121.68	146.60
R245fa-90%/R152a-10%	-	-	-	127.25	149.94
R600 (butane)	0	3.3	A3	58.12	151.98
R245fa	0	794	A1	134.05	154.01
R245fa-50%/Isopentane-50%	-	-	-	103.10	170.61
R245fa-50%/R365mfc-50%	-	-	-	141.70	171.92
R245ca	0	693	Slightly flammable	134.05	174.42
R245fa-50% / Pentane-50%	-	-	-	103.10	175.28
R245ca-50%/R365mfc-50%	-	-	-	141.06	180.64
R123	0.02	120	B1		183.68
R601a (isopentane)	0	11	A3	72.15	187.20
R601 (pentane)	0	10	Moderate toxicity, Flammable	72.15	196.55
R11	1	4600	A1		197.96
R141b	0.11	700	A1	116.95	204.35
R113	0.8	6000	A1	187.38	214.06
Benzene	0		Flammable carginogenic	78.11	288.90
Toluene	0	2.7	Moderate health hazard, Flammable	92.14	318.60
R718 (Water)	0	0	A1	18.02	373.95

Table 3.7: Organic and other fluids proposed for ORC in Relevant Literature Continued						
Name	***Critical density***	***Latent heat***	***Thermal Conduct.***	***Heat Capacity***	***Atm. BP***	***Viscosity***
	(kg/m^3)	***(kJ/kg)***	***(W/m.K)x 100***	***(kJ/kgK)***	***(°C)***	***(µPa/s)***
R50	162.66		33.93	2.23	-161.64	11.07
R744	467.60	119.64	16.64	0.85	-78.62	14.93
R170	206.18	167.94	20.98	1.76	-88.82	9.35
R41	316.51	235.50	17.16	1.12	-78.55	10.96
R125	573.58	110.39	14.02	0.80	-48.36	12.96
R410a	500.57		13.46	0.81	-51.07	13.35
R218	627.98	76.01	12.54	0.80	-37.08	12.49
R143a	431.00	159.35	14.87	0.95	-47.52	11.09
R32	424.00	270.91	12.52	0.85	-51.91	12.61
R421a	552.82		13.76	0.82	-41.72	12.50
R407a	520.36		13.74	0.82	-43.63	12.51
R407c	519.40		13.74	0.83	-42.97	12.46
R417a	533.41		13.79	0.84	-40.05	12.30
R407d	506.91		13.65	0.84	-37.00	12.06
R413a	530.54		13.48	0.86	-35.42	12.03
R32-30%/R134a-70%	475.41		13.68	0.85	-37.82	11.81
R290	220.48	335.74	18.31	1.68	-42.41	8.15
R134a	511.90	177.79	13.39	0.85	-26.36	11.82
R227ea	594.25	111.60	13.34	0.81	-16.65	11.59
R152a	368.00	279.36	14.16	1.05	-24.32	10.08
RC318	620.00	104.23	12.18	0.79	-6.29	11.50
R124	560.00	146.56	11.85	0.74	-12.28	11.59
R236fa	551.29	145.92	12.63	0.84	-1.75	10.96
R717	225.00	1165.76	24.93	2.16	-33.59	10.09
R600a	225.50	328.92	16.89	1.69	-12.08	7.50
R236ea	563.00	155.61	14.44	0.87	5.87	10.90
R245fa-65%/R152a-55%	475.93		13.50	0.94	-8.28	10.57
R114	579.97	128.07	10.21	0.70	3.25	10.81
R245fa-45%/R152a-10%	496.37		13.24	0.92	-0.23	10.50
R245fa-90%/R152a-10%	505.53		13.11	0.92	5.39	10.46
R600	228.00	361.48	16.56	1.73	-0.84	7.41
R245fa	516.08	190.32	12.91	0.92	14.81	10.30
R245fa-50%/Isopentane-50%	364.65		14.05	1.19	13.03	9.40
R245fa-50%/R365mfc-50%	491.13				23.02	
R245ca	523.59	201.03	13.29	0.93	24.79	10.12
R245fa-50%/Pentane-50%	361.29		13.64	1.21	17.31	9.24
R245ca-50%/R365mfc-50%	496.24		85.72	1.36	29.12	446.01
R123	550.00	171.37	76.42	1.02	27.46	417.60
R601a	236.00	345.45	107.35	2.27	27.45	216.43
R601	232.00	366.29	111.40	2.32	35.68	217.90
R11	554.00	180.88	8.45	0.61	23.34	10.16
R141b	458.56	226.07	90.64	1.15	31.67	408.35
R113	560.00	151.34	68.27	0.92	47.19	653.61
Benzene	309.00	432.94		1.70	79.66	
Toluene	291.99	412.85		1.70	110.13	
R718 (Water)	322.00	2441.68	607.19	4.18	99.61	890.08

4 Applications of Organic Rankine Cycles

The first studies on ORC applications appeared in the 1960s, however it was not until much later that their potential for low-grade waste heat recovery was further examined and applied. The number and size of such applications in the industry has markedly increased in the last 30 years, as can be seen in Figure 4.1 [40].

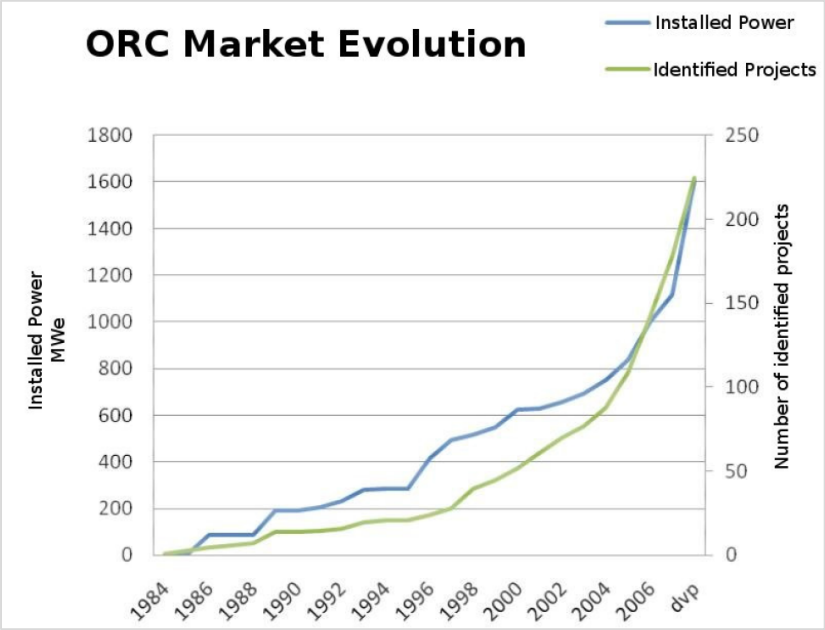

Figure 4.1: ORC applications on the market [40]

4.1 Land-based ORC Applications

Typical applications of ORC technology on land include geothermal and solar energy conversion, biomass applications and waste heat recovery.

Geothermal energy conversion uses subterranean heat to produce electric power. Several configurations can be employed including binary plants in which the thermal energy of the geothermal source is transferred to a secondary working fluid for use in a Rankine cycle. The first such application was developed in Russia in 1967, while by 2010, binary power plants were the most common type of geothermal power solution with 162 units worldwide generating 373 MW of power [41]. Geothermal energy can provide heat for ORC applications at a range of temperatures from as low as 100^0C to above 200^0C. High temperature sources allow for combined heat and power generation (CHP) meaning that the cooling water for the power-producing ORC cycle can be used for space heating [40].

While utilizing *solar power* through concentrating collectors such as parabolic troughs is a well-known technology, the combination of this technology with ORC systems is still relatively rare with few such plants available on the market [40]. Nevertheless, the system has proven to be both technically and economically feasible by nine parabolic trough plants in California developed between 1984 and 1990. Since then, research has intensified and a larger number of applications have been examined with much focus being given to small-scale ORC systems which could be applied in off-grid areas and developing

countries [41]. An important characteristic of concentrated solar applications is the trade-off that must be made between the efficiency of the collector and the thermal efficiency of the Rankine cycle. While high collector temperatures increase ORC efficiency, they lead to higher ambient heat losses and therefore lower efficiency in the collectors themselves [40].

Biomass energy ORC systems use the heat produced from the burning of organic compounds like wood or agricultural waste to produce useful energy [40]. Biomass is the fourth largest energy source in the world contributing to nearly 10% of global energy demand, a percentage much higher in developing nations. As with geothermal applications, biomass systems can be used for combined heat and power generation with high temperature exhaust from the combustion of biomass serving as the ORC hot stream via an intermediate thermal oil while the cooling water serving as the ORC cold stream is further utilized for space heating. More than one hundred biomass-ORC plants have been installed worldwide with most applications being in Europe [41].

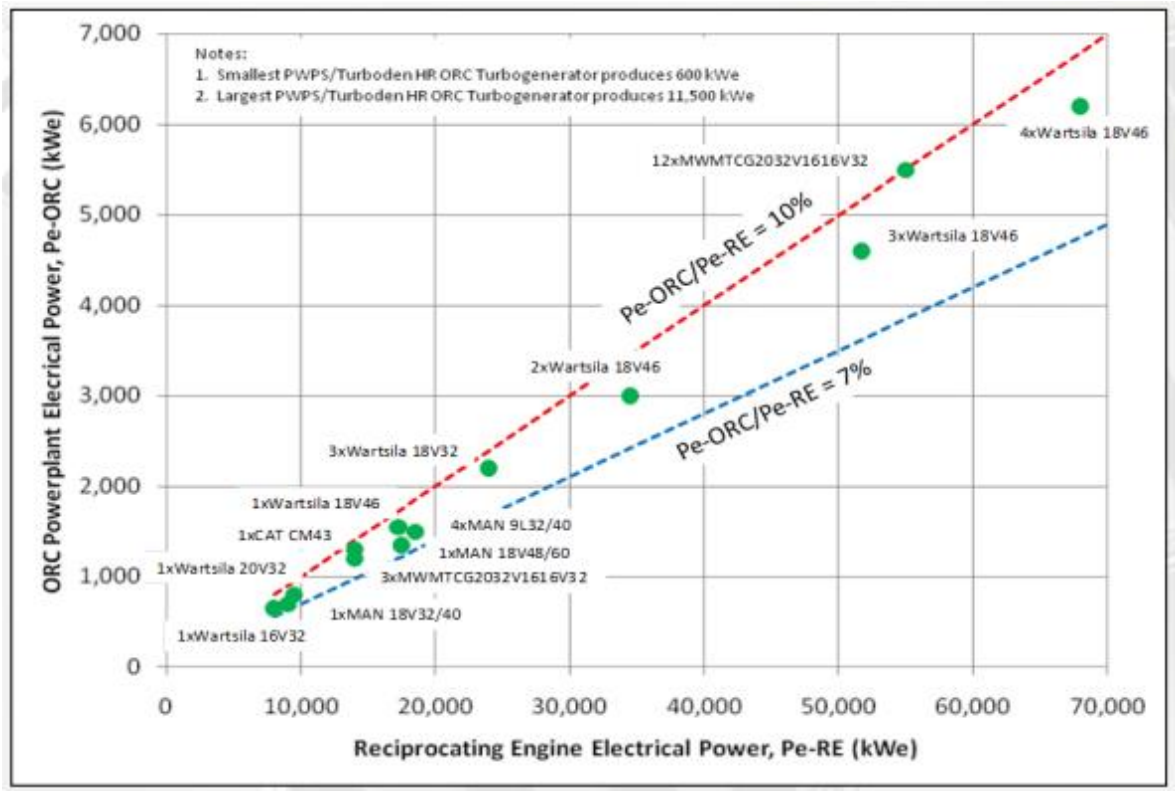

Figure 4.2: ORC with existing internal combustion engines [20]

Finally, a promising application of ORC technology which is examined further in this study is in *waste heat recovery* through which the excess heat rejected by fuel combustion or other chemical reactions is converted to useful energy through a thermodynamic cycle. Such applications show huge potential considering that, in many industrial applications, up to 70% of input energy is rejected to the environment as heat. Among waste heat recovery applications, recovery from internal combustion engines is a prime area for ORC applications since rejected heat is generally at low temperatures [41]. This type of system was first examined in the wake of the energy crisis of the 1970s when Mack Trucks installed a prototype ORC system which recovered heat from the exhaust of the 288 HP Diesel engine resulting in a 12.5% decrease in fuel consumption [6]. A few

decades later, such installations are becoming more common. The coupling of such systems with existing engines ranging from 10 to 70 MW can be seen in Figure 4.2. The produced electric power in the coupled ORC system can reach 6 MWe with the recovered power ranging from 7-10% of the reciprocating engine power [20].

A qualitative comparison of the above applications can be seen in Table 4.1.

Table 4.1: Qualitative comparison of land-based ORC applications [41]

Applications	***Technological maturity***	***Greenhouse gas emissions***	***Complexity, Operation and Maintenance***
Geothermal	Mature	Very low	Simple plants
Solar	Under development	None	Plants with complex operation and maintenance
Biomass	Mature	Yes	Suitable for distributed generation
Waste heat recovery	Very promising	None	Economics depend on the heat availability of the application

4.2 Marine ORC Applications

In marine technology, organic Rankine cycles can be employed for waste heat recovery (WHR) from propulsion engines. In addition to the thermodynamic advantages provided by all ORC systems, existing ORC technologies provide certain operational advantages which make them good candidates for use onboard ships. These include [20], [42]:

(1) High turbine efficiencies but low turbine speeds meaning low mechanical stresses and the possibility of direct drive of electrical generators
(2) Turbines are protected from erosion by the use of dry fluids
(3) Low operating temperatures
(4) Automated plants with continuous operation and simple start up procedures
(5) Minimal operator intervention required with simple maintenance procedures (for certain systems around 3 hours per week)
(6) Long life cycle (up to 20 years)
(7) Systems are usually installed on existing installations while the original installation is left in place resulting in failsafe operation.

Despite the advantages, the application of ORC-WHR systems on ships has gained ground only in the past couple of years with an increasing number of academic studies on the subject since 2013.

Yue et al. [43] examined a subcritical marine ORC system using the dry fluid isopentane as a working fluid and recovering heat from the engine exhaust and cooling water streams. Both first and second law efficiencies were calculated as well as the total fuel savings per year. Turbine design was also attempted using computer-aided design.

Burel et al. [24] researched the application of heat recovery on an LNG fueled handysize tanker operating largely in ECA areas. The study showed that an annual reduction of 5% in fuel consumption was noted by using an ORC-WHR system even when compared to a system already using heat recovery in a conventional exhaust gas boiler.

Larsen et al. [44] used genetic algorithms to find the optimum parameters for ORC systems in marine applications with waste heat at levels from 180 to 360°C. The design parameters in the studied systems included the working fluid, boiler pressure (sub or supercritical) and cycle parameters such as preheating, superheating and recuperation. A total of 109 dry, isentropic and wet organic fluids were examined. The optimization criteria included thermodynamic performance, the hazard levels of the fluids and system pressures, external constraints (such as minimum exhaust outlet temperature for sulphuric acid condensation or liquid in the expander) as well as environmental parameters. The researchers found that for systems with recuperation, dry type fluids (hydrocarbons) were most efficient. On the contrary, for non-recuperated processes, wet and isentropic fluids had better performance. When recuperation was used, for high temperature cases, high pressures (supercritical) were generally more effective. For lower temperature cases, lower pressures (subcritical) were optimal. On the contrary, for ORC systems without recuperation, optimum pressures were subcritical even for heat sources up to 360°C.

Kalikatzarakis [6] focused more specifically on the design of a marine ORC system, examining various parameters including fluid selection and cycle design. The goal of the study was to select the best system based on a multi-criteria selection including thermodynamic, economic and environmental factors. The study revealed that among a simple Rankine cycle, a recuperated cycle and a combined cycle with a high and low-temperature loop, the recuperated cycle using R245fa 50% / R-355mfc 50% was the best thermodynamically. However, when taking into account economic criteria (such as the cost of the cycle parts as well as the net present value and payback period of the system throughout its lifetime), the two-cycle system with R-245fa and R413a was superior. The study highlighted the important role of the ship operational profile on ORC system design and optimization. For example, in ships employing slow-steaming, an increasingly common fuel-saving technique, recovery of certain waste heat streams from the engine was not economically practical.

Similarly, Mancini's work [27] examined a subcritical ORC installation on a tanker vessel initially using pinch point analysis to analyze the maximum benefit of a proposed ORC system. Finally, six different heat exchanger networks were proposed employing various combinations of waste heat sources (such a lubricant oil, air coolers and jacket water) and various heat sinks (such as sea water and fresh water from the main water cooler). An optimization was carried out with the objective function being work output.

Finally, Soffiato in [17] examined the potential for an ORC system on an LNG carrier. Three possible layouts were proposed, one as an addition to the existing system and two which would require a redesign of the system allowing direct heat transfer from hot streams to the ORC working fluid. After the Heatstep method was used to examine the possible thermal coupling with a simple, regenerative and two-stage ORC cycle, the heat exchanger network for each system was proposed in greater detail. Finally, an economic analysis of the possible energy savings by using the optimal ORC systems was included.

The economic analysis did not consider the effect of the natural boil-off speed on the net present value of a waste heat recovery system which is an important point that will be analyzed later in this work.

The use of ORC systems for marine applications is not limited to academic research, but is being actively pursued in the maritime industry. Certain marine ORC systems have already been installed, while others are designed and available, though not yet tried on ships.

The first ORC system installation resulted from the collaboration of Swedish company Opcon marine with Ro-Ro shipper Wallenius Marine with the support of the Swedish Energy Agency in 2011. Installed on M/V Figaro, a 75,000 GT large car truck carrier, the system made use of cooling water from the vessel's 19 MW Diesel engine to produce up to 500 kW of electric energy [2], [1]. Along with a wet steam turbine installed on the vessel which was designed to withstand humidity in the expansion process eliminating the need for superheating, the company claimed energy savings could be around 4-6%, while, depending on the studied vessel and operational profile, other installations could reach savings of 10% [2]. Opcon's installations are applicable for vessels with installed power of more than 5 MW. An example Sankey diagram for a vessel with 15 MW engines is shown in Figure 4.3. According to the manufacturer, by using an Opcon Marine Wet Steam Turbine (OPB-WST) system to recover flue gas heat, an additional 2-4% of the consumed fuel energy can be utilized to produce electric power. Additionally, using an Opcon Powerbox ORC (OPB-ORC) system, an additional 3-6% of the consumed fuel energy can be utilized to produce electric power [45].

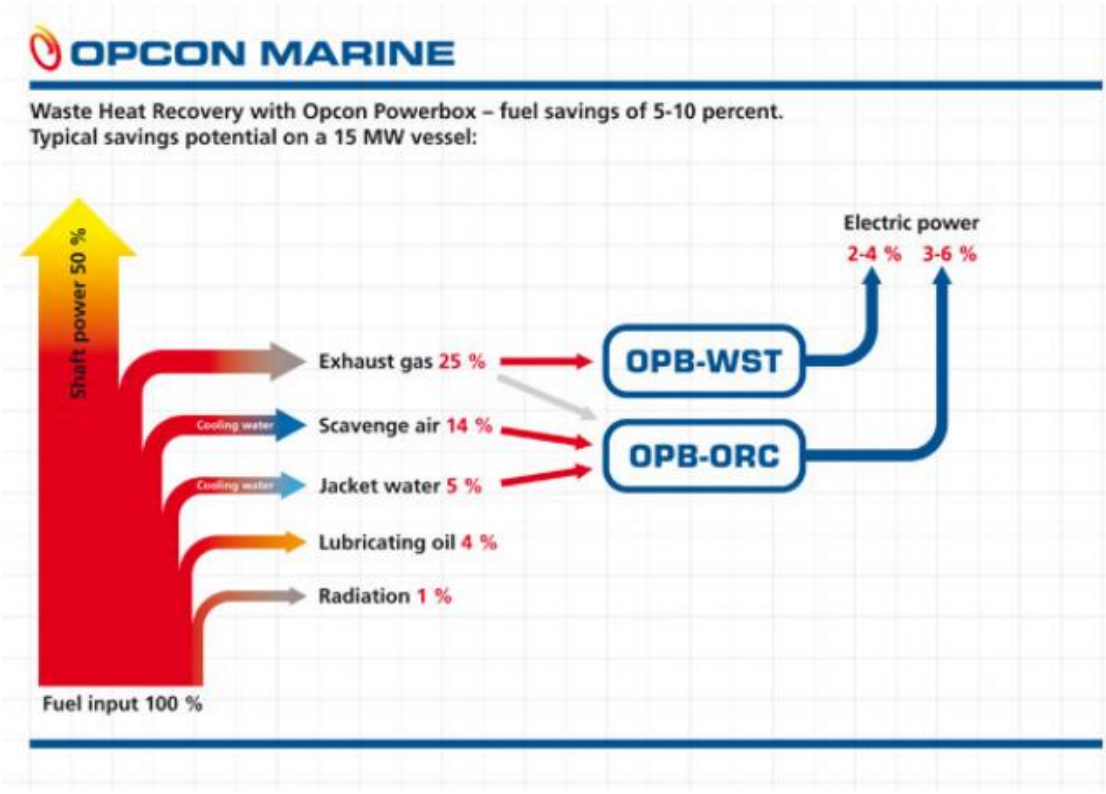

Figure 4.3: Potential savings from Opcon Marine's heat recovery system [45]

Though they have not yet installed ORC systems on merchant vessels, many other companies with experience in waste heat recovery have designed systems for marine applications. Enertime, a France based company which specializes in ORC systems for various conventional applications like geothermal energy, biomass plants and power plants, has developed an ORC system for marine Diesel engines. Their systems are designed to recover heat both from the engine exhaust gasses as well as from the high temperature cooling water cycle using HFC-245fa. They can produce between 500 kW to 1 MW of electrical power. The company claims that their system can reduce fuel consumption by up to 10% [46]. Enertime carried out a feasibility study for the application of such a system on a passenger ferry with four dual-fuel engines in an electric propulsion scheme with a total power of 40 MW. The ORC system selected could produce 700 kW of electric power, had dimensions of 7.5×2.5×4 m and a total weight of 25 tons. Despite the studied vessel's limited sailing time of only 4000 h/year, the payback period was found to be less than 6 years [46].

An Italian ORC technology company, Turboden, has also designed ORC systems for engine heat recovery that can produce between 500 kW to 10 MW of electric energy from exhaust gas and jacket water heat sources. While the company experience is rooted in land-based ORC systems and they have applied or are constructing eleven such systems since 2010, Turboden has also collaborated with marine engine maker Wärtsilä to produce the Wärsilä Marine Engine Combined Cycle (ECC), an ORC system specifically designed for marine applications. Again, the potential savings are said to be up to 10% [20], [46].

5 Analysis of the Existing Marine Propulsion System

The present study will examine the potential of installing an ORC system onboard an LNG carrier. In the following sections, the design of this carrier is detailed and examined.

5.1 Power production system and Main Generator Engines

The studied vessel has a Diesel Electric power production system. Four triple-fuel main generator engines (MGEs) with incorporated alternators produce electric power. The majority of this electricity serves the needs of propulsion while the remainder is used to cover the ship's electrical power needs (cargo switchboard, bow thruster, accommodation power, etc.). Power for propulsion passes through the main switchboard, a voltage transformer, a frequency converter and finally reaches two electric propulsion motors that re-convert it to mechanical energy. Finally, the two propulsion motors rotate a single axis and propeller through the reduction gearbox. The assumed efficiencies of the aforementioned major components are given in Table 5.1 [47].

Table 5.1: Propulsion system efficiency

Component	***Symbol***	***Efficiency***
Switchboard	η_{SB}	0.999
Transformer	η_{TF}	0.985
Frequency converter	η_{FC}	0.986
Electric propulsion motor	η_{EPM}	0.980
Gearbox	η_{GB}	0.980

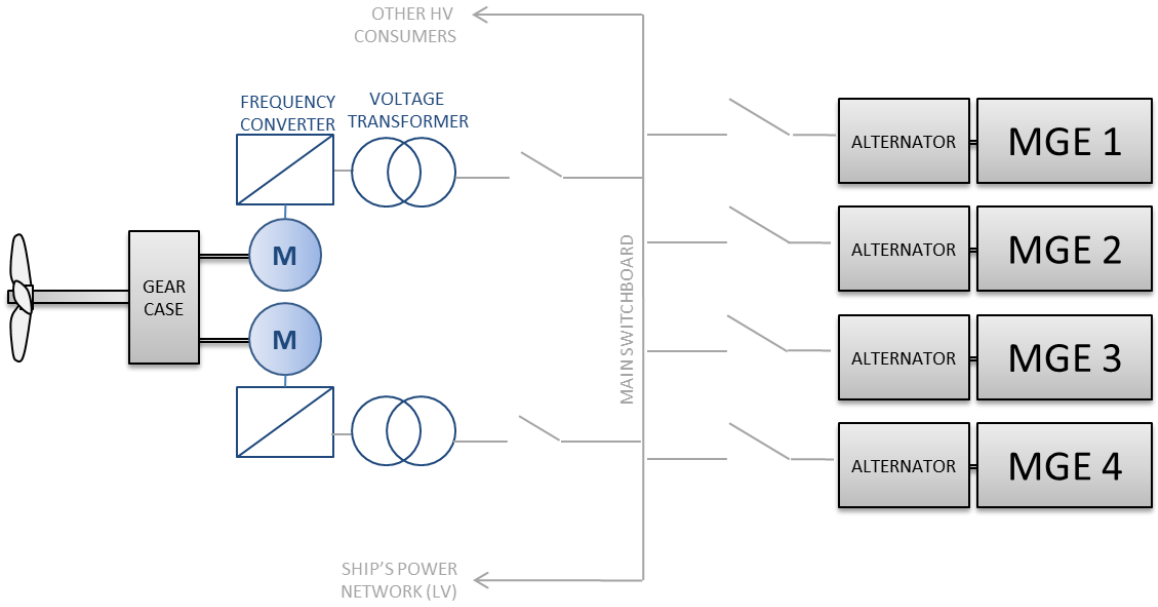

Figure 5.1: Propulsion system overview

The specifications of the main propulsion components on the studied vessel are given in Table 5.2, Table 5.3 and Table 5.4.

Table 5.2: Main Generator Engines and coupled Alternators		
Number	4	-
Mechanical output	8775	kW
Engine shaft speed	514	RPM
Electrical output	9389	kVA
Electrical voltage	6600	V (AC)
Electrical frequency	60	Hz

Table 5.3: Electric Propulsion Motors		
Number	2	-
Mechanical output	13260	kW
Shaft speed	651-720	RPM

Table 5.4: Reduction Gearbox		
Propulsion motor speed	651-720	RPM
Propeller Speed	80.92-89.5	RPM
Reduction Ratio	8.05:1	-

The main engines are 4-stroke, non-reversible, turbocharged and intercooled with direct fuel injection. They are capable of burning three types of fuel: natural gas, heavy fuel oil and marine Diesel oil (as well as low-sulfur marine gas oil).

5.2 Fuel consumption modes

As mentioned in the previous section, the main engines can meet the power demands of the ship by burning natural gas or liquid fuel (including heavy fuel oil, marine Diesel oil and marine gas oil which serves as pilot fuel). The process for fuel burning in each of these modes is analyzed in the following sections.

5.2.1 Liquid fuel burning mode

Liquid fuel burning on an LNG vessel with a triple-fuel engine is similar to fuel burning on most other liquid-fuel powered ships. Heavy fuel oil (HFO) is stored in various bunker tanks. The HFO is sent via the FO transfer pumps to the settling tanks in order for suspended water and solids to be removed and the fuel thermally stabilized. The HFO is then centrifuged and transferred to the service tanks.

The main feeder pumps then force the fuel through the FO filter before the booster pumps send it to be heated. The heating medium in the FO heaters is service steam, the supply of which is modulated so as to provide fuel at up to 150°C at the engine. Once heated, the fuel passes through the viscosity controller, which ensures it has the correct viscosity for burning. Finally, it passes through one last filter before being fed to the engine cylinders by the high pressure fuel injection pumps.

If the fuel used is Diesel Oil then the pre-heating of the fuel is omitted.

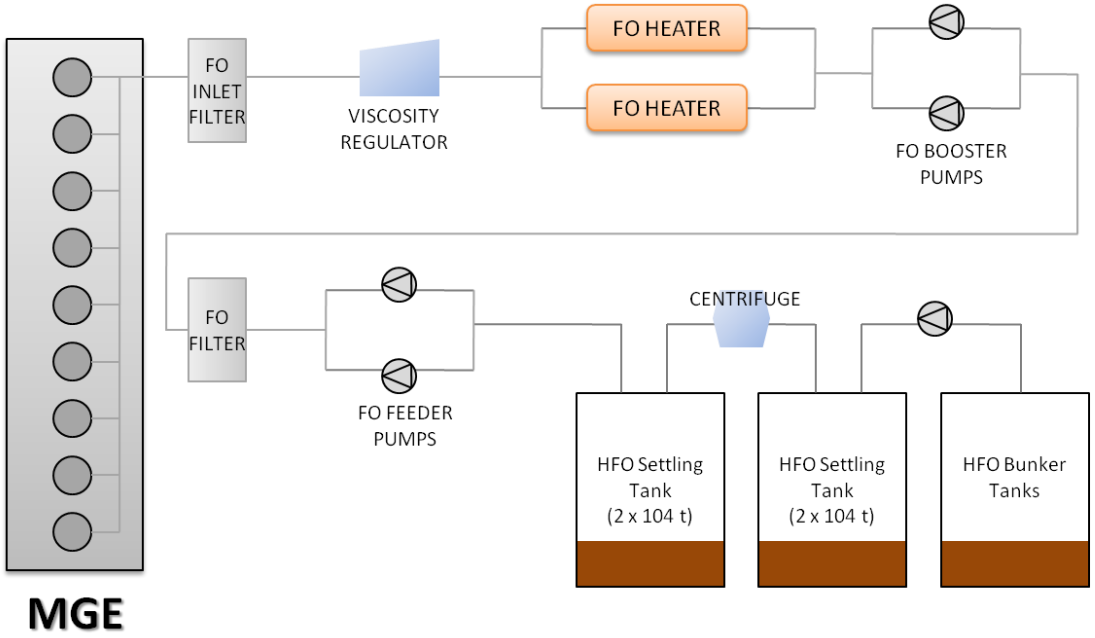

Figure 5.2: Fuel oil feed system

5.2.2 Gas burning mode: Natural and forced boil-off gas

LNG carriers are unique in that the ship's cargo, natural gas, can also be used as fuel. Natural gas, a hydrocarbon mixture composed primarily of methane (CH_4), is in gaseous form at atmospheric temperature and pressure. However, gaseous methane is uneconomic to carry due to its very small density. In fact, 600 m^3 of gaseous methane have the same mass as just 1 m^3 of liquid methane. Therefore, natural gas must be liquefied to be transported by ship. The phase shift from gas to liquid can be achieved either though compression or through cooling.

Generally, the natural gas is liquefied through cooling at the LNG source. When loaded, it is at approximately atmospheric pressure, but chilled to its boiling point, around -160°C with the exact temperature depending on the cargo source and composition. The studied vessel is not fitted with any refrigeration or re-liquefaction capabilities: cargo is kept cold only by the effective thermal insulation of the cargo tanks. Even the best insulation, however, cannot completely stop heat transfer from the environment to the LNG. As a result, a small amount of cargo boils and becomes vapor every day. This vaporized cargo is called natural boil-off gas (NBOG).

In order to keep the cargo cold and the pressure within allowable levels in the tanks, the produced NBOG must be removed. While, in the past, the boil-off gas was burned in the ship's mast, today's energy prices have put this practice to an end. Boil-off gas is directed to the engine, where it is burned as fuel. When NBOG is used as fuel, no pre-heating of the gas is required. The boil-off leaves the tanks at a temperature around -110°C and a pressure around 50-180 mbarg. However, in order to be used as fuel in the main engines, the gas pressure must be increased to approximately 5 barg. Due to the compression process, the gas is heated so that it finally reaches the engine around 37-45°C.

During the ballast passage or for high ship speeds, the energy provided by the natural boil-off gas may not be sufficient for the vessel's propulsion and other energy needs. In this case, the ship has two options: burn liquid fuel or create more boil-off gas. Additional boil-off gas, or forced boil-off gas (FBOG) is produced by pumping LNG from the cargo tanks at its boiling point around -160°C. The liquid is then heated by steam up to a temperature similar to that of the natural boil-off around -110°C. It can then be sent to the engine and burned with the same process as the natural boil-off (compression and simultaneous heating).

The processes for gas burning with natural and forced boil-off gas are described in further detail below.

It should be noted that at lower speeds, the NBOG is more than what is required for the ship's propulsion. In this case, excess BOG can be burned in a gasification unit and discharged as exhaust or re-liquefied. The second case is a newer option and less common due to cost.

5.2.2.1 *Gas burning: Natural boil-off gas*

Figure 5.3 shows the process of gas burning with natural boil-off gas. As mentioned in the previous section, the actual natural boil-off temperature depends on cargo tank pressure and the loaded cargo composition, but it is around -110°C while the pressure is only slightly higher than atmospheric.

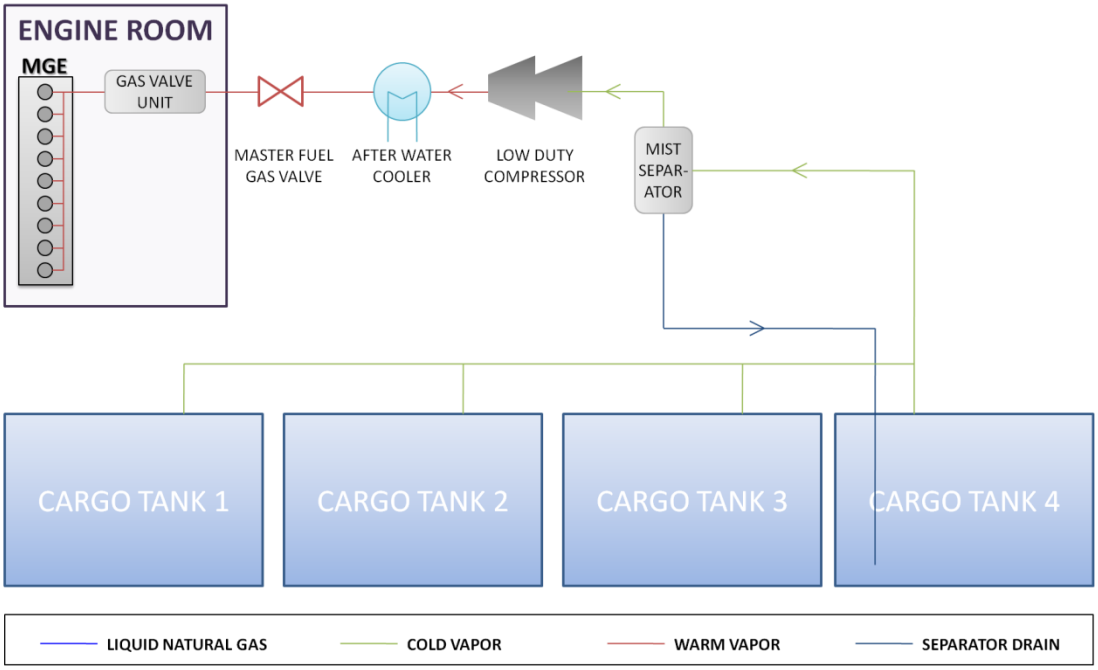

Figure 5.3: Fuel gas burning with Natural Boil-off Gas

The boil-off gas is first passed through a mist separator, where any liquid particles are extracted and returned to the tanks. This is to avoid any damage to the low duty (LD) compressor through which the vapor passes next and which is responsible for providing the engine with the required gas pressure for ignition. The LD compressor increases the gas pressure from around 1.06 to 6.5 bar. As a result of the compression, the gas temperature will increase to around 55-80°C, depending on the inlet temperature and gas composition.

The gas is then cooled as needed in the after-cooler, a shell-and-tube heat exchanger fed with fresh water. It then passes through the Master Fuel Gas Valve, required by the relevant IMO rules (IGC Code) [48] to insulate the cargo and machinery areas, on its way to the engine room.

Once inside the engine room, and before entering the engine, the fuel gas passes through a Gas Valve Unit (GVU). This device, separate from the engine, serves to filter the natural gas fuel as well as to monitor and regulate the gas feed pressure to the engine. Each of the four engines has its own GVU. At the GVU inlet, the gas temperature should be around 0-60°C. The required pressure is a function of the lower heating value (LHV) of the specific cargo as well as of the engine load. The pressure at the engine inlet will be approximately 1.2 bar lower due to losses in the GVU.

After the GVU the gas finally enters the engine, where it is ignited with the injection of a small amount of pilot liquid fuel. The pilot fuel consumption is of the order of 1 g/kWh even at 100% engine load.

5.2.2.2 *Gas burning: Forced boil-off gas*

As previously mentioned, when the energy provided by the natural boil-off gas is not sufficient, the ship can create more boil-off gas, known as forced boil-off gas (FBOG). The gas burning process with FBOG is shown in Figure 5.4.

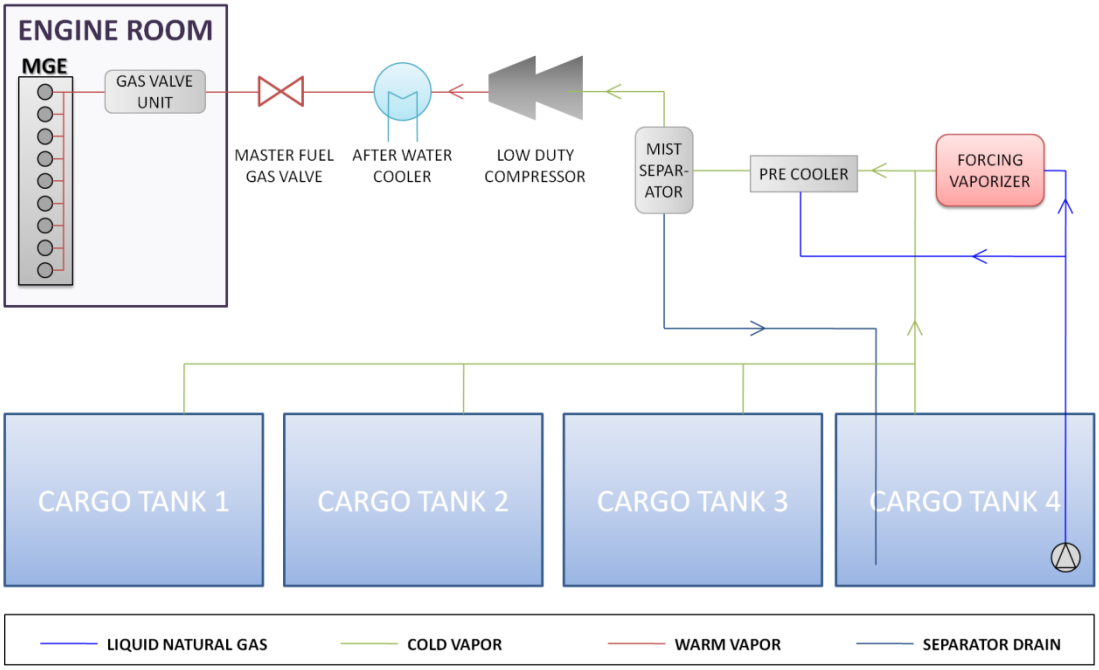

Figure 5.4: Fuel gas burning with Forced and Natural Boil-off Gas

The LNG from the cargo tanks is first pumped to the forcing vaporizer, a steam-fed shell and tube heater. The natural gas enters the forcing vaporizer tubes in liquid state, around -160°C. There it is warmed by steam and exits in a gaseous state. Depending on the mass flow through the forcing vaporizer, the outlet temperature can range from -20 to 85°C, however, the temperature is generally regulated to -100°C using a by-pass. Depending on the type of LD compressor in use, the forced boil-off may be further cooled

up to -120°C using cold liquid in the pre-cooler (also called the in-line mixer). Along with the natural boil-off gas, the forced boil-off then passes through the LD compressor, aftercooler, master fuel gas valve and finally the GVU on its way to the engine. Once again, a small amount of pilot fuel is required.

Table 5.5: Atmospheric boiling points of natural gas components		
Fluid	***Composition***	***Atmospheric boiling point***
Nitrogen	N_2	-195.91^{0}C
Methane	CH_4	-161.64^{0}C
Ethane	C_2H_6	-88.82^{0}C
Propane	C_3H_8	-42.41^{0}C
Butane	C_4H_{10}	-0.84^{0}C
Pentane	C_5H_{12}	35.68^{0}C
Hexane	C_6H_{14}	68.30^{0}C

An important distinction must be made regarding the composition and therefore thermal characteristics of the gas burned in the engines depending on whether it is the result of natural or forced boil-off processes. Forced boil-off gas will have the same mass composition as the liquid from which it is produced. The same is not true for natural boil-off gas which will be composed primarily of the more volatile components of the LNG – methane and nitrogen – while the heavier components of the LNG – ethane, propane, butane, pentane and hexane – will remain in liquid form. The key characteristics of the BOG, such as density or energy content, will vary accordingly.

The atmospheric boiling points for the main BOG components are given in Table 5.5 in order of volatility.

5.3 Fresh Water and Steam Systems

The engine system and the fresh water and steam systems are closely related. Waste heat from the engine exhaust is used for the production of steam while the warm jacket cooling water provides the energy for producing fresh water.

The ship is fitted with two fresh water generators (FWG), each with the capacity to produce 30 m^3 of fresh water per day. Specifications of each can be seen in Table 5.6.

Table 5.6: Fresh Water Generators		
Number	2	-
Capacity	30	m^3/day
Heat consumption at capacity	857.9	kW

In Figure 5.5, the vessel's steam system can be seen. The steam plant consists of two exhaust gas boilers (on MGEs 1 and 4) as well as two oil-fired boilers which can produce steam in case the engine load is too low for the vessel's steam demands.

The exhaust gas boilers (EGBs) and oil fired boilers functions are closely intertwined. The auxiliary boilers are filled to a certain level with water at saturation

temperature. The unfilled top portion of the boiler serves as the steam space for the entire system. Circulation pumps transfer water at saturation temperature from the auxiliary boilers to the EGBs. There, as the water rises through the boiler, it is heated by the engine exhaust gases and is converted to a mixture of hot water and saturated steam. The steam-water mixture is discharged into the steam space of the oil-fired boiler where steam separates from water. The dry saturated steam is then sent for service at a working pressure of 7 bar. A small amount of steam is siphoned from the service system to pass through the boiler water and maintain it at saturation temperature.

If the EGB steam production is more than the vessel's steam needs, the excess steam can be sent to the steam dump condenser, where it is cooled by sea water. The condensate will then flow to the cascade tank, where it is joined with the cooled steam and condensate returning from the steam service system. This collected water is sent with feed pumps to replenish the water level in the oil-fired boilers.

If the EGB steam production is less than the vessel's steam needs, for example during maneuvering or on a slow-steaming passage, the auxiliary boilers will burn liquid fuel to produce hot flue gases to heat the water in the boilers. The light steam bubbles produced when the water begins to boil rise to the surface reaching the steam drum where they are separated from any water particles which flow back into the boiler water. The steam is then sent to the service system via the same line as used by the EGB.

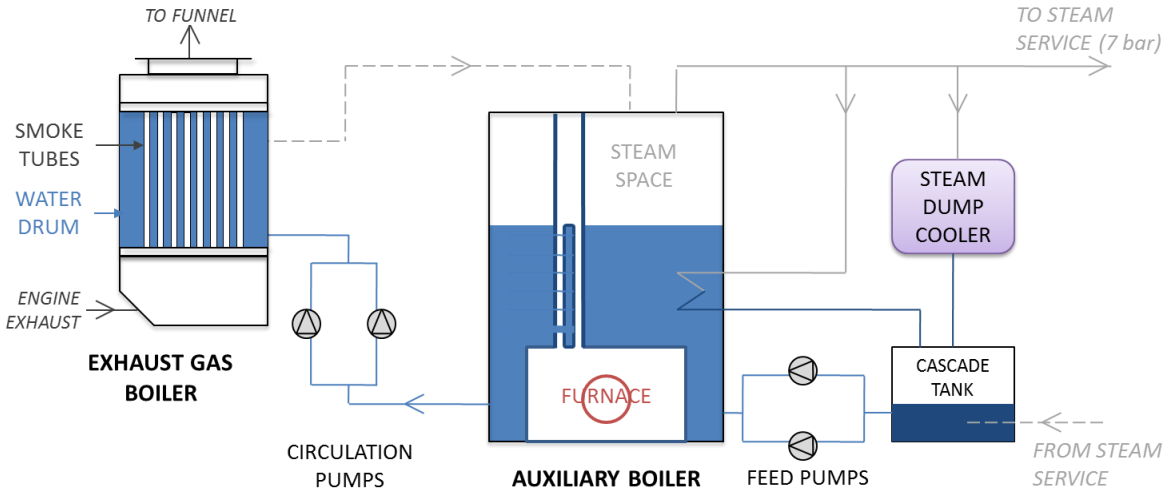

Figure 5.5: Steam system of the studied vessel

5.4 Operating Profile

5.4.1 Voyage and speed profile

The studied vessel is a project LNG ship on a fairly steady trading route. The time period examined spans two years of data. The vessel’s operating profile can be seen in Figure 5.6 (where the percentages refer to the whole year) and the speed profile in Figure 5.7 (where the percentages refer only to the steaming time).

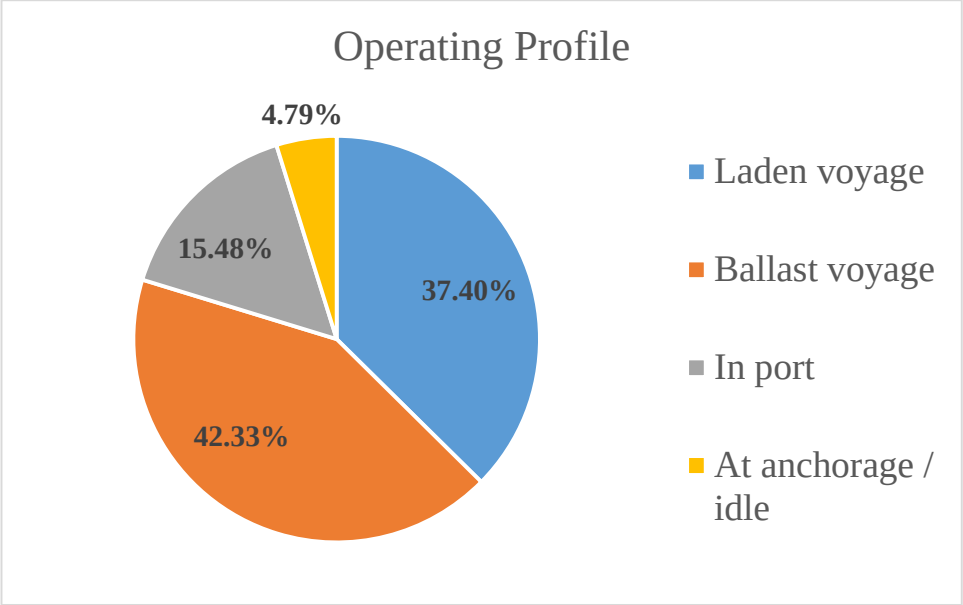

Figure 5.6: Studied vessel operational profile

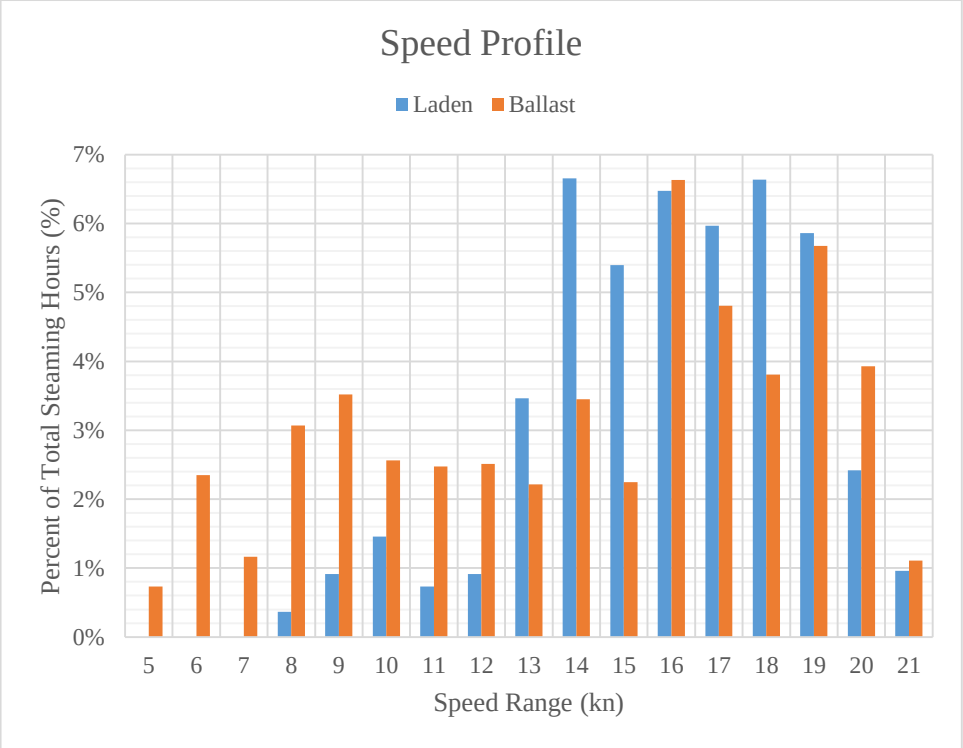

Figure 5.7: Speed profile of the studied vessel

The average speed for each voyage mode is listed in Table 5.7.

Table 5.7: Average speed per voyage mode

Mode	***Average speed (kn)***
Laden time	15.97
Ballast time	13.99
Total time	14.93

5.4.2 Engine working profile

The Diesel-electric configuration aboard the studied ship means that the electricity consumption is related to engine and propeller load. The electrical energy requirements of the vessel's machinery and accommodation are met by the main generator engines.

In Table 5.8 and Table 5.9, the power requirements for each speed can be seen for the laden and ballast conditions respectively. Furthermore, the required number of engines to produce this power and the symmetric load of the engines is shown. For each speed / power requirement, the minimum number of engines are used with engines not being allowed to exceed the NCR or 85% of the MCR[7]. Finally, the fuel energy consumption for each speed is shown based on the specific fuel energy consumption provided by the engine maker.

The speed range examined is 5 to 21 knots with the former being the maneuvering speed of the vessel and the latter being the maximum sea trial speed. The vessel design service speed is 19.5 knots. More details about the construction of these tables based on statistical data measured from the ship can be found in the Appendices.

Table 5.8: Power distribution - Laden voyages

Speed	**Steaming Time**		$\dot{W}_{ep}$	$\dot{W}_{eo}$	$\dot{W}_{e,tot}$	**Required Engines**	**Load per MGE**	**Fuel Energy Consumption**
(kn)	(hrs)	(%)	(kW)	(kW)	(kW)	(-)	(%)	(kW)
5	0.0	0.0%	664	1500	2164	1	24.66%	6822
6	0.0	0.0%	1072	1625	2697	1	30.73%	7753
7	0.0	0.0%	1607	1750	3357	1	38.25%	8906
8	48.0	0.3%	2281	1875	4156	1	47.37%	10303
9	120.0	0.9%	3109	2000	5109	1	58.22%	11967
10	191.0	1.4%	4100	2125	6225	1	70.94%	13917
11	96.0	0.7%	5266	2250	7516	2	42.83%	19214
12	120.0	0.9%	6618	2375	8993	2	51.24%	21795
13	454.0	3.3%	8166	2500	10666	2	60.78%	24719
14	872.0	6.2%	9921	2625	12546	2	71.49%	28004
15	707.0	5.1%	11892	2750	14642	3	55.62%	34708
16	848.5	6.1%	14089	2875	16964	3	64.44%	38765
17	782.2	5.6%	16521	3000	19521	3	74.16%	43233
18	869.7	6.2%	19198	3125	22323	4	63.60%	51168
19	768.0	5.5%	22127	3250	25377	4	72.30%	56505
20	317.0	2.3%	25318	3375	28693	4	81.75%	62300
21	125.5	0.9%	28780	3500	32280	4	91.97%	68567
Laden time below 5 or above 21 kn				0.0 hrs		0.0% of steaming time		

[7] The vessel design speed is 19.5 knots. Therefore, the fact that the NCR is exceeded at 21 knots as can be seen in Table 5.8 and Table 5.9 is acceptable and to be expected.

Table 5.9: Power distribution - Ballast voyages								
Speed	**Steaming Time**		$\dot{W}_{ep}$	$\dot{W}_{eo}$	$\dot{W}_{e,tot}$	**Required Engines**	**Load per MGE**	**Fuel Energy Consumption**
(kn)	(hrs)	(%)	(kW)	(kW)	(kW)	(-)	(%)	(kW)
5	96.0	0.7%	732	2000	2732	1	31.14%	7815
6	308.0	2.2%	1162	2125	3287	1	37.46%	8785
7	152.5	1.1%	1717	2250	3967	1	45.21%	9973
8	402.0	2.9%	2408	2375	4783	1	54.51%	11398
9	461.0	3.3%	3245	2500	5745	1	65.47%	13079
10	336.0	2.4%	4237	2625	6862	1	78.20%	15031
11	324.4	2.3%	5393	2750	8143	2	46.40%	20311
12	329.0	2.4%	6723	2875	9598	2	54.69%	22853
13	290.0	2.1%	8234	3000	11234	2	64.01%	25710
14	452.3	3.2%	9933	3125	13058	2	74.41%	28899
15	294.7	2.1%	11830	3250	15080	3	57.28%	35471
16	869.0	6.2%	13930	3375	17305	3	65.74%	39360
17	630.0	4.5%	16241	3500	19741	3	74.99%	43617
18	499.0	3.6%	18771	3625	22396	4	63.81%	51296
19	743.5	5.3%	21525	3750	25275	4	72.01%	56327
20	515.0	3.7%	24510	3875	28385	4	80.87%	61762
21	145.0	1.0%	27734	4000	31734	4	90.41%	67612
Ballast time below 5 or above 21 kn				216.0 hrs		1.8% of steaming time		

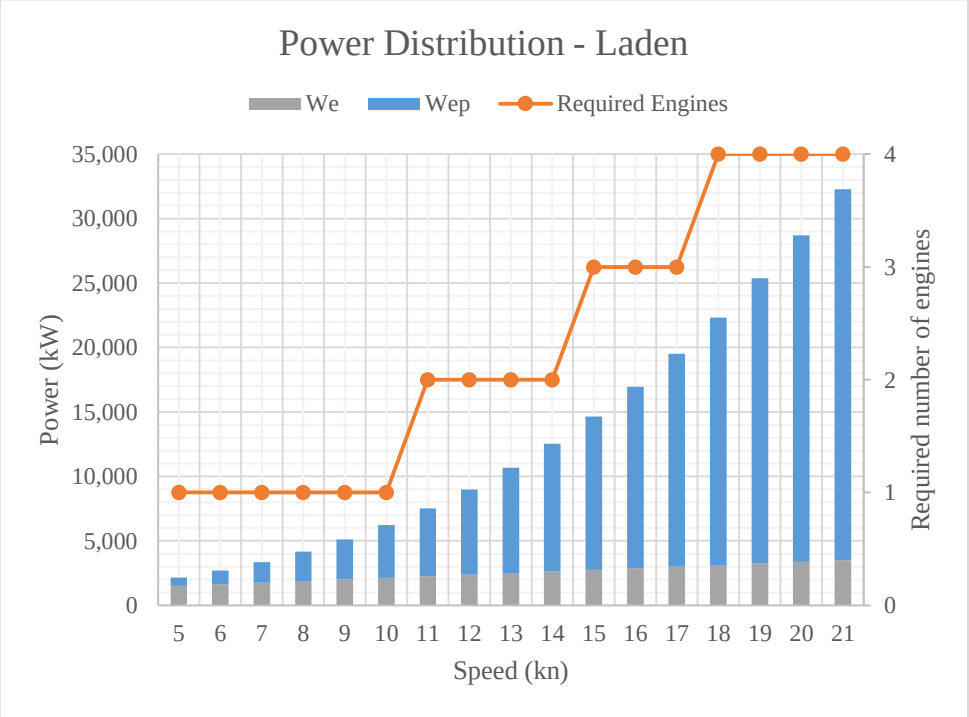

Figure 5.8: Power distribution and engines used for laden condition

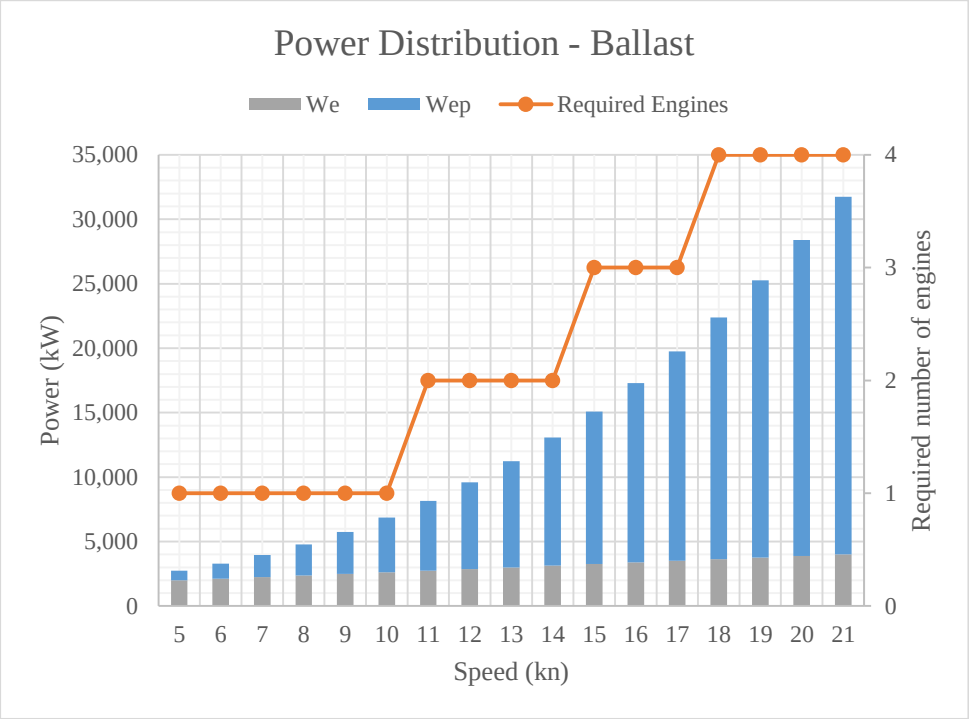

Figure 5.9: Power distribution and engines used for ballast condition

5.4.3 Consumption profile

The dual fuel engines installed onboard the studied vessel are capable of running on both natural gas or liquid fuel. From Table 5.10, however, it can be clearly seen that LNG is used preferentially. This study will therefore examine the engines in gas mode.

Table 5.10: Consumption by fuel type in examined period

Fuel type	***Total Consumption***	***LHV***	***Fuel Energy Consumed in Examined Period***	
(-)	(MT)	(kJ/kg)	(MJ)	(%)
HFO	4585.7	40.8	187096.6	12.2%
MGO	105.6	43.0	4540.8	0.3%
LNG	30555.3	43.9	1341257	87.5%
Total	35246.6	-	1532895	100.0%

5.4.4 Fresh water consumption profile

No strong correlation was found between fresh water consumption and speed. Therefore, for the present model, it will be assumed that the daily fresh water production is constant and equal to the average consumption from the measured data, 18.31 m^3/day. This consumption is sufficiently small that it can be covered by operating only one of the two available FWG at a time.

Furthermore, a linear relationship is assumed between fresh water production and the heat consumption for fresh water generation. Based on the nominal FWG characteristics in Table 5.6, this means that the average energy requirement per day is $\dot{Q}_{FWG} = 523.53\ kW$.

Since a regulating valve is used to ensure that the outflow of the HT cooling water from the engine system is constant and regulated to 91^{0}C, the inflow to the fresh water

generator will also have this same constant temperature. For this study it is assumed that the outflow of the fresh water generator will be maintained at its nominal temperature, 70.7°C, and only the water flow through the generator will be changed as needed to provide the necessary energy.

5.4.5 Steam consumption profile

In order to create a model of the vessel steam system, assumptions will have to be made about the available and the required steam onboard.

Steam production is from two sources: the exhaust gas boilers (EGBs) and the auxiliary boilers. The exhaust gas boilers are used preferentially while the auxiliary boilers are only used if the steam production from the former is insufficient.

The water which will be evaporated in the EGB is supplied as saturated water with a pressure of 7 bar. The produced steam-water mixture then passes through the auxiliary boiler where the steam is separated from the water. Therefore it can be assumed that the steam which exits the auxiliary boiler, acting as the steam drum, is saturated steam at 7 bar.

The steam consumption can be divided into three categories:

(1) Steam required for glycol heating:

A heated glycol water mixture is used to maintain the cofferdam spaces between the cargo tanks at a temperature of +5°C. This is necessary to avoid brittle fracture of the steel in these spaces. Since, in ballast condition, the tanks will be much warmer than in laden condition, the required steam for the glycol system is correspondingly reduced.

(2) Steam required for vaporizing FBOG:

Forced boil-off gas is produced in a steam-fed, shell and tube heater. The required mass of FBOG depends on the natural boil off rate of the cargo system and the speed. The required mass of steam to produce this FBOG varies accordingly. The heat exchange as a function of the methane flow is known and can be seen in the makers drawing in Figure 5.10. Furthermore, it is known that the vaporizer is fed with saturated steam at 7 bar and the condensate outlet is set to +90^{0}C. From this, the required steam flow can be calculated as in Table 5.11. Here, the pressure drop in the heat exchanger is ignored. Furthermore, the manufacturer of the vaporizer provides data about the design point of the exchanger using pure methane, not an LNG mixture. The difference in steam consumption that would result from vaporizing LNG instead of pure methane is not taken into account.

(3) Steam for other uses:

Other consumers of steam within the vessel (when in normal sailing mode, either laden or ballast) are heating for the bunker tanks, heating for the lube oil tanks, heating for bunker and lube oil purifiers, the accommodation heating system and the calorifier (which produces hot water for the accommodation). From the steam consumption calculation drawing of the vessel, it can be seen that these

requirements are practically constant between laden and ballast mode and among various engine loads. Therefore, they will be assumed constant here as well.

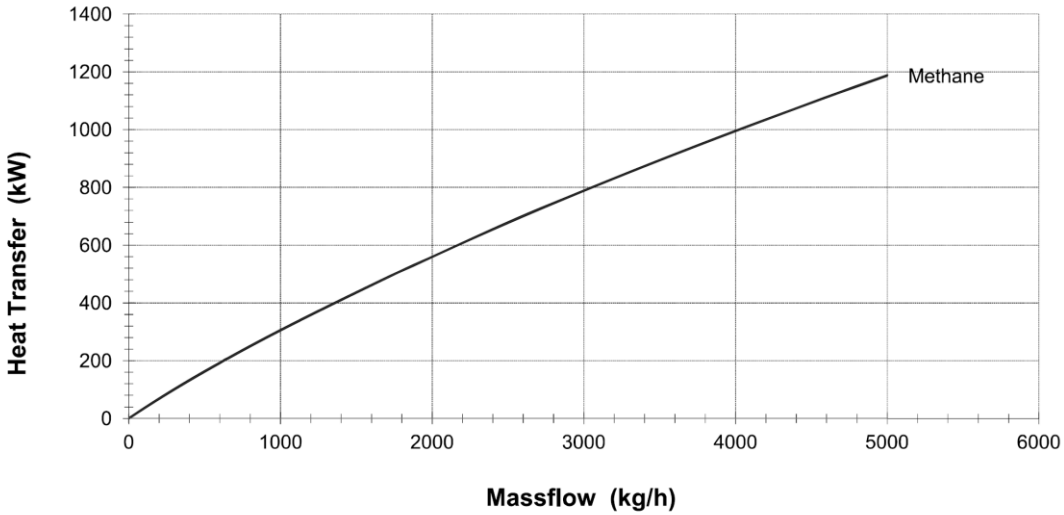

Figure 5.10: Forcing vaporizer characteristic curve [49]

Table 5.11: Forcing vaporizer design curve			
Steam inlet condition:		Saturated steam 7 bar	
Condensate outlet condition:		Water +90^{0}C	
Methane mass flow	***Heat Transfer***	***Required steam***	
(kg/h)	(kW)	(kg/s)	(kg/h)
0	0	0.00	0
500	160	0.07	241
1000	300	0.13	453
1500	450	0.19	679
2000	580	0.24	875
2500	690	0.29	1041
3000	790	0.33	1192
3500	900	0.38	1358
4000	1000	0.42	1509
4500	1100	0.46	1660
5000	1190	0.50	1796

The aforementioned steam requirements can be seen in Table 5.12 for ISO environmental conditions[8]. It is noted that all consumers require saturated steam at 7 bar. Finally, as per the steam consumption calculation for the ship, a 5% margin is assumed for pipe losses.

[8] ISO environmental conditions assume that the ambient temperature of the atmosphere, sea water, ballast water, cofferdam spaces and engine room is 25°C.

Table 5.12: Vessel steam requirements	
Usage	***Required Steam (kg/h)***
For glycol heating (laden)	803
For glycol heating (ballast)	64
For forcing vaporizer	Variable as in Table 5.11
For other uses (laden/ballast)	1038

5.5 Energy Balance and Quality of Rejected Heat

The overall engine system can be seen in Figure 5.11. The main engine requires several supporting systems including: the turbocharger, the charge air coolers and the lubricating oil cooler. These systems are interconnected via the cooling water system as can be seen in Figure 5.12. The cooling water system is divided into a high temperature loop (responsible for cooling the jacket water and the HT air cooler as well as feeding the FWG) and a low temperature loop (responsible for cooling the LT air cooler, the lube oil and the alternators).

5.5.1 Energy Balance

The energy balance of the engine system can be written as follows:

$$\dot{H}_f = \dot{q}_f \dot{W}_m = \dot{W}_e + \dot{Q}_{jw} + \dot{Q}_{lo} + \dot{Q}_{caH} + \dot{Q}_{caL} + \dot{Q}_G + \dot{Q}_{g2} + \dot{Q}_a \qquad (5.1)$$

where

- $\dot{H}_f$ the total fuel energy requirement from the fuel
- $\dot{q}_f$ the specific fuel energy consumption
- $\dot{W}_m$ the available mechanical power
- $\dot{W}_e$ the alternator output or produced electric energy
- $\dot{Q}_{jw}$ the heat loss to cool the cylinder jackets in the engine
- $\dot{Q}_{caH}$ the heat loss to cool the charge air in the high temperature intercooler
- $\dot{Q}_{caL}$ the heat loss to cool the charge air in the low temperature intercooler
- $\dot{Q}_G$ the heat loss to cool the alternator
- $\dot{Q}_{g2}$ the thermal power of the flue gasses
- $\dot{Q}_a$ the unaccounted heat losses or radiation

Assuming that heat transfer losses are negligible for all components except the exhaust gas boiler, the following equations result:

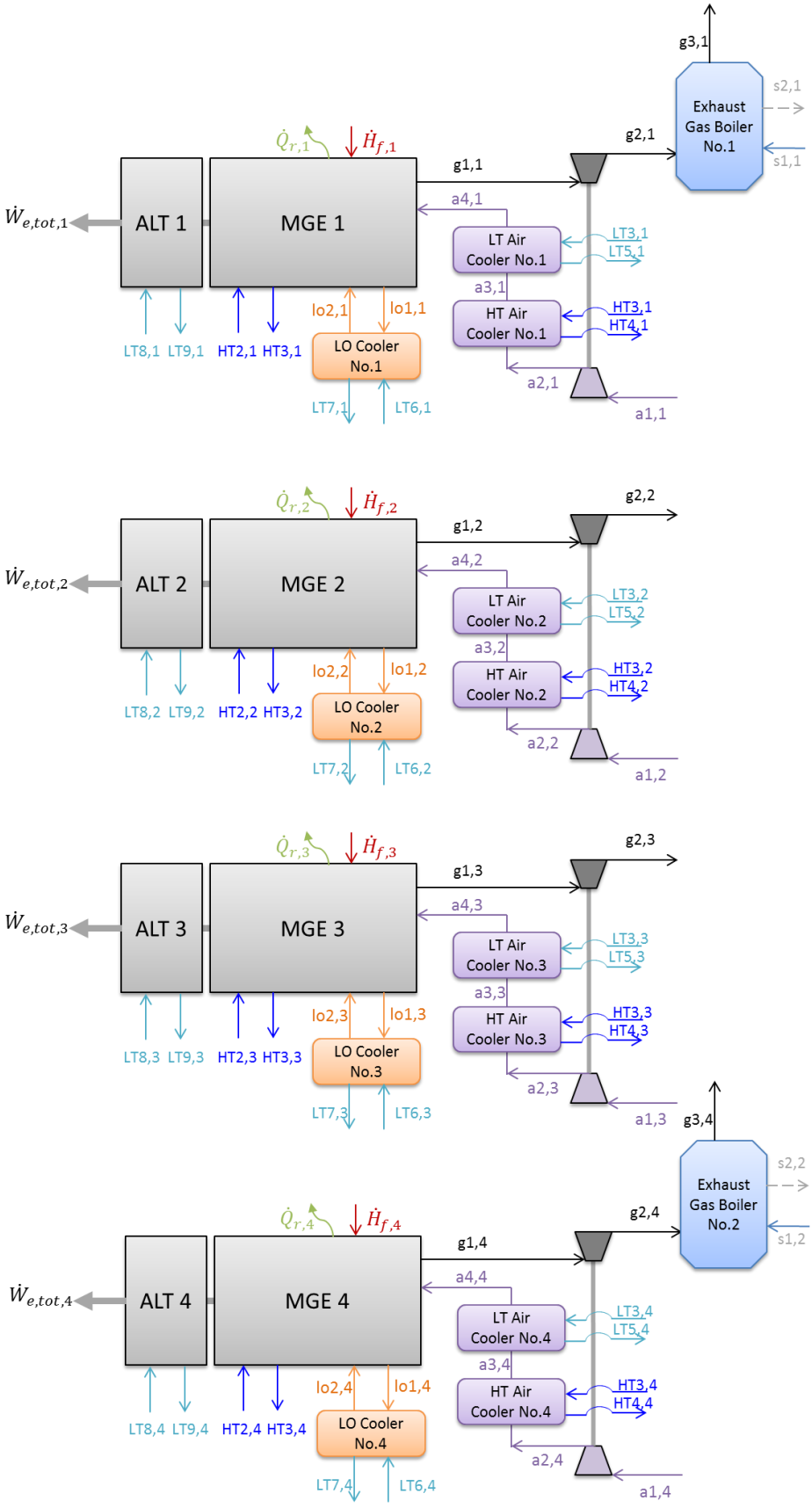

Figure 5.11: Main generator engines and supporting systems

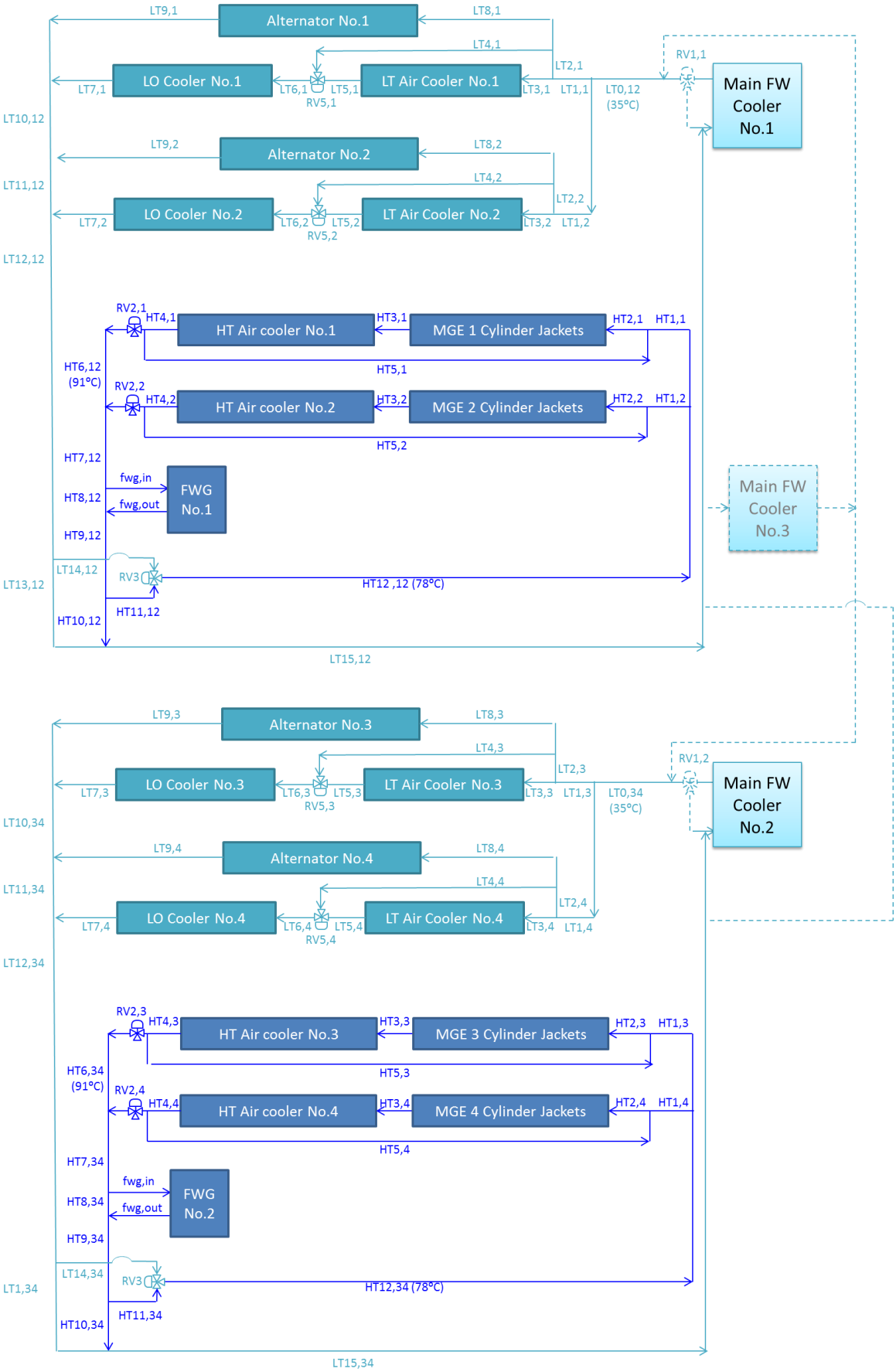

Figure 5.12: Main engines cooling water systems

Jacket Water Cooler

$$\dot{Q}_{jw} = \dot{m}_{w,HT1}\,(h_{HT2} - h_{HT1}) \tag{5.2}$$

LO Cooler

$$\dot{Q}_{lo} = \dot{m}_{lo} c_{plo} (T_{lo1} - T_{lo2}) = \dot{m}_{wLT1} (h_{LT5} - h_{LT4}) \tag{5.3}$$

Intercooler HT Stage

$$\dot{Q}_{caH} = \dot{m}_a (h_{a2} - h_{a3}) = \dot{m}_{wHT1} (h_{HT3} - h_{HT2}) \tag{5.4}$$

Intercooler LT Stage

$$\dot{Q}_{caL} = \dot{m}_a (h_{a3} - h_{a4}) = \dot{m}_{wLT1} (h_{LT3} - h_{LT1}) \tag{5.5}$$

Alternator Cooling

$$\dot{Q}_G = \dot{m}_{LT6} (h_{LT7} - h_{LT6}) \tag{5.6}$$

Flue Gas Heat

$$\dot{Q}_{g2} = \dot{m}_g c_{pg} (T_{g2} - T_0) \tag{5.7}$$

Finally, the available energy for steam production in the exhaust gas boiler can be found as follows:

$$\dot{Q}_{EGB} = \eta_q \dot{m}_g c_{pg} (T_{g2} - T_{g3}) = \dot{m}_s (h_{s2} - h_{s1}) \tag{5.8}$$

The magnitude of the above components can be found based on the available literature ([17], [50], [51]) and is shown in Table 5.13.

Table 5.13: Heat Balance - Gas Mode

Engine load	-	50%	75%	85%	100%
Specific fuel energy consumption (kJ/kWh)	$\dot{q}_f$	8860	7902	7688	7599
Engine output (kW)	$\dot{W}_m$	4388	6581	7459	8775
Total fuel energy consumption (kW)	$\dot{H}_f$	10798	14446	15929	18523
Output electric power (kW)	$\dot{W}_e$	4225	6338	7183	8450
Flue gas heat (kW)	$\dot{Q}_{g2}$	4161	4820	5009	5668
Jacket water cooler losses (kW)	$\dot{Q}_{jw}$	780	915	962	1065
Lube oil cooler losses (kW)	$\dot{Q}_{lo}$	645	720	729	765
Intercooler HT stage losses (kW)	$\dot{Q}_{caH}$	270	645	916	1260
Intercooler LT stage losses (kW)	$\dot{Q}_{caL}$	695	695	695	695
Alternator losses (kW)	$\dot{Q}_G$	162	244	276	325
Radiation / Unaccounted heat loss (kW)	$\dot{Q}_a$	270	270	261	240
Efficiency	$\eta = 1/\dot{q}_f$	40.6%	45.6%	46.8%	47.4%

The power distribution for each studied engine load can be seen in Figure 5.13.

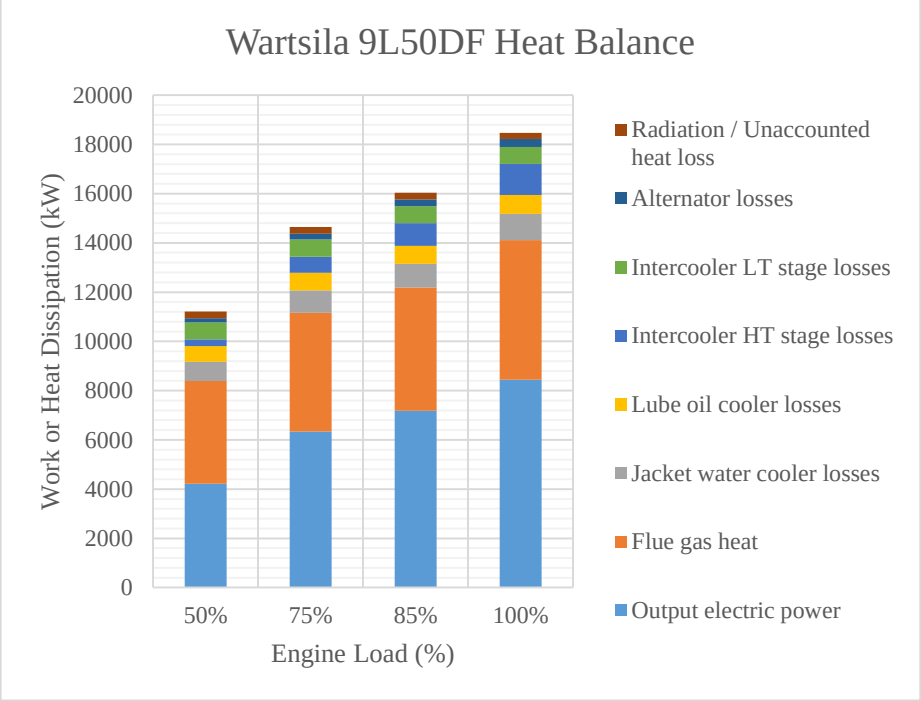

Figure 5.13: Engine system power distribution vs. Engine load

5.5.2 Quality of Rejected Heat

In order to examine the possibility of applying a waste heat recovery system to the existing power production plant, it is necessary to know not only the magnitude of available heat sources, but also their quality (in other words, temperature, pressure and enthalpy).

The quality of the available flows for certain parts of the system is available from existing literature [17], [50], [51]. For the remaining points, it must be calculated as below. For each calculation, the known quantities and assumptions are stated followed by the calculation of the missing quantity. Heat transfer losses are not taken into account.

5.5.2.1 *Charge air quality*

Known quantities: $\dot{m}_a, p_{a1}, T_{a1}, h_{a1} = f(p_{a1}, T_{a1}), p_{a4}, T_{a4}, h_{a4} = f(p_{a4}, T_{a4}), \dot{Q}_{caL}, \dot{Q}_{caH}$

Assumptions: $p_{a2} = p_{a3} = p_{a4}$

Calculation of missing quantities:

$$\dot{Q}_{caL} = \dot{m}_a(h_{a3} - h_{a4}) \rightarrow h_{a3} = h_{a4} + \frac{\dot{Q}_{caL}}{\dot{m}_a} \tag{5.9}$$

$$h_{a3}, p_{a3} \rightarrow T_{a3} \tag{5.10}$$

$$\dot{Q}_{caH} = \dot{m}_a(h_{a2} - h_{a3}) \rightarrow h_{a2} = h_{a3} + \frac{\dot{Q}_{caH}}{\dot{m}_a} \tag{5.11}$$

$$h_{a2}, p_{a2} \rightarrow T_{a2} \tag{5.12}$$

5.5.2.2 *Lube oil quality*

Known quantities: $\dot{m}_{lo}, T_{lo2}, \dot{Q}_{lo}$
Assumptions: $c_{plo} = 1.88\, kJ/kgK = const.$
Calculation of missing quantities:

$$\dot{Q}_{lo} = \dot{m}_{lo} c_{plo} (T_{lo1} - T_{lo2}) \rightarrow T_{lo1} = T_{lo2} + \frac{\dot{Q}_{lo}}{\dot{m}_{lo} c_{plo}} \tag{5.13}$$

5.5.2.3 *Cooling water quality*

Low-temperature cycle

Known pump capacities: $\dot{m}_{LT1} = \dot{m}_{LT6} = 72.3 \frac{kg}{s}, \dot{m}_{LT8} = \dot{m}_{LT9} = 16.8\, kg/s,$
Known nominal temperatures (regulated by valves): $T_{LT1} = 35℃, T_{LT6} = 38℃$
Known pressures: $p_{LT1} = 3.9\, bar$
Assumptions: $p_{LTi} = p_{LT1}\, for\, i = 2 \ldots 15$
Known enthalpies:

$$h_{LT1} = h_{LT2} = h_{LT3} = h_{LT4} = h_{LT8} = f(T_{LT1}, p_{LT1}), h_{LT6} = f(T_{LT6}, p_{LT6})$$

Unknowns: $\dot{m}_{LT2}, \dot{m}_{LT3}, \dot{m}_{LT4}, \dot{m}_{LT5}, h_{LT5}$

$$\dot{m}_{LT1} = \dot{m}_{LT2} + \dot{m}_{LT3} \tag{5.14}$$

$$\dot{m}_{LT2} = \dot{m}_{LT4} + \dot{m}_{LT8} \tag{5.15}$$

$$\dot{m}_{LT4} + \dot{m}_{LT5} = \dot{m}_{LT6} \tag{5.16}$$

$$\dot{m}_{LT4} h_{LT4} + \dot{m}_{LT5} h_{LT5} = \dot{m}_{LT6} h_{LT6} \tag{5.17}$$

$$\dot{m}_{LT5} = \dot{m}_{LT3} \tag{5.18}$$

Equations (5.14) to (5.18) provide a closed system of five equations with five unknowns. Once solved, this system also allows for the calculation of the following figures:

$$T_{LT5} = f(h_{LT5}, p_{LT5}) \tag{5.19}$$

$$\dot{Q}_{caL} = \dot{m}_{LT3} (h_{LT5} - h_{LT3}) \tag{5.20}$$

$$h_{LT9} = h_{LT8} + \dot{Q}_{Alt} / \dot{m}_{LT8} \tag{5.21}$$

$$\dot{m}_{LT7} = \dot{m}_{LT6} \tag{5.22}$$

$$\dot{m}_{LT10} = \dot{m}_{LT7} + \dot{m}_{LT9} \tag{5.23}$$

$$h_{LT10} = (\dot{m}_{LT7} h_{LT7} + \dot{m}_{LT9} h_{LT9}) / \dot{m}_{LT10} \tag{5.24}$$

If one MGE is on line per set of Main Cooler:

$$\dot{m}_{LT11} = \dot{m}_{LT12} = \dot{m}_{LT10} \tag{5.25}$$

$$h_{LT11} = h_{LT12} = h_{LT10} \tag{5.26}$$

If two MGE are on line per set of Main Cooler:

$$\dot{m}_{LT11} = \dot{m}_{LT9} + \dot{m}_{LT10} \tag{5.27}$$

$$h_{LT11} = (\dot{m}_{LT9} h_{LT9} + \dot{m}_{LT10} h_{LT10})/\dot{m}_{LT11} \tag{5.28}$$

$$\dot{m}_{LT12} = \dot{m}_{LT7} + \dot{m}_{LT11} \tag{5.29}$$

$$h_{LT12} = (\dot{m}_{LT7} h_{LT7} + \dot{m}_{LT11} h_{LT11})/\dot{m}_{LT12} \tag{5.30}$$

$$h_{LT12} = h_{LT13} = h_{LT14} \tag{5.31}$$

High-temperature cycle

Known heat exchange: $\dot{Q}_{caH}, \dot{Q}_{jw}, \dot{Q}_{fwg}$

Known pump capacities: $\dot{m}_{HT2} = \dot{m}_{HT3} = \dot{m}_{HT4} = 55.6\ kg/s$

Known nominal temperatures (regulated by valves): $T_{HT6} = 91°C, T_{HT12} = 78°C$

Other known temperatures: $T_{fwg,out} = 70.7°C$

Known pressures: $p_{HT1} = 4.8\ bar$

Assumptions: $p_{HTi} = p_{HT1}\ for\ i = 2 \dots 12\ and\ p_{fwg,in} = p_{fwg,out} = p_{HT1}$

Known enthalpies: $h_{HT4} = h_{HT5} = h_{HT6} = f(T_{HT6}, p_{HT6}) = h_{HT7} = h_{HT8} = h_{fwg,in}, h_{fwg,out} = f\left(T_{fwg,out}, p_{fwg,out}\right), h_{HT12} = f(T_{HT12}, p_{HT12}), h_{LT12} = h_{LT13} = h_{LT14}$

From the above known quantities, the following can be immediately calculated:

$$h_{HT3} = h_{HT4} - \frac{\dot{Q}_{caH}}{\dot{m}_{HT3}} \tag{5.32}$$

$$h_{HT2} = h_{HT3} - \frac{\dot{Q}_{jw}}{\dot{m}_{HT2}} \tag{5.33}$$

$$\dot{m}_{fwg} = \frac{\dot{Q}_{fwg}}{h_{fwg,in} - h_{fwg,out}} \tag{5.34}$$

However, the following quantities still remain unknown:

$\dot{m}_{HT1}, \dot{m}_{HT5}, \dot{m}_{HT6}, \dot{m}_{HT7}, \dot{m}_{HT8}, \dot{m}_{HT9}, \dot{m}_{HT10}, \dot{m}_{HT11}, \dot{m}_{HT12}, \dot{m}_{LT14}$

$h_{HT1}, h_{HT2}, h_{HT9}, h_{HT10}, h_{HT11}, h_{LT14}$

The following equations are valid:

$$\dot{m}_{HT4} - \dot{m}_{HT5} = \dot{m}_{HT6} \tag{5.35}$$

$$\dot{m}_{HT7} = \dot{m}_{HT6} \cdot n_{MGE} \tag{5.36}$$

$$\dot{m}_{HT7} - \dot{m}_{fwg} = \dot{m}_{HT8} \tag{5.37}$$

$$\dot{m}_{HT8} + \dot{m}_{fwg} = \dot{m}_{HT9} \tag{5.38}$$

$$\dot{m}_{HT8} h_{HT8} + \dot{m}_{fwg} h_{fwg,out} = \dot{m}_{HT9} h_{HT9} \tag{5.39}$$

$$\dot{m}_{HT9} = \dot{m}_{HT10} + \dot{m}_{HT11} \tag{5.40}$$

$$h_{HT9} = h_{HT10} \tag{5.41}$$

$$h_{HT10} = h_{HT11} \tag{5.42}$$

$$\dot{m}_{HT11} + \dot{m}_{LT14} = \dot{m}_{HT12} \tag{5.43}$$

$$\dot{m}_{HT11} h_{HT11} + \dot{m}_{LT14} h_{LT14} = \dot{m}_{HT12} h_{HT12} \tag{5.44}$$

$$\dot{m}_{HT12} = \dot{m}_{HT1} \cdot n_{MGE} \tag{5.45}$$

$$h_{HT12} = h_{HT1} \tag{5.46}$$

$$\dot{m}_{HT1} + \dot{m}_{HT5} = \dot{m}_{HT2} \tag{5.47}$$

$$\dot{m}_{HT1} h_{HT1} + \dot{m}_{HT5} h_{HT5} = \dot{m}_{HT2} h_{HT2} \tag{5.48}$$

$$\dot{m}_{HT9} = \dot{m}_{HT12} \tag{5.49}$$

Equations (5.35) to (5.49) constitute a closed system of fifteen equations with fifteen unknowns which can be solved for the missing quantities.

Finally, the available heat for heat recovery from the cooling water system can be calculated as:

$$\dot{Q}_{HT,avail} = \sum_{j=1}^{4} \left(\dot{Q}_{JW} + \dot{Q}_{caH} \right) - \dot{Q}_{FWG} \tag{5.50}$$

$$\dot{Q}_{LT} = \sum_{j=1}^{4} (\dot{Q}_{caL} + \dot{Q}_{lo} + \dot{Q}_{G}) \tag{5.51}$$

5.5.2.4 ***Flue gas quality***

Known quantities: $p_{s1}, h_{s1}, p_{s2}, h_{s2}, \dot{m}_s, \dot{m}_g, c_{pg}$[9]
Assumptions: $\eta_q = 0.95$,

$$\dot{Q}_{EGB} = \dot{m}_s(h_{s2} - h_{s1}) \tag{5.52}$$

$$\dot{Q}_{EGB} = \eta_q \dot{m}_g c_{pg}(T_{g2} - T_{g3}) \rightarrow T_{g3} = T_{g2} - \frac{\dot{Q}_{EGB}}{\eta_q \dot{m}_g c_{pg}} \tag{5.53}$$

The available heat for recovery for the two engines without EGBs is:

$$\dot{Q}_{g2} = \dot{m}_g c_{pg}(T_{g2} - T_{g,min}) \tag{5.54}$$

while the available heat for the two engines with EGBs is:

$$\dot{Q}_{g2} = \dot{m}_g c_{pg}(T_{g3} - T_{g,min}) \tag{5.55}$$

where $T_{g,min}$ is the minimum allowable temperature of the exhaust gas based on the sulphur content of the fuel.

The summary of the above can be seen in Table 5.14 where the calculated values are shaded.

[9] See Appendix B

Table 5.14: Quality of waste heat streams

		50% Load				75% Load				85% Load				100% Load			
		$\dot{m}$ (kg/s)	h (kJ/kg)	T (^{0}C)	p (bar)	$\dot{m}$ (kg/s)	h (kJ/kg)	T (^{0}C)	p (bar)	$\dot{m}$ (kg/s)	h (kJ/kg)	T (^{0}C)	p (bar)	$\dot{m}$ (kg/s)	h (kJ/kg)	T (^{0}C)	p (bar)
EXH	g1	8.10	-	525.00	-	10.60	-	543.00	-	12.00	-	542.00	-	14.10	-	542.00	-
	g2		-	430.00	-		-	420.00	-		-	404.00	-		-	383.00	-
	g3		-	310.31	-		-	328.30	-		-	322.67	-		-	313.41	-
CH AIR	a1	7.88	298.45	25.00	1.02	10.30	298.45	25.00	1.02	11.67	298.45	25.00	1.02	13.72	298.45	25.00	1.02
	a2		441.07	165.99	1.25		448.51	173.32	1.82		456.38	181.05	2.18		460.75	185.36	2.73
	a3		406.80	132.31	1.25		385.91	111.78	1.82		377.94	103.95	2.18		368.92	95.13	2.73
	a4		318.54	45.00	1.25		318.43	45.00	1.82		318.35	45.00	2.18		318.24	45.00	2.73
LO	lo1	32.50	-	69.56	4.90	32.50	-	70.78	4.80	32.50	-	71.92	4.80	32.50	-	72.52	4.70
	lo2		-	59.00	4.90		-	59.00	4.80		-	60.00	4.80		-	60.00	4.70
HT CW	HT1	19.24	326.91	78.00	4.80	28.58	326.91	78.00	4.80	34.41	326.91	78.00	4.80	42.59	326.91	78.00	4.80
	HT2	55.60	362.61	86.49	4.80	55.60	353.43	84.31	4.80	55.60	347.71	82.94	4.80	55.60	339.67	81.03	4.80
	HT3		376.63	89.83	4.80		369.89	88.22	4.80		365.02	87.06	4.80		358.83	85.59	4.80
	HT4		381.49	91.00	4.80		381.49	91.00	4.80		381.49	91.00	4.80		381.49	91.00	4.80
	HT5	36.36	381.49	91.00	4.80	27.02	381.49	91.00	4.80	21.20	381.49	91.00	4.80	13.01	381.49	91.00	4.80
	HT6	19.24	381.49	91.00	4.80	28.58	381.49	91.00	4.80	34.41	381.49	91.00	4.80	42.59	381.49	91.00	4.80
	HT7 (1)	19.24	381.49	91.00	4.80	28.58	381.49	91.00	4.80	34.41	381.49	91.00	4.80	42.59	381.49	91.00	4.80
	HT8 (1)	13.09	381.49	91.00	4.80	22.43	381.49	91.00	4.80	28.26	381.49	91.00	4.80	36.45	381.49	91.00	4.80
	HT9 (1)	19.24	354.27	84.51	4.80	28.58	363.17	86.62	4.80	34.41	366.27	87.36	4.80	42.59	369.20	88.06	4.80
	HT10 (1)	2.81	354.27	84.51	4.80	5.32	363.17	86.62	4.80	6.85	366.27	87.36	4.80	9.12	369.20	88.06	4.80
	HT11 (1)	16.43	354.27	84.51	4.80	23.26	363.17	86.62	4.80	27.55	366.27	87.36	4.80	33.48	369.20	88.06	4.80
	HT12 (1)	19.24	326.91	78.00	4.80	28.58	326.91	78.00	4.80	34.41	326.91	78.00	4.80	42.59	326.91	78.00	4.80

		50% Load				75% Load				85% Load				100% Load			
		$\dot{m}$ (kg/s)	h (kJ/kg)	T (^{0}C)	p (bar)	$\dot{m}$ (kg/s)	h (kJ/kg)	T (^{0}C)	p (bar)	$\dot{m}$ (kg/s)	h (kJ/kg)	T (^{0}C)	p (bar)	$\dot{m}$ (kg/s)	h (kJ/kg)	T (^{0}C)	p (bar)
HT CW cont.	HT7 (2)	38.47	381.49	91.00	4.80	57.16	381.49	91.00	4.80	68.81	381.49	91.00	4.80	85.19	381.49	91.00	4.80
	HT8 (2)	32.33	381.49	91.00	4.80	51.01	381.49	91.00	4.80	62.66	381.49	91.00	4.80	79.04	381.49	91.00	4.80
	HT9 (2)	38.47	367.88	87.75	4.80	57.16	372.33	88.80	4.80	68.81	373.88	89.17	4.80	85.19	375.34	89.52	4.80
	HT10 (2)	7.84	367.88	87.75	4.80	12.73	372.33	88.80	4.80	15.75	373.88	89.17	4.80	20.26	375.34	89.52	4.80
	HT11 (2)	30.64	367.88	87.75	4.80	44.43	372.33	88.80	4.80	53.06	373.88	89.17	4.80	64.93	375.34	89.52	4.80
	HT12 (2)	38.47	326.91	78.00	4.80	57.16	326.91	78.00	4.80	68.81	326.91	78.00	4.80	85.19	326.91	78.00	4.80
	fwg,in	6.15	381.49	91.00	4.80	6.15	381.49	91.00	4.80	6.15	381.49	91.00	4.80	6.15	381.49	91.00	4.80
	fwg,out		296.32	70.70	4.80		296.32	70.70	4.80		296.32	70.70	4.80		296.32	70.70	4.80
LT CW	LT1	72.39	146.99	35.00	3.90	72.39	146.99	35.00	3.90	72.39	146.99	35.00	3.90	72.39	146.99	35.00	3.90
	LT2	18.37	146.99	35.00	3.90	18.37	146.99	35.00	3.90	18.37	146.99	35.00	3.90	18.37	146.99	35.00	3.90
	LT3	54.02	146.99	35.00	3.90	54.02	146.99	35.00	3.90	54.02	146.99	35.00	3.90	54.02	146.99	35.00	3.90
	LT4	1.58	146.99	35.00	3.90	1.58	146.99	35.00	3.90	1.58	146.99	35.00	3.90	1.58	146.99	35.00	3.90
	LT5	54.02	159.86	38.08	3.90	54.02	159.86	38.08	3.90	54.02	159.86	38.08	3.90	54.02	159.86	38.08	3.90
	LT6	55.60	159.50	38.00	3.90	55.60	159.50	38.00	3.90	55.60	159.50	38.00	3.90	55.60	159.50	38.00	3.90
	LT7	55.60	171.10	40.77	3.90	55.60	172.45	41.10	3.90	55.60	172.61	41.13	3.90	55.60	173.26	41.29	3.90
	LT8	16.79	146.99	35.00	3.90	16.79	146.99	35.00	3.90	16.79	146.99	35.00	3.90	16.79	146.99	35.00	3.90
	LT9	16.79	152.11	36.23	3.90	16.79	154.67	36.84	3.90	16.79	155.69	37.08	3.90	16.79	166.35	39.64	3.90
	LT10	72.39	166.69	39.72	3.90	72.39	168.32	40.11	3.90	72.39	168.68	40.19	3.90	72.39	171.65	40.90	3.90
	LT11 (1)	72.39	166.69	39.72	3.90	72.39	168.32	40.11	3.90	72.39	168.68	40.19	3.90	72.39	171.65	40.90	3.90
	LT12 (1)	72.39	166.69	39.72	3.90	72.39	168.32	40.11	3.90	72.39	168.68	40.19	3.90	72.39	171.65	40.90	3.90
	LT13 (1)	69.58	166.69	39.72	3.90	67.07	168.32	40.11	3.90	65.54	168.68	40.19	3.90	63.27	171.65	40.90	3.90
	LT14 (1)	2.81	166.69	39.72	3.90	5.32	168.32	40.11	3.90	6.85	168.68	40.19	3.90	9.12	171.65	40.90	3.90
	LT15 (1)	72.39	173.96	41.46	3.90	72.39	182.64	43.53	3.90	72.39	187.39	44.67	3.90	72.39	196.54	46.86	3.90

		50% Load				75% Load				85% Load				100% Load			
		$\dot{m}$	h	T	p	$\dot{m}$	h	T	p	$\dot{m}$	h	T	p	$\dot{m}$	h	T	$\dot{m}$
		(kg/s)	(kJ/kg)	(^{0}C)	(bar)	(kg/s)	(kJ/kg)	(^{0}C)	(bar)	(kg/s)	(kJ/kg)	(^{0}C)	(bar)	(kg/s)	(kJ/kg)	(^{0}C)	(kg/s)
LT CW cont.	LT11 (2)	89.18	163.95	39.06	3.90	89.18	165.75	39.49	3.90	89.18	166.24	39.61	3.90	89.18	170.65	40.66	3.90
	LT12 (2)	144.78	166.69	39.72	3.90	144.78	168.32	40.11	3.90	144.78	168.68	40.19	3.90	144.78	171.65	40.90	3.90
	LT13 (2)	136.94	166.69	39.72	3.90	132.05	168.32	40.11	3.90	129.03	168.68	40.19	3.90	124.52	171.65	40.90	3.90
	LT14 (2)	7.84	166.69	39.72	3.90	12.73	168.32	40.11	3.90	15.75	168.68	40.19	3.90	20.26	171.65	40.90	3.90
	LT15 (2)	144.78	177.58	42.32	3.90	144.78	186.25	44.40	3.90	144.78	191.01	45.54	3.90	144.78	200.15	47.72	3.90
FUEL	f_{FO}	0.0028	-	26.00	8.50	0.0017	-	29.00	8.50	0.0014	-	34.00	8.50	0.0014	-	35.00	8.50
	f_G	0.2183	-	41.00	2.26	0.2938	-	41.00	2.83	0.3237	-	41.00	3.25	0.3768	-	41.00	3.77
STM	s1	0.5556	697.00	164.95	7.00	0.5556	697.00	164.95	7.00	0.5556	697.00	164.95	7.00	0.5556	697.00	164.95	7.00
	s2		2762.75	164.95	7.00		2762.75	164.95	7.00		2762.75	164.95	7.00		2762.75	164.95	7.00

6 Initial Design Parameters of the Studied Rankine System

In the studied system, the sources of waste heat are as follows:

(1) Jacket water
(2) Cooling water for the alternator
(3) Lube oil
(4) Charge air
(5) Exhaust gas

However, the cooling systems for the jacket water, alternator, lube oil and charge air are complex and intertwined, and consequently it is considered that an attempt to intervene in these cycles at multiple points would result in a complicated and costly system. Furthermore, to modify in the internal engine cycles as a retrofit would be difficult due to the compact system design.

Therefore, an ORC system will be examined which extracts waste heat from only a few points:

(1) From the outlet of the LT water from the engine cooling system (point $LT12$ as per Figure 5.12) with temperatures ranging from 39.72 to 40.1°C
(2) From the outlet of the HT cooling water from the fresh water generator (point $HT7$ as per Figure 5.12) with temperatures ranging from 84.51 to 88.06°C
(3) From the exhaust gas with temperatures ranging from 310-430°C

A simple schematic of the existing system where the above mentioned waste heat streams can be seen is shown in Figure 6.1.

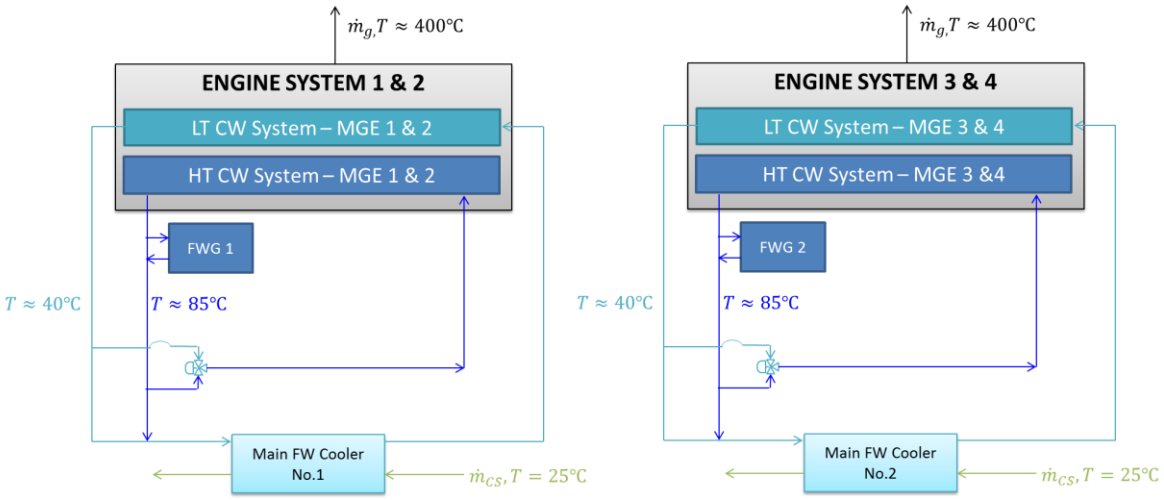

Figure 6.1: Simplified schematic of propulsion system waste heat streams

One immediate observation is that temperature of the waste heat for the flue gas stream is much higher than that of the cooling water streams. The particularities of using an ORC system for such high temperature heat recovery as well as for recovery of sources with such varied temperatures merits further examination so that appropriate initial cycle parameters can be found.

6.1 ORC cycles for Exhaust Gas Recovery

Departing from the more common low-grade waste heat sources normally employed in ORC systems (cooling water, lubricating oil and charge air), this study will additionally examine the use of the high temperature exhaust gas (reaching up to 430°C).

The difficulty in using ORC to exploit high temperature sources is matching the high exhaust temperatures with appropriate working fluids [52]. Above certain temperatures, refrigerants can become chemically unstable, breaking down to form toxic products like hydrogen fluoride.

Fluids do not begin to degrade immediately but after a heating period of 5-50 hours, suggesting that for use in cyclic processes even fluids with degradation temperatures below the maximum cycle temperatures might be able to be used. However, this must be examined further before any such applications can be safely employed [53].

In Table 6.1, various organic fluids along with their critical temperature and maximum allowed temperature for avoiding thermal degradation are listed. It is notable that there is not a direct correlation between critical temperature and thermal degradation. Furthermore, different literature sources calculate the maximum allowable temperature for avoiding thermal degradation differently, suggesting that it is a topic which still requires further experimental study before safe conclusions can be drawn.

Table 6.1: Thermal degradation of various refrigerants

Fluid	Critical temperature	Maximum temperature for avoiding thermal degradation	Source
R-141b	204.35	90	[54]
R-227ea	101.74	235	[53]
R-245fa	153.86	300	[53]
R-134a	100.95	368, 500	[54] , [55]
R-23	25.6	400	[53]
R-1234yf	95	<500	[55]
R-32	78.4	570-590	[55]

In recent years the search for the proper fluids, cycle parameters and layouts to exploit medium to high-grade exhaust energy has intensified.

J. Larjola in 1994 [56] suggested toluene as a fluid for heat recovery from a 425°C source citing its low rate of thermal decomposition at high temperatures. Toluene is a dry fluid with the benefit of a high critical temperature and low critical pressure. However, it is moderately toxic and flammable with a flash point of 6°C.

In 2013, Hossain et al. [57] examined water (R-718), R-134a and ammonia (R-717) as working fluids to exploit the exhaust gas of a Diesel engine generator set with temperatures up to 479°C. They found that, while the organic fluids resulted in higher thermal efficiencies, water outperformed the other two in terms of power output. Notable was that the organic fluids required higher pressures (up to 48 bar for ammonia and 36 bar for R-134a) to achieve comparable power results with water (at a pressure of 10-15 bar).

The use of a zeotropic mixture for high temperature exhaust recovery was examined by Song et al. in 2015 [58]. Working on a stationary compressed natural gas engine with exhaust temperatures between 495 and 555°C, they employed R-416A for increased power output and improved efficiency. Examining the effect of cycle pressure, they found that thermal efficiency and net power output increased with added pressure, while exergy destruction decreased. In this study, pressures from 10 to 35 were used, however the results suggest that even higher pressures could be beneficial.

The fluids which are appropriate for extracting high temperature heat may not be equally suitable for lower temperature heat sources like cooling water or charge air. This problem can be addressed by using two separate cycles in a dual-loop ORC.

This concept has roots in the automotive industry where BMW first designed a dual loop RC-ORC cycle dubbing the system the "turbosteamer" in 2005 [59]. The HT water loop absorbed waste heat from exhaust while the LT loop absorbed residual exhaust heat, heat from the steam loop and heat from the engine coolant.

Zhang et al. researched the same idea in 2013 [60] employing R-245fa to recover exhaust gas heat at 175 to 505°C and R-134a to recover heat from cooling water and air at a temperature up to 120°C. Pressures were limited to 24 bar in the high temperature cycle and slightly less in the low temperature cycle. The result was an improvement in the brake specific fuel consumption of up to 12-14% at the engine operating loads with already high efficiency and up to 30% at engine loads with low efficiency.

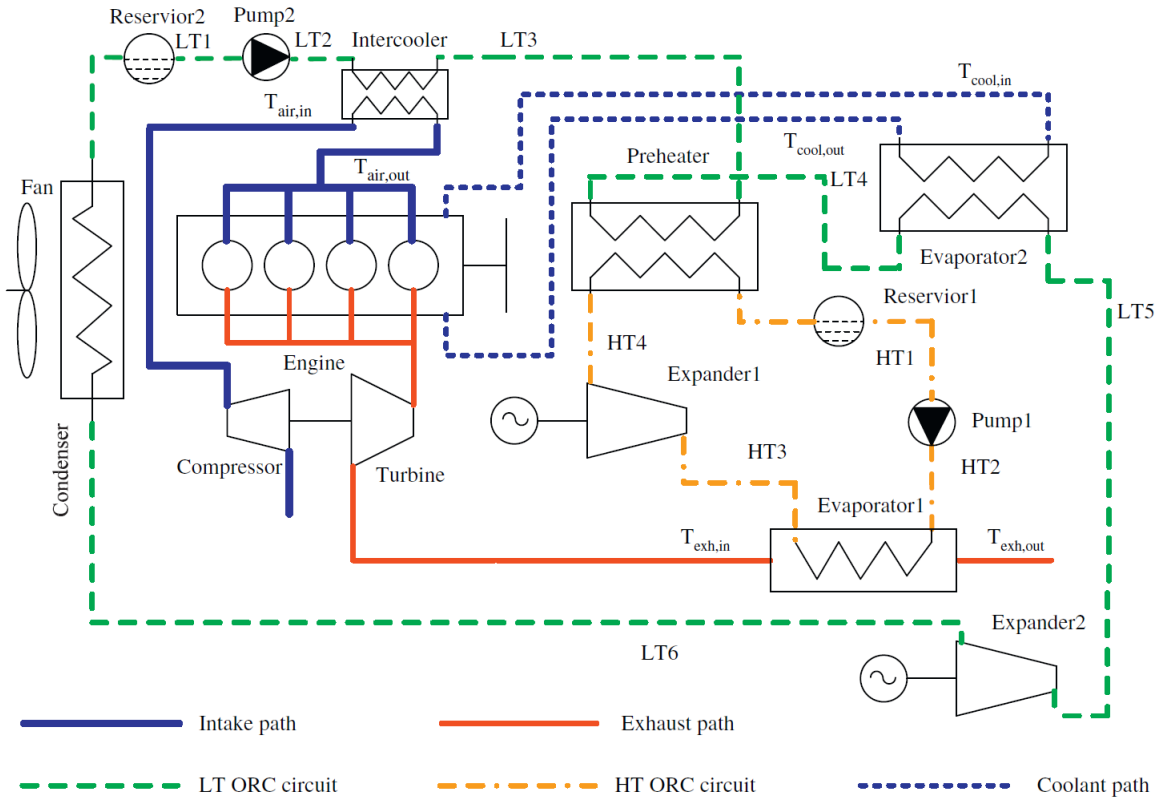

Figure 6.2: Proposed dual cycle system by Zhang et al. [60]

Shu et al. [52] built further on this topic in 2014 examining a dual ORC cycle with a topping water loop and a bottoming organic fluid loop. The high-temperature loop

recovered exhaust heat from a diesel engine at temperatures between 326 and 519°C while the low temperature loop recovered heat from the already partially cooled exhaust as well as from the engine coolant around 80°C. The organic fluids they examined for the bottoming loop were R-124, R-134a, R-1234yf (which performed best in terms of power output), R-600a, R-245fa and R-600 (of which the latter two performed best in terms of efficiency).

Song and Gu continued in this vein in [61]. In their work, exhaust gas heat at 300°C is recovered using water, and jacket cooling water heat at 90°C is recovered using R-123, R-236fa or R-245fa. For the studied 996 kW Diesel engine, an additional 55 kW could be produced by the HT-loop and another 60 kW from the LT loop.

Zhang et al. [62] analyzed the potential of coupling a bottoming ORC cycle with various types of topping cycles including a steam Rankine cycle, a Brayton cycle and a thermoelectric generator. Of the three possibilities, the steam Rankine cycle performed the best. In this system the low-temperature cycle did not recover heat from engine coolant but from the exhaust gas after it passed through the high temperature loop and from the working fluid of the loop itself. The HT loop employed water, while the LT loop employed the dry organic fluid R-123, suitable for this application due to its relatively high decomposition temperature, around 330°C. Due to uncertainty about the variable thermo-physical properties of fluids near their critical point, the researchers chose to use only subcritical pressure values in the organic cycle. However, for the water cycle, pressures up to 70 bar were examined with increased evaporating temperatures showing an improvement for overall work output.

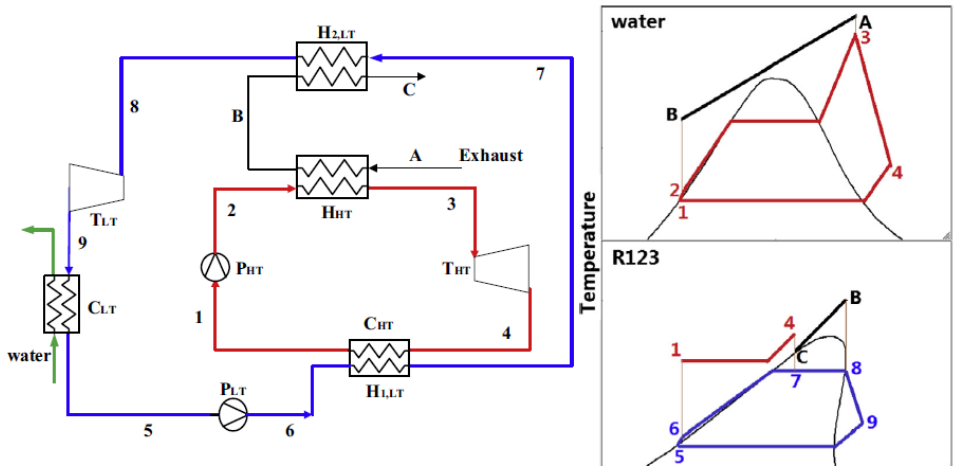

Figure 6.3: Dual Cycle System proposed by Zhang et al. [62]

Dual loop cycles recovering high temperature exhaust heat have even been examined for marine applications. Choi and Kim [63] examined the use of an upper trilateral cycle (in which saturated water is directly injected into the turbine) and lower ORC cycle to extract heat from the exhaust gas (around 227°C) from the main engine of a 6800 TEU Containership to produce additional propulsion power. The topping cycle used water and the bottoming cycle R1234yf. The resulting reductions in the specific fuel oil consumption of the main engine resulted in 98 tons of fuel savings per voyage (for the vessels China-Korea-USA route).

Panesar and Heikal 2014 [64] employed both the concept of a dual loop cycle and the search for a better working fluid to recover heat from a Heavy Duty Diesel Engine. Their system employed a high-temperature loop, recovering heat from exhaust and from the high-temperature portion of an exhaust gas recirculation system, and a low-temperature loop, recovering heat from the low-temperature portion of the exhaust gas recirculation system and from the charge air. The maximum temperature in the system was that of the exhaust gas at 466 °C. The researchers chose to face the problem of thermal instability of organic fluids by using water-based blends which met several practical and environmental criteria (including having an ODP of 0, a GWP less than 150, good thermal stability and an auto-ignition temperature above 360°C). The studied mixtures which met these criteria were: water 25% / acetone 75%, water 25% / methanol 75%, water 35% / ethanol 75%, water 75% / acetone 25%, water 75% / ethanol 25%, water / acetonitrile (ratio not specified), water / 2butanol (ratio not specified) and water / diacetone alcohol (ratio not specified). Pressures were allowed to reach up to 35 bar.

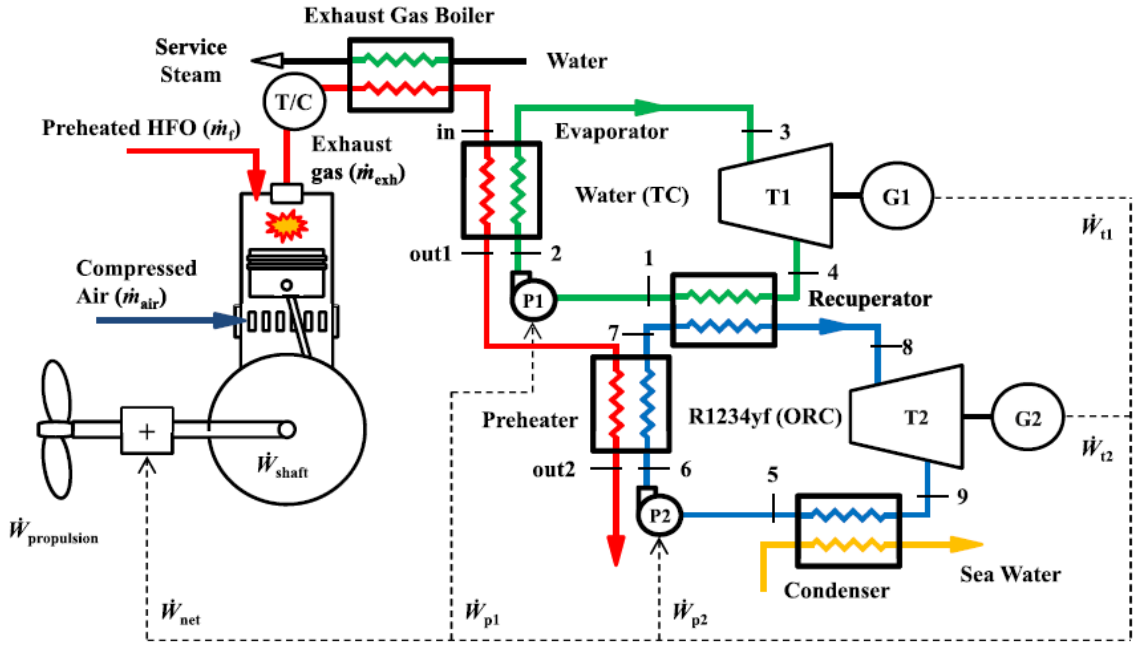

Figure 6.4: Dual ORC cycle for containership propulsion proposed by Choi and Kim [63]

6.2 Conclusions Based on Literature Review

From the above literature review, a few important conclusions can be drawn. The pool of fluids which lend themselves to high temperature heat recovery is often different from that used for lower temperature sources, primarily due to problems with thermal stability. Improved thermal matching using dual-loop cycles can be beneficial, especially when two, varied temperature sources will be used. It is notable that many researchers employ pressures well-above the 20 bar limit often found in low-grade recovery applications [6]. Additionally, some researchers use a large pinch temperature of 30°C in the exchangers involving exhaust gas ([64], [56], [62], [52]) while others use pinch points from 6-10°C ([63], [61]).

Based on the above, the following design decisions are made for the system at hand:

(1) A dual-loop system will be used with the high temperature cycle recovering heat from the exhaust gas streams and the low temperature cycle recovering heat from the cooling water stream as well as from the condenser of the high temperature cycle. The proposed cycle arrangement can be seen in Figure 6.5.

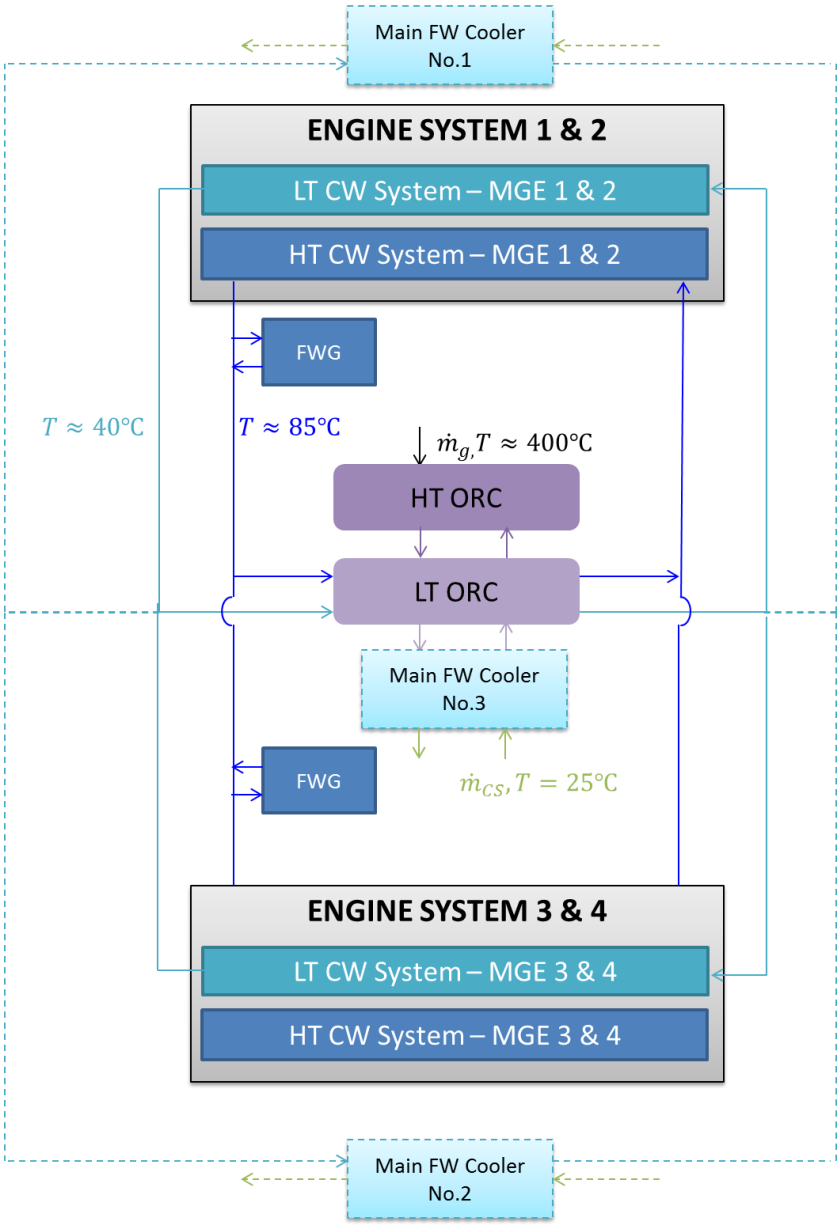

Figure 6.5: Schematic of proposed system

(2) It is considered for simplicity that the flows from all four engines will be combined into one common dual cycle system. Furthermore, the connection of the LT cooling system to the main freshwater cooler will remain in place in case all of the energy from the LT cooling system cannot be absorbed. In fact, all existing piping would remain in place so that the engine system can run independently of the Rankine system.

(3) The cold stream for the LT cycle will be provided by seawater with an inlet temperature of 25°C. The flow of the seawater is taken to be equal to the capacity of one of the existing pumps which are responsible for supplying seawater to the main freshwater coolers. There are three such pumps on board, one for each main freshwater cooler, however only two are used at a time since only two main coolers are used at a time. Therefore it is considered that the spare pump and freshwater cooler could be used with minimum modification for the Rankine system.

(4) The fluids to be examined for use in the high-temperature cycle, taking into account the examined fluids for HT loops in the available literature, the thermal degradation characteristics listed in Table 6.1 and safety requirements, are: R-416a, ammonia, R-245fa and water.

(5) For the low-temperature cycle, R-134a is chosen having been studied for both topping ([57]) and bottoming ([52], [60]) cycles in the reviewed works, as well as having both appropriate critical parameters for low-temperature heat recovery and resistance to chemical degradation in case of contact with high temperatures. The environmental, safety and thermodynamic characteristics of the fluids to be examined are given in Table 6.2 and Table 6.3.

Table 6.2: Environmental and Safety Characteristics of Examined Fluids

HT Group			
Name	ODP	GWP	ASHRAE Safety Group
R416a	0.01	1000	A1/A1/A3
Ammonia	0	0	B2
R245fa	0	794	A1
Water	0	0	A1
LT Group			
R-134a	0	1430	A1

Table 6.3: Thermodynamic Characteristics of Examined Fluids

HT Group										
Name	Type	Molar Mass	Crit Temp.	Crit. Pres.	Crit. Dens.	Latent heat	Thermal Conduct.	Heat Cap.	Atm. BP	Visc.
	(-)	(kg/ kmol)	(^{0}C)	(bar)	(kg/m^3)	(kJ/kg)	(W/m.K) x100	(kJ/ kgK)	(^{0}C)	(μPa/s)
R416a	Isen.	115	108.3	39.3	522.3	-	12.85	0.81	-23.22	11.74
Ammonia	Wet	17	132.3	113.3	225.0	1165.8	24.93	2.16	-33.59	10.09
R245fa	Dry	134	154.0	36.5	516.1	190.3	12.91	0.92	14.81	10.30
Water	Wet	18	374.0	220.1	322.0	2441.7	607.19	4.18	99.61	890.1
LT Group										
R134a	Isen.	102	101.1	4.06	511.9	177.8	13.39	0.85	-26.36	11.82
Properties are given for the reference point of 25°C and 1 bar										

(6) Considering that in the reviewed literature, dual cycles have not used an intermediate fluid between the topping and bottoming cycle, the same tactic will be followed here.

(7) It is considered that pressures above 50 bar are not practical for the onboard system. Nevertheless, the potential of higher cycle pressures will be examined. The lower limit on pressure will be atmospheric (to avoid infiltration) except in the case of water as a working fluid.
(8) The minimum pinch point for the exhaust gas heat exchanger will be set at 30°C. The minimum pinch point for other exchangers, including the common exchanger between the topping and bottoming cycle, will be set at 5°C based on the literature review in [6].
(9) The isentropic and mechanical efficiencies of all pumps / turbines will be taken as in [17].

All fluids selected based on the literature analysis are at acceptable levels of ODP and GWP. However, it is noted that, compared to the other fluids, ammonia has a lower safety rating.

Ammonia is a Class B2 refrigerant, meaning it displays a certain level of toxicity and flammability. Though not considered a fire hazard at normal operating conditions, for concentrations of 16-25% ammonia in air and at temperatures above 850˚C it can also be flammable [65]. In the present work the expected temperatures are less than this limit, so it can be considered that the flammability is not a concern. The issue of toxicity remains, though, as noted in [66], ammonia is toxic in high concentrations while it has a sharp smell which makes any leakage quickly detectable. Furthermore, it is lighter than air suggesting that any leaks will rise and scatter so that usage with proper ventilation can be appropriate.

The critical temperatures of the high temperature fluids, with the exception of water, are such that supercritical cycles can be achieved. However it is noted that due to the high critical pressure of ammonia, this would require high cycle pressures.

For the low temperature group, supercritical cycles can only be achieved if the waste heat from the cooling water system is not exploited as the critical temperature of R-134a is 101.1°C while the cooling water maximum temperature is around 88°C.

7 Proposed Model, Analysis and Optimization

Based on the initial design decisions made in Chapter 6, a more detailed model of the proposed dual cycle system can be determined. The layout of the system can be seen in Figure 7.1.

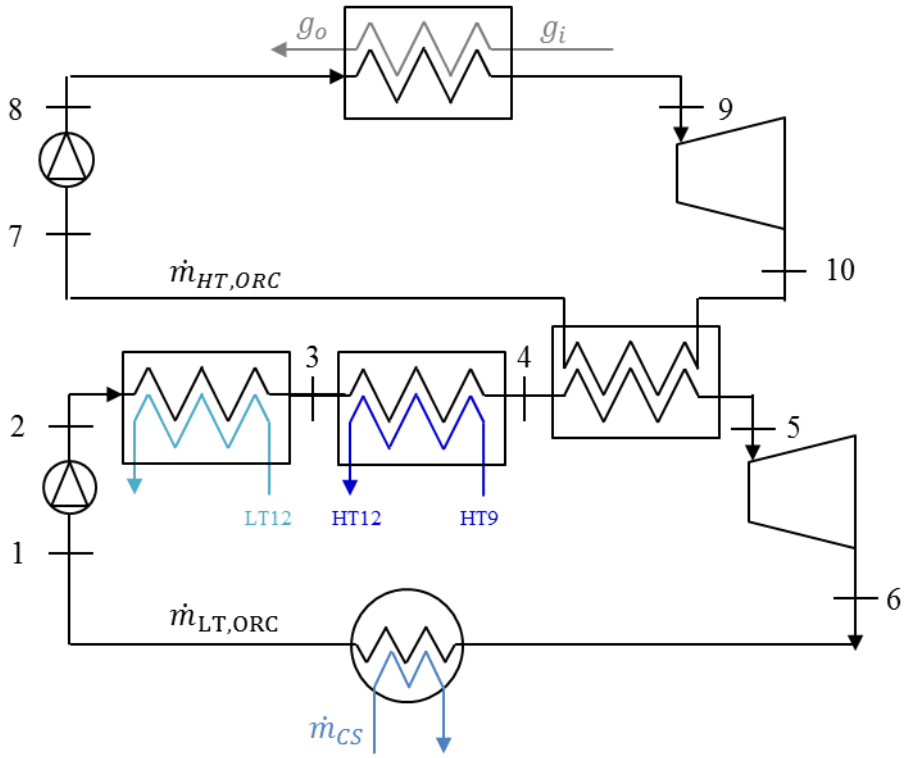

Figure 7.1: Proposed layout of dual cycle system

Initially, the only known parameters of the design are the waste heat flows and the potential fluid candidates. In order to choose the best parameters for the remaining elements, pinch point analysis will be used.

7.1 Analytical approach: Pinch analysis

Pinch analysis is a useful tool of process integration, a term which is used to describe the analysis and optimization of systems in order to maximize their effective use of energy and raw materials. In a pinch analysis of heat transfer, available streams of hot fluids which need to be cooled and cold fluids which need to be heated are examined. The goal is to match these streams in the best way possible so as to maximize the efficiency of heat transfer and reduce the use of external utilities [67]. In essence, the available cold streams should be heated as much as possible by the available hot streams and as little as possible by external components (like an electric heater). At the same time, the available hot streams should be cooled as much as possible by the available cold streams and as little as possible by external components (like an additional cooling water system).

A basic technique of pinch analysis is the construction of hot and cold composite curves which represent heat availability of the hot streams and heat demands of the cold streams, respectively. These curves are graphically represented on temperature-enthalpy

diagrams and the degree to which they overlap indicates the potential for heat recovery as can be seen in Figure 7.2.

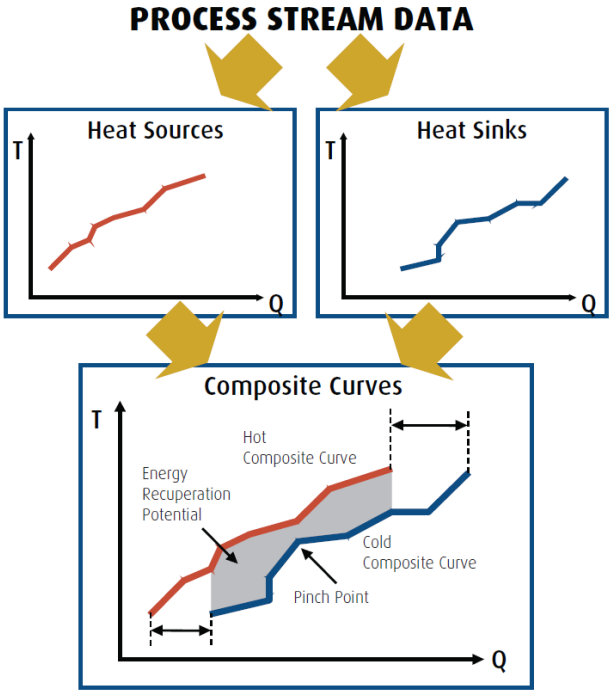

Figure 7.2: Pinch analysis [67]

In order for heat recovery to be maximum, the overlap of the curves must be maximized. This is achieved by approaching the two curves until their closest approach is equal to the minimum allowable temperature difference or pinch point.

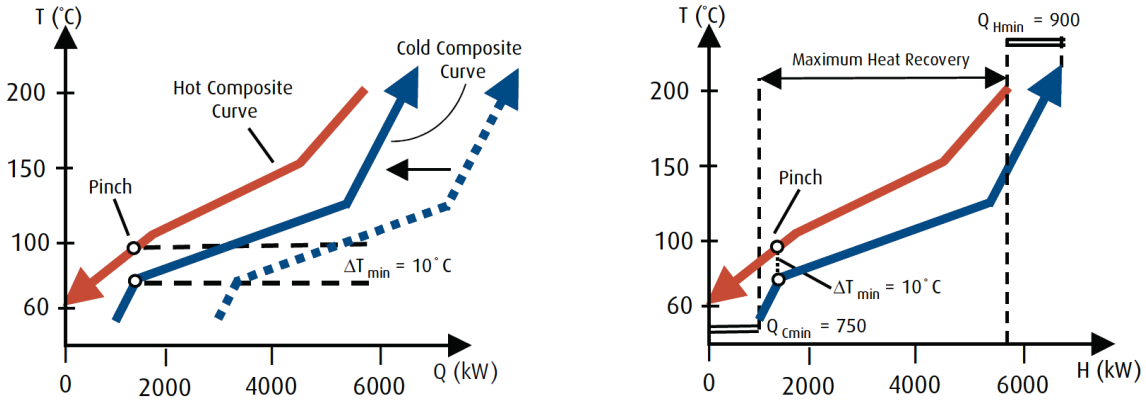

Figure 7.3: Using the composite curves to determine energy targets [67]

The pinch point, as mentioned above, is the minimum temperature difference between the hot and cold streams allowed in the heat exchanger. A smaller pinch point allows for a better match between the hot and cold streams and subsequent maximization of the heat recovery potential. However, as the pinch point difference decreases, the size and capital costs of the required heat exchanger increase. Therefore there is an optimal pinch point temperature which minimizes the total cost of the system [67].

In the present study, the pinch point which will be applied has already been decided based on the available literature in Section 6.2. The next step is to find the optimal cycle

parameters which will maximize the heat recovery and as a result the work output of the system while respecting this pinch point.

7.2 Optimization problem

Pinch point analysis is employed to examine the optimum heat transfer in the system. The ultimate goal is to solve the following optimization problem:

Objective function:

$$\max\left(\dot{W}_{net,2R}\right)$$

Constraints and Assumptions

(1) Heat transfer in all exchangers must be feasible meaning that the hot stream temperature must be higher than the cold stream temperature plus the pinch point difference at all times.
(2) The quality at the turbine exit must be sufficient to avoid droplet formation, i.e. $x \geq 0.9$. This applies to both cycles.
(3) It is considered that the low temperature cycle will be exclusively responsible for condensing the HT cycle and cooling the engine HT Cooling Water. However, to what extent it will be cooling the engine LT cooling water will be left as an open parameter of the optimization. This is because this waste stream is at a low temperature and may not be possible to exploit or worth exploiting. Furthermore, the main fresh water coolers are already in place and can be used if needed.

Like with all pinch point analyses, the present work makes the following assumptions [68]:

(1) Heat exchange will take place in counter-flow heat exchangers.
(2) Pressure losses in the exchangers are ignored.
(3) Heat loss to the environment is ignored.
(4) Changes in kinetic and potential energy are ignored.
(5) Specific heat capacity is considered constant.

The following parameters in Table 7.1 will be assumed to be constant and equal to the values shown based on the available literature and design decisions.

Table 7.1: Dual cycle constant parameters

Parameter	Symbol	Value
LT cooling source (sea water) temperature	T_{CS}	25^0C
LT cooling source flow	$\dot{V}_{CS}$	770 m^3/hr
Pinch point with exhaust gas	PP_G	30^0C
Pinch point in other heat exchangers	PP	5^0C
Pump isentropic efficiency	η_P	0.70
Pump mechanical efficiency	η_{mP}	0.90
Turbine isentropic efficiency	η_T	0.85
Turbine mechanical efficiency	η_{mT}	0.90

Decision variables

These variables constitute the defining parameters of each studied system

(1) Fluid types
(2) Fluid flows: $\dot{m}_{ORC,HT}, \dot{m}_{ORC,LT}$
(3) Superheating of HT fluid: $\Delta T_{sup,HT}$
(4) Evaporation pressures for both fluids: $P_{ev,HT},\ P_{ev,LT}$
(5) Portion of cooling of the engine system LT cooling water by the ORC: $\%CW$

Dependent/performance variables

The variables which will be calculated for each cycle based on the above and which will be used for a qualitative comparison of the cycles are listed below:

(1) $\dot{W}_{net}$
(2) $\dot{W}_{net}/\dot{m}$
(3) η_R
(4) η_Q
(5) η_{tot}
(6) ζ_R
(7) SP
(8) VFR
(9) RSP

The relevant equations of the proposed system as in Figure 7.1 are given below:

LT Cycle

Available energy:

$$\dot{Q}_{Av,LT} = \dot{Q}_{Av,LT,HT\_ORC} + \dot{Q}_{Av,HT,CW} + \dot{Q}_{Av,LT,CW} \tag{7.1}$$

$$\dot{Q}_{Av,LT,HT\_ORC} = \dot{m}_{ORC,HT}(h_{10} - h_7) \tag{7.2}$$

$$\dot{Q}_{Av,HT,CW} = \dot{m}_{HT9,12}\left(h_{HT9,12} - h_{HT12,12}\right) + \dot{m}_{HT9,34}\left(h_{HT9,34} - h_{HT12,34}\right) \tag{7.3}$$

$$\dot{Q}_{Av,LT,CW} = \dot{m}_{LT12,12}\left(h_{LT12,12} - h_{LT0,12}\right) + \dot{m}_{LT12,34}\left(h_{LT12,34} - h_{LT0,34}\right) \tag{7.4}$$

where the subscripts of Equation (7.3) and (7.4) refer to Figure 5.12.

Cycle parameters:

$$T_1 = T_{CS} + PP, x_1 = 0 \rightarrow P_1 = P_{cond,LT}, h_1, s_1, \rho_1 \tag{7.5}$$

$$P_{2is} = P_{ev,LT}, s_{2is} = s_1 \rightarrow h_{2is} \tag{7.6}$$

$$h_2 = h_1 + \frac{h_{2is} - h_1}{\eta_{isP}} \tag{7.7}$$

$$\dot{Q}_{H,LT} = \dot{Q}_{Av,LT,HT\_ORC} + \dot{Q}_{Av,HT,CW} + \%CW \cdot \dot{Q}_{Av,LT,CW} \tag{7.8}$$

$$\dot{m}_{ORC,LT}(h_5 - h_2) = \dot{Q}_{in,LT} \tag{7.9}$$

$$h_5 = h_2 + \frac{\dot{Q}_{in,LT}}{\dot{m}_{ORC,LT}} \tag{7.10}$$

$$P_5 = P_{ev,LT}, h_5 \rightarrow T_5, s_5, x_5, \rho_5 \tag{7.11}$$

$$P_{6is} = P_{cond,LT}, s_{6is} = s_5 \rightarrow h_{6is} \tag{7.12}$$

$$h_6 = h_5 - \eta_{isT}(h_5 - h_{6is}) \tag{7.13}$$

Energy parameters:

$$\dot{W}_{P,LT} = \dot{m}_{ORC,LT}(h_2 - h_1)/\eta_{mP} \tag{7.14}$$

$$\dot{W}_{T,LT} = \dot{m}_{ORC,LT}(h_5 - h_6)\eta_{mT} \tag{7.15}$$

$$\dot{W}_{net,LT} = \dot{W}_{T,LT} - \dot{W}_{P,LT} \tag{7.16}$$

$$\dot{Q}_{H,LT} = \dot{m}_{ORC,LT}(h_5 - h_2) \tag{7.17}$$

$$\dot{Q}_{C,LT} = \dot{m}_{ORC,LT}(h_6 - h_1) \tag{7.18}$$

$$\eta_{R,LT} = \frac{\dot{W}_{net,LT}}{\dot{Q}_{H,LT}} \tag{7.19}$$

$$\eta_{Q,LT} = \frac{\dot{Q}_{H,LT}}{\dot{Q}_{Av,LT}} \tag{7.20}$$

$$\eta_{TOT,LT} = \eta_{R,LT} \cdot \eta_{Q,LT} \tag{7.21}$$

Exergy parameters:

$$\dot{E}_{H,LT} = \dot{m}_{ORC,LT}[h_4 - h_2 - T_0(s_4 - s_2)] \tag{7.22}$$

$$\Delta\dot{E}_{loss,LT} = \dot{m}_{ORC,LT}[h_6 - h_1 - T_0(s_6 - s_1)] \tag{7.23}$$

$$\zeta_{R,LT} = \frac{\dot{W}_{net,LT}}{\dot{E}_{H,LT}} \tag{7.24}$$

HT Cycle

Available energy:

$$\begin{aligned}\dot{Q}_{Av,HT} = \dot{m}_{g,1}c_{pg}(T_{g3,1} - T_{gmin}) + \dot{m}_{g,2}c_{pg}\left(T_{g2,2} - T_{gmin}\right) \\ + \dot{m}_{g,3}c_{pg}\left(T_{g2,3} - T_{gmin}\right) + \dot{m}_{g,4}c_{pg}(T_{g3,4} - T_{gmin})\end{aligned} \tag{7.25}$$

where $T_{gmin} = 120℃$ is the lowest temperature to which it is considered the exhaust can be cooled without fear of acid condensation[10].

Cycle parameters:

$$T_7, x_7 = 0 \rightarrow P_7, h_7, s_7, \rho_7 \tag{7.26}$$

$$P_{8is} = P_{ev,HT}, s_{8is} = s_7 \rightarrow h_{8is} \tag{7.27}$$

$$h_8 = h_7 + \frac{h_{8is} - h_7}{\eta_{isP}} \tag{7.28}$$

$$P_8 = P_{ev,HT}, h_8 \rightarrow T_8, s_8, x_8, \rho_8 \tag{7.29}$$

$$T_{max,HT} = \begin{cases} T_{sat}\left(P_{ev,HT}\right) + \Delta T_{sup,HT}, for\ P_{ev,HT} < P_{crit,HT} \\ T_{crit,HT} + \Delta T_{sup,HT}, for\ P_{ev,HT} > P_{crit,HT} \end{cases} \tag{7.30}$$

$$P_9 = P_{ev,HT}, T_9 = T_{max,HT} \rightarrow h_9, s_9, x_9, \rho_9 \tag{7.31}$$

$$P_{10is} = P_{cond,HT}, s_{10is} = s_9 \rightarrow h_{10is} \tag{7.32}$$

$$h_{10} = h_9 - \eta_{isT}(h_9 - h_{10is}) \tag{7.33}$$

$$P_{10} = P_{cond,HT}, h_{10} \rightarrow T_{10}, s_{10}, x_{10}, \rho_{10} \tag{7.34}$$

Energy parameters:

$$\dot{W}_{P,HT} = \dot{m}_{ORC,HT}(h_8 - h_7)/\eta_{mP} \tag{7.35}$$

[10] The actual value of T_{gmin} should be calculated more exactly based on the combustion equations and sulphur content of the pilot fuel. However, such a calculation goes beyond the scope of the present work.

$$\dot{W}_{T,HT} = \dot{m}_{ORC,HT}(h_9 - h_{10})\eta_{mT} \tag{7.36}$$

$$\dot{W}_{net,HT} = \dot{W}_{T,HT} - \dot{W}_{P,HT} \tag{7.37}$$

$$\dot{Q}_{H,HT} = \dot{m}_{ORC,HT}(h_9 - h_8) \tag{7.38}$$

$$\dot{Q}_{C,HT} = \dot{m}_{ORC,HT}(h_{10} - h_7) \tag{7.39}$$

$$\eta_{R,HT} = \frac{\dot{W}_{net,HT}}{\dot{Q}_{H,HT}} \tag{7.40}$$

$$\eta_{Q,HT} = \frac{\dot{Q}_{H,HT}}{\dot{Q}_{Av,HT}} \tag{7.41}$$

$$\eta_{TOT,HT} = \eta_{R,HT} \cdot \eta_{Q,HT} \tag{7.42}$$

Exergy parameters:

$$\dot{E}_{H,HT} = \dot{m}_{ORC,HT}[h_9 - h_8 - T_0(s_9 - s_8)] \tag{7.43}$$

$$\dot{E}_{loss,HT} = \dot{m}_{ORC,HT}[h_{10} - h_7 - T_0(s_{10} - s_7)] \tag{7.44}$$

$$\zeta_{R,HT} = \frac{\dot{W}_{net,HT}}{\dot{E}_{H,HT}} \tag{7.45}$$

7.3 Simulation Algorithm

The simulation algorithm used to solve the above optimization problem is the Generalized Reduced Gradient (GRG2) Algorithm as applied in Microsoft Excel Solver [69]. The algorithm seeks to maximize a non-linear objective function for several independent or optimization variables. Constraints for all independent variables must be applied.

The algorithm applies trial values for the optimization variables through an iterative process. For each trial value, the partial derivative of the objective function in respect to each variable is calculated using finite difference estimates. This is done by calculating the value of the objective function for values of the independent variable slightly above and slightly below the initial trial point and observing the rate of change of the objective function. The partial derivative for each variable is then used to determine the next trial value for that variable. Finally, when the partial derivatives of the objective function for all independent variables are zero, it is considered that the optimum point has been determined.

A weakness of this method is the inability of the algorithm to distinguish between globally optimal and locally optimal points. As a result, the produced optimal values must

be evaluated based on the physical knowledge of the studied system or by observing the solver behavior for varying initial values of the optimization variables.

8 Simulation Results

An initial selection of four HT fluids and one LT fluid was made based on the available literature for similar applications. A further narrowing of the choices will be made by examining the fluids behavior at a design point.

Based on the speed profile of the vessel, and keeping in mind that the ORC system can be most beneficial in ballast mode and at high speeds, the initial design point is chosen to be the speed of 16 knots for the vessel in ballast mode. For this operating point and resulting waste heat streams, all combinations of fluids are examined to find the optimal parameters for the ORC system design.

8.1 Comparison of the Optimal Parameters for each Fluid Combination in the Dual Cycle

For each fluid, the design parameters which produce the best results and the results themselves are shown in Table 8.1 to Table 8.7.

The numbering of points in Table 8.4 to Table 8.7 is as per Figure 7.1.

Table 8.1: Dual Cycle Optimization Results

	Fluid combination	***R416a - R134a***	***Ammonia - R134a***	***R245fa - R134a***	***Water - R134a***	-
Optimal Decision Variables	$\dot{m}_{ORC,HT}$	23.2	5.2	20.6	2.0	kg/s
	$\dot{m}_{ORC,LT}$	43.0	43.9	42.1	43.4	kg/s
	$\Delta T_{sup,HT}$	213	207	164	199	°C
	$T_{max,HT}$	322	340	318	379	°C
	$P_{ev,HT}$	130	150	100	10	bar
	$P_{ev,LT}$	28.30	28.30	27.92	26.23	bar
	$\%CW$	0.0%	0.0%	0.0%	0.0%	-
Dual Cycle Performance	$\dot{W}_{net,2R}$	1366	1643	1572	1471	kW
	$\eta_{R,2R}$	0.079	0.093	0.090	0.108	-
	$\eta_{Q,2R}$	0.774	0.787	0.782	0.667	-
	$\eta_{TOT,2R}$	0.061	0.073	0.070	0.072	-
	$\zeta_{R,2R}$	0.084	0.100	0.096	0.116	-

Table 8.2: HT Cycle Optimization Results						
	Fluid combination	***R416a - R134a***	***Ammonia - R134a***	***R245fa - R134a***	***Water - R134a***	
HT Cycle Performance	$\dot{m}_{ORC,HT}$	23.2	5.2	20.6	2.0	kg/s
	$\dot{W}_{net,HT}$	625.1	905.5	840.5	928.0	kW
	$\dot{W}_{net,HT}/\dot{m}_{ORC,HT}$	27.0	173.5	84.0	456.5	kJ/kg
	$\eta_{R,HT}$	0.083	0.116	0.109	0.160	-
	$\eta_{Q,HT}$	0.933	0.967	0.954	0.717	-
	$\eta_{TOT,HT}$	0.077	0.112	0.104	0.115	-
	$\zeta_{R,HT}$	0.088	0.123	0.115	0.170	-
	SP_{HT}	12.13	7.24	16.74	28.38	-
	VFR_{HT}	4.55	2.54	10.64	9.08	-
	RSP_{HT}	0.062	0.227	0.050	0.086	-
HT Cycle Components	$\dot{Q}_{AV,HT}$	8075.27	8075.27	8075.27	8075.27	kW
	$\dot{W}_{P,HT}$	378.73	168.69	254.48	3.12	kW
	$\dot{Q}_{H,HT}$	7532.79	7805.60	7701.78	5789.96	kW
	$\dot{W}_{T,HT}$	1003.82	1074.14	1094.94	931.15	kW
	$\dot{Q}_{C,HT}$	6758.29	6763.92	6714.20	4758.15	kW

Table 8.3: LT Cycle Optimization Results						
	Fluid combination	***R416a - R134a***	***Ammonia - R134a***	***R245fa - R134a***	***Water - R134a***	
LT Cycle Performance	$\dot{m}_{ORC,LT}$	43.0	43.9	42.1	43.4	kg/s
	$\dot{W}_{net,LT}$	740.6	737.7	731.5	543.3	kW
	$\dot{W}_{net,LT}/\dot{m}_{ORC,LT}$	17.22	16.80	17.39	12.53	kJ/kg
	$\eta_{R,LT}$	0.076	0.075	0.075	0.070	-
	$\eta_{Q,LT}$	0.685	0.685	0.684	0.634	-
	$\eta_{TOT,LT}$	0.052	0.052	0.051	0.044	-
	$\zeta_{R,LT}$	0.081	0.081	0.081	0.075	-
	SP_{LT}	27.76	27.93	27.65	27.44	-
	VFR_{LT}	2.91	2.92	2.86	3.10	-
	RSP_{LT}	0.018	0.018	0.018	0.016	-
LT Cycle Components	$\dot{Q}_{AV,LT}$	14285.99	14291.63	14241.90	12285.85	kW
	$\dot{W}_{P,LT}$	107.82	109.96	103.32	98.80	kW
	$\dot{Q}_{H,LT}$	9784.49	9790.13	9740.40	7784.35	kW
	$\dot{W}_{T,LT}$	848.46	847.66	834.83	642.12	kW
	$\dot{Q}_{C,LT}$	8938.79	8947.25	8905.80	7159.81	kW

Table 8.4: Extensive and Intensive Properties for Optimal R416a-R134a Dual Cycle						
		$\dot{m}$	$\dot{V}$	T	P	h
		(kg/s)	(m^3/h)	(°C)	(bar)	(kJ/kg)
LT Cycle	1	43.00	134.87	39.76	10.10	256.05
	2		134.03	41.47	28.30	258.31
	3		134.03	41.47	28.30	258.31
	4		171.49	83.26	28.30	328.69
	5		1344.78	121.74	28.30	485.86
	6		3914.19	81.61	10.10	463.94
HT Cycle	7	23.17	89.59	88.41	26.84	324.62
	8		80.15	105.45	130.00	339.34
	9		243.46	321.52	130.00	664.46
	10		1107.75	256.79	26.84	616.32
	g_i	29.02	-	423.71	-	-
	g_o		-	203.88	-	-

Table 8.5: Extensive and Intensive Properties for Optimal Ammonia-R134a Dual Cycle						
		$\dot{m}$	$\dot{V}$	T	P	h
		(kg/s)	(m^3/h)	(°C)	(bar)	(kJ/kg)
LT Cycle	1	43.90	137.73	39.85	10.13	256.19
	2		136.88	41.56	28.30	258.44
	3		136.88	41.56	28.30	258.44
	4		173.83	82.66	28.30	327.38
	5		1342.62	118.31	28.30	481.46
	6		3919.52	77.86	10.13	460.00
HT Cycle	7	5.22	38.61	88.41	49.51	792.27
	8		37.85	96.17	150.00	821.36
	9		337.57	339.72	150.00	2317.14
	10		858.84	228.74	49.51	2088.43
	g_i	29.02	-	423.71	-	-
	g_o		-	195.92	-	-

Table 8.6: Extensive and Intensive Properties for Optimal R245fa-R134a Dual Cycle						
		$\dot{m}$	$\dot{V}$	T	P	h
		(kg/s)	(m^3/h)	(°C)	(bar)	(kJ/kg)
LT Cycle	1	42.07	131.93	39.73	10.09	256.01
	2		131.13	41.41	27.92	258.22
	3		131.13	41.41	27.92	258.22
	4		184.46	82.77	27.92	330.16
	5		1362.40	124.44	27.92	489.76
	6		3892.65	85.23	10.09	467.71
HT Cycle	7	20.63	65.20	88.41	9.69	321.86
	8		63.17	96.35	100.00	332.96
	9		219.55	317.89	100.00	706.20
	10		2335.00	240.31	9.69	647.24
	g_i	29.02	-	423.71	-	-
	g_o		-	198.95	-	-

Table 8.7: Extensive and Intensive Properties for Optimal Water-R134a Dual Cycle						
		$\dot{m}$	$\dot{V}$	T	P	h
		(kg/s)	(m^3/h)	(°C)	(bar)	(kJ/kg)
LT Cycle	1	43.37	135.06	37.82	9.58	253.17
	2		134.33	39.35	26.23	255.22
	3		134.33	39.35	26.23	255.22
	4		191.22	79.82	26.23	325.00
	5		1068.54	82.96	26.23	434.72
	6		3312.61	37.82	9.58	418.27
HT Cycle	7	2.03	7.57	88.41	0.66	370.36
	8		7.57	88.57	10.00	371.74
	9		2170.29	379.09	10.00	3219.99
	10		19707.00	115.42	0.66	2711.03
	g_i	29.02	-	423.71	-	-
	g_o		-	254.74	-	-

As can be readily seen from the above, as well as from Figure 8.1, the Ammonia-R134a has the highest overall power output, though the R245fa-R134a and Water-R134a cycles follow closely behind achieving 95.7% and 89.5% of the maximum dual cycle output, respectively.

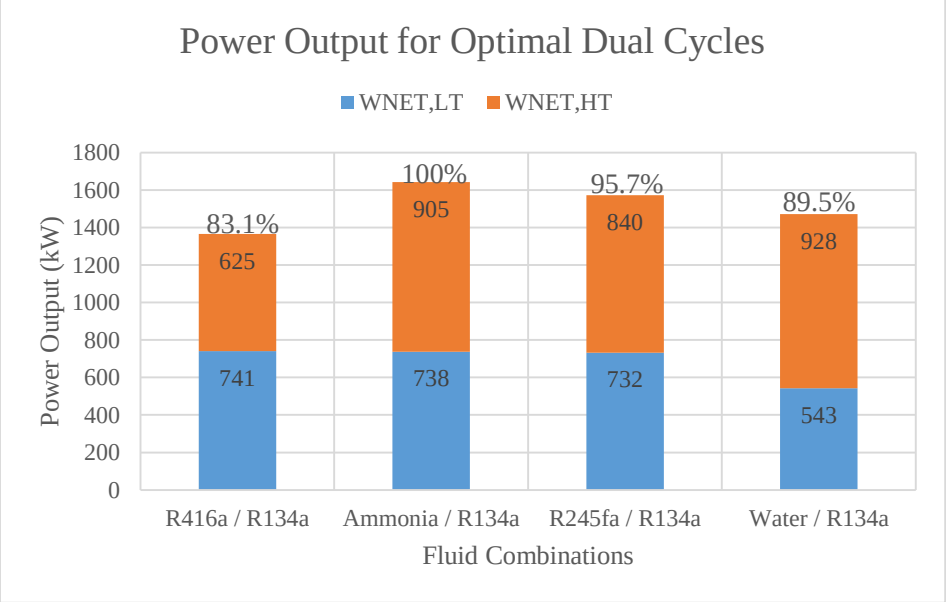

Figure 8.1: Optimum Dual Cycle Power Output

In terms of first and second law efficiency, the Water-R134a cycle takes the lead with the dual cycles topped by ammonia and R245fa following.

The mass flows for the optimum HT cycles are markedly lower for the two wet fluids (for ammonia, $\dot{m}_{ORC,HT} = 5.2\ kg/s$ and for water $\dot{m}_{ORC,HT} = 2\ kg/s$) compared to the dry R245fa ($\dot{m}_{ORC,HT} = 20.6\ kg/s$) and the isentropic R416a ($\dot{m}_{ORC,HT} = 23.2\ kg/s$). This can be attributed to to the larger enthalpy of vaporization for wet fluids.

The mass flows for the optimum LT cycles are similar, around $\dot{m}_{ORC,LT} = 42 - 43\ kg/s$ in all cases.

Due to its high optimal pressure, in terms of the size parameter and volume flow ratio, ammonia outperforms the other HT fluids, having the lowest SP and VFR value among the four, a fact which suggests a compact turbine size. However its rotational speed parameter exceeds that of the other four fluids indicating that a tradeoff for the small turbine size could be high turbine speeds.

The most notable and important difference among the cycles is the HT evaporation pressure, which is markedly lower for water than for the other cycles. In fact, when the maximum evaporation pressure is limited to 50 bar, the picture for overall cycle performance changes significantly, as can be seen in Figure 8.2.

Ammonia is completely excluded as its condensation pressure is already above 50 bar and the performance of both the R416a and R245fa topped cycles is reduced. The Water-R134a cycle is the best performer but is very closely followed by the R245fa-R134a cycle, which, while having a reduced power output compared to the case with unlimited pressure, still performs well.

The new optimum cycle parameters for the fluids whose power output is reduced by the 50 bar limit are shown in Table 8.8 to Table 8.12.

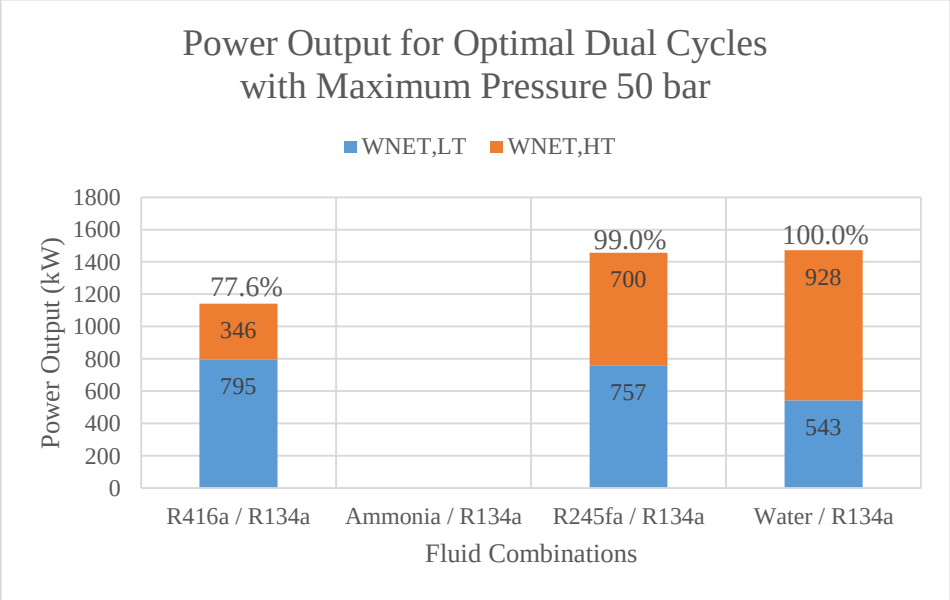

Figure 8.2: Optimum Dual Cycle Power Output with Maximum Pressure 50 bar

Table 8.8: Dual Cycle Optimization Results with Maximum Pressure 50 bar				
Optimal Decision Variables	***Fluid combination***	***R416a-R134a***	***R245fa-R134a***	-
	$\dot{m}_{ORC,HT}$	27.8	20.9	kg/s
	$\dot{m}_{ORC,LT}$	44.9	42.4	kg/s
	$\Delta T_{sup,HT}$	158	149	°C
	$T_{max,HT}$	266.0	302.8	°C
	$P_{ev,HT}$	50	50	bar
	$P_{ev,LT}$	28.33	27.85	bar
	$\%CW$	0.0%	0.0%	-
Dual Cycle Performance	$\dot{W}_{net,2R}$	1142	1457	kW
	$\eta_{R,2R}$	0.061	0.080	-
	$\eta_{Q,2R}$	0.805	0.796	-
	$\eta_{TOT,2R}$	0.049	0.064	-
	$\zeta_{R,2R}$	0.065	0.086	-

Table 8.9: HT Cycle Optimization Results with Maximum Pressure 50 bar				
	Fluid combination	***R416a-R134a***	***R245fa-R134a***	
HT Cycle Performance	$\dot{m}_{ORC,HT}$	27.77	20.86	kg/s
	$\dot{W}_{net,HT}$	346.3	700.2	kW
	$\dot{W}_{net,HT}/\dot{m}_{ORC,HT}$	12.47	70.02	kJ/kg
	$\eta_{R,HT}$	0.043	0.088	-
	$\eta_{Q,HT}$	0.995	0.983	-
	$\eta_{TOT,HT}$	0.043	0.087	-
	$\zeta_{R,HT}$	0.046	0.093	-
	SP_{HT}	16.64	18.45	-
	VFR_{HT}	1.85	5.23	-
	RSP_{HT}	0.028	0.039	-
HT Cycle Components	$\dot{Q}_{AV,HT}$	8075.27	8075.27	kW
	$\dot{W}_{P,HT}$	107.11	115.99	kW
	$\dot{Q}_{H,HT}$	8037.84	7939.32	kW
	$\dot{W}_{T,HT}$	453.38	816.18	kW
	$\dot{Q}_{C,HT}$	7630.48	7136.85	kW

Table 8.10: LT Cycle Optimization Results with Maximum Pressure 50 bar				
	Fluid combination	***R416a-R134a***	***R245fa-R134a***	
LT Cycle Performance	$\dot{m}_{ORC,LT}$	44.87	42.45	kg/s
	$\dot{W}_{net,LT}$	795.3	756.5	kW
	$\dot{W}_{net,LT}/\dot{m}_{ORC,LT}$	17.72	17.82	kJ/kg
	$\eta_{R,LT}$	0.075	0.074	-
	$\eta_{Q,LT}$	0.703	0.693	-
	$\eta_{TOT,LT}$	0.052	0.052	-
	$\zeta_{R,LT}$	0.080	0.080	-
	SP_{LT}	28.44	27.90	-
	VFR_{LT}	2.81	2.79	-
	RSP_{LT}	0.018	0.018	-
LT Cycle Components	$\dot{Q}_{AV,LT}$	15158.19	14664.55	kW
	$\dot{W}_{P,LT}$	111.53	103.28	kW
	$\dot{Q}_{H,LT}$	10656.69	10163.05	kW
	$\dot{W}_{T,LT}$	906.79	859.81	kW
	$\dot{Q}_{C,LT}$	9749.52	9300.66	kW

Table 8.11: Extensive and Intensive Properties for Optimal R416a-R134a Dual Cycle with Maximum Pressure 50 bar						
		$\dot{m}$	$\dot{V}$	T	P	h
		(kg/s)	(m^3/h)	(°C)	(bar)	(kJ/kg)
LT Cycle	1	44.87	141.20	40.65	10.34	257.38
	2		140.31	42.36	28.33	259.62
	3		140.31	42.36	28.33	259.62
	4		177.36	82.52	28.33	327.06
	5		1478.29	130.71	28.33	497.13
	6		4156.22	92.22	10.34	474.67
HT Cycle	7	27.77	107.39	88.41	26.84	324.62
	8		103.27	93.38	50.00	328.09
	9		689.88	266.02	50.00	617.50
	10		1279.45	242.37	26.84	599.36
	g_i	29.02	-	423.71	-	-
	g_o		-	189.14	-	-

Table 8.12: Extensive and Intensive Properties for Optimal R245a-R134a Dual Cycle with Maximum Pressure 50 bar						
		$\dot{m}$	$\dot{V}$	T	P	h
		(kg/s)	(m^3/h)	(°C)	(bar)	(kJ/kg)
LT Cycle	1	42.45	133.34	40.16	10.21	256.65
	2		132.52	41.82	27.85	258.84
	3		132.52	41.82	27.85	258.84
	4		187.70	82.64	27.85	330.13
	5		1434.10	131.18	27.85	498.26
	6		4004.67	93.10	10.21	475.75
HT Cycle	7	20.86	65.90	88.41	9.69	321.86
	8		64.87	92.14	50.00	326.87
	9		465.16	302.80	50.00	707.55
	10		2433.49	253.79	9.69	664.07
	g_i	29.02	-	423.71	-	-
	g_o		-	192.01	-	-

8.2 Parametric Analysis per Fluid Combination in the Dual Cycle

8.2.1 R416a-R134a Dual Cycle

Among the examined HT fluids, R-416a is the only zeotropic mixture. It also has the lowest critical properties with a critical temperature just above that of the LT fluid R134a. At the designed condensation temperature, its saturation pressure is 26.8 bar, corresponding to a reduced evaporation pressure of 0.68. This means that the examined evaporation pressures for the HT cycle must be above this point and will therefore be mostly supercritical.

For supercritical cycles, as the pressure in the HT cycle rises, the power output of the HT cycle predictably increases. Simultaneously, the load on the HT condenser falls. As a result, the heat input to the LT cycle falls and the power output of the LT cycle falls with it. This effect produces the result shown in Figure 8.3. It is notable that for this fluid combination, the LT cycle has a higher output than the HT cycle.

As can be seen in Figure 8.4, the power output for the LT cycle is reduced with higher HT evaporation pressures, as can be expected since the cycle mass flow is falling. The LT evaporation pressure is fairly steady, limited by the pinch point restriction in the HT condenser. The mass flow and superheating in the HT cycle vary conversely as the pinch point limitation shifts from a point near the HT evaporator outlet for low pressures to a point near the HT evaporator inlet for high pressures.

As can be seen in Figure 8.5, the thermal efficiency is increased for higher pressures, while the heat recovery efficiency is slightly decreased. The maximum values for heat recovery efficiency are around 0.8. This is because, due to the pinch point limitation in the condenser of the LT cycle, it is not possible to absorb heat from the engine LT cooling water. In order to cool the LT working fluid, the sea water in the LT condenser is heated

by around 10°C from 25 to around 35°C. The engine LT cooling water is at a temperature near 40°C. In case it were to be cooled by the LT ORC fluid, the load on the LT condenser would increase. The temperature of the seawater at the condenser outlet would increase as well and the pinch point limitation would be exceeded.

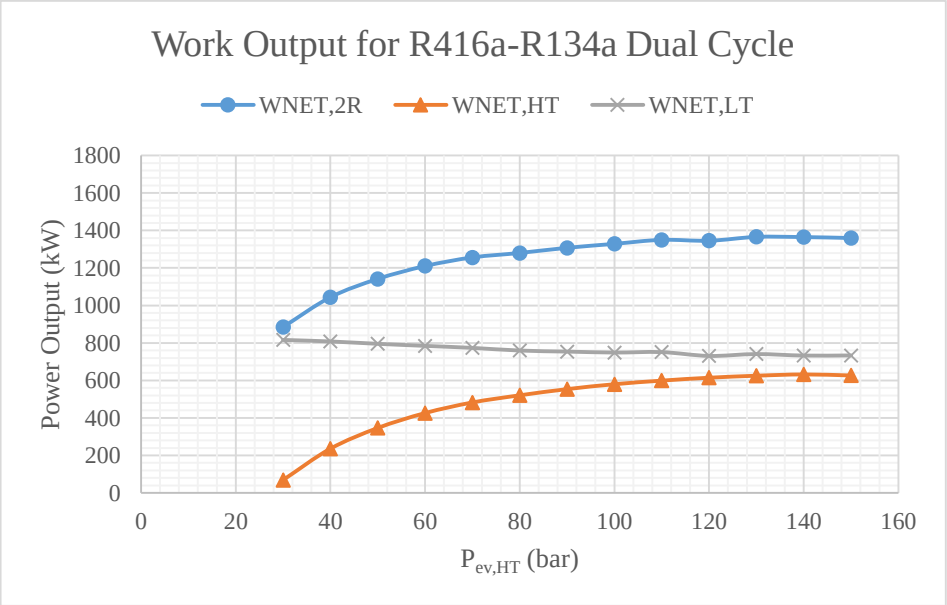

Figure 8.3: Power Output for R416a-R134a Dual Cycle

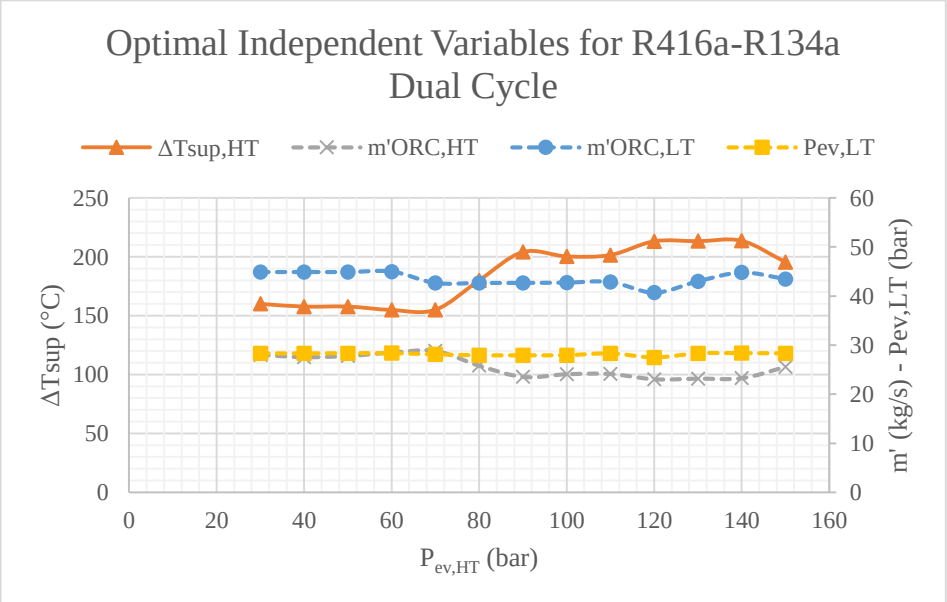

Figure 8.4: Optimal Independent Variables for R416a-R134a Dual Cycle

Interesting observations can be drawn from Figure 8.6 which shows the parameters which indicate the potential system size for the HT cycle. For high HT evaporation pressures, the size parameter (SP) is reduced, suggesting that the turbine will be smaller as pressure is increased. The power-mass flow ratio is similarly increased meaning the overall system will be more compact. The tradeoff for these benefits is the higher volume flow ratio (VFR) at high pressures, indicating a larger flow but also a worse isentropic turbine

efficiency. Furthermore, at high pressures the rotational speed parameter is increased, indicating higher turbine speeds.

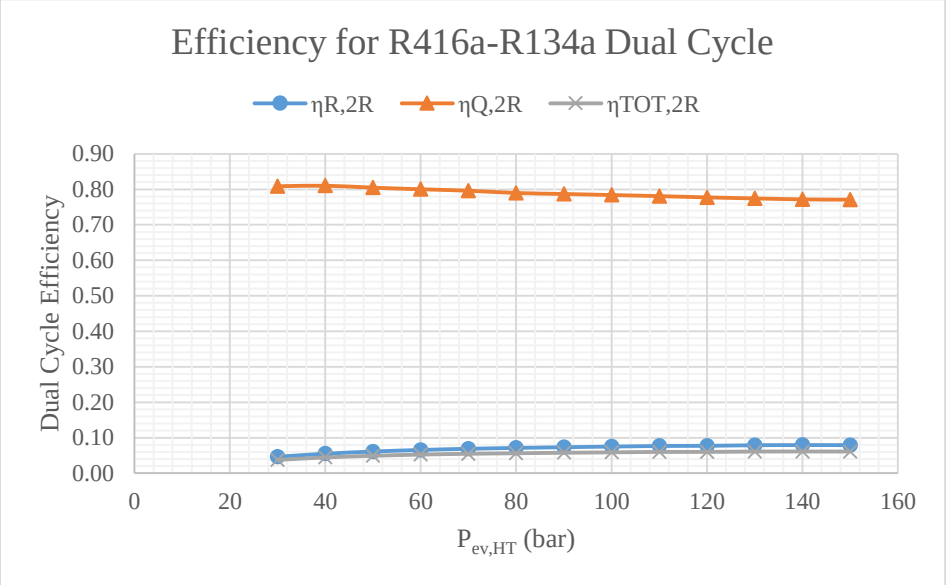

Figure 8.5: Efficiency for R416a-R134a Dual Cycle

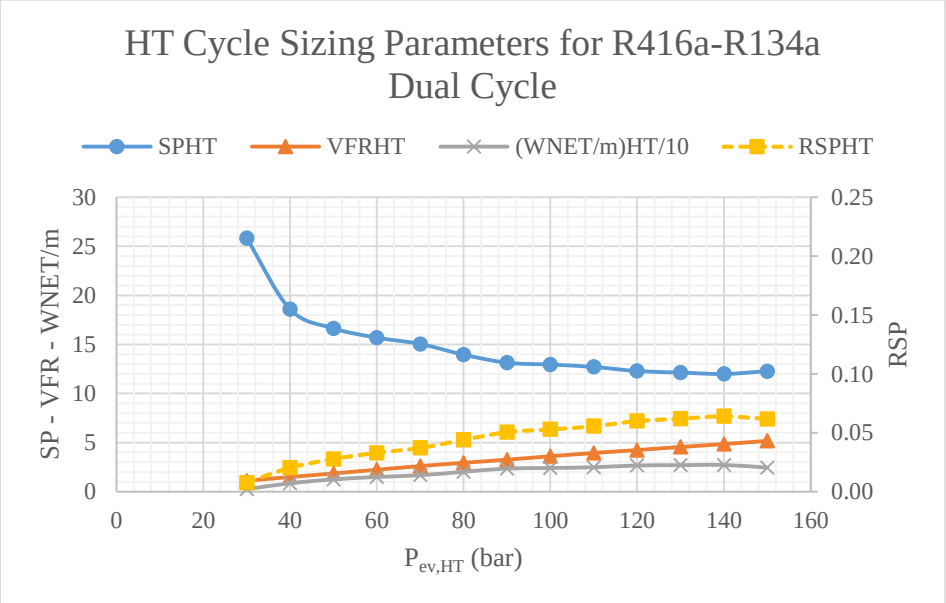

Figure 8.6: HT Cycle Sizing Parameters for R416a-R134a Dual Cycle

8.2.2 Ammonia-R134a Dual Cycle

Ammonia is a wet fluid with a moderate critical temperature (132.3°C) and a relatively high critical pressure (113.3 bar) which means high pressures will be required to achieve supercritical cycles.

In fact, at the designed condensation temperature of 88^{0}C, the corresponding saturation pressure is 49.5 bar, meaning all evaporation pressures must be above this point. This limitation seems to matter little for the performance of the Ammonia-R134a dual cycle as the power output of both the HT cycle and the dual cycle overall steadily increase

for increasing HT evaporation pressures, as can be seen in Figure 8.7. The power output follows a similar trend to that seen for the R416a-R134a dual cycle, with the explanations given for that cycle being applicable here as well.

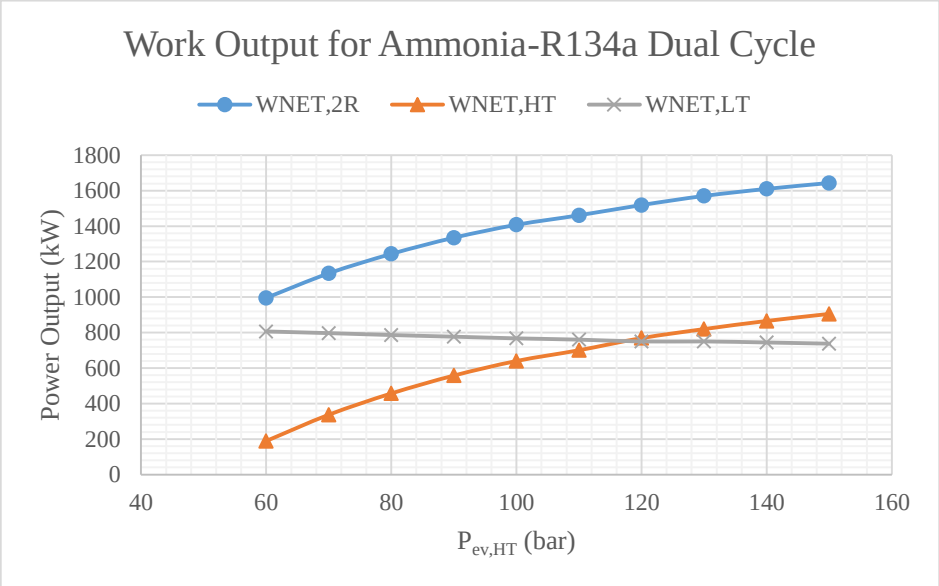

Figure 8.7: Power Output for Ammonia-R134a Dual Cycle

In fact, as depicted in Figure 8.8, the independent variables for the optimum cycle at each evaporation temperature vary quite little with the superheating ranging from 200-230°C, the HT mass flow taking values around 5.2-5.4 kg/s, the LT mass flow taking values around 44-46 kg/s and the LT evaporation pressure hovering at 28.3 bar. It is clear that the decisive parameter in this case is the HT evaporation pressure.

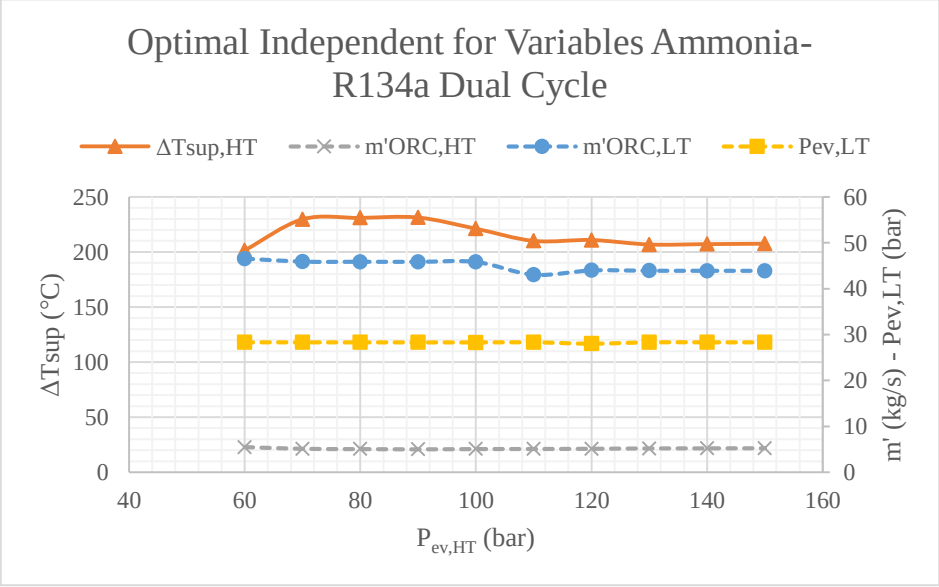

Figure 8.8: Optimal Independent Variables for Ammonia-R134a Dual Cycle

The heat recovery efficiency varies quite little as well. Again the recovery of the engine LT cooling water heat is not possible. The thermal efficiency in this case is a more

crucial parameter, increasing with increased HT evaporation pressure, but still being limited to values around 0.10, as can be seen in Figure 8.9.

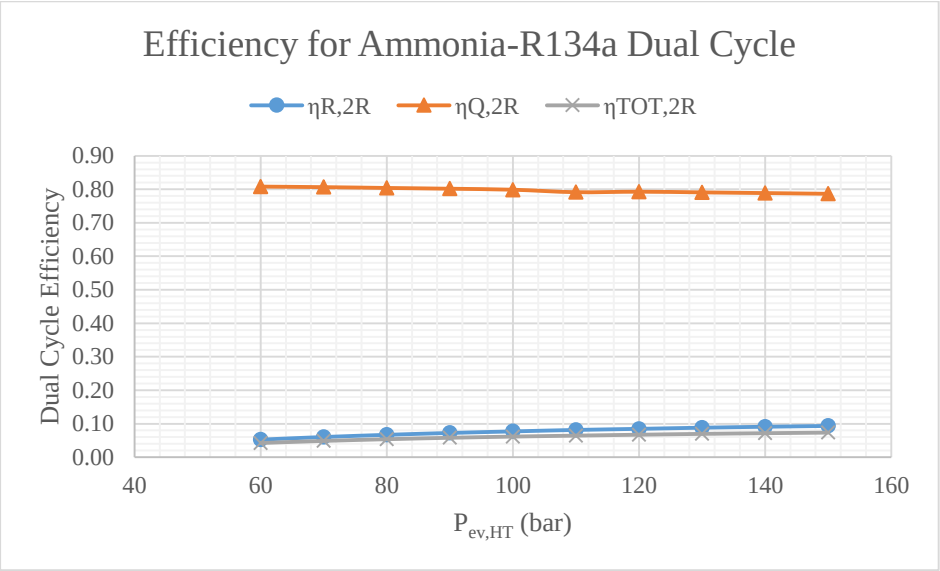

Figure 8.9: Efficiency for Ammonia-R134a Dual Cycle

While the benefit of high pressure can be clearly seen from the above, it can be noted once again that high HT evaporation pressures, while having a positive effect on the size parameter and power-mass flow ratio of the HT cycle, are accompanied by higher vlaues of the volume flow ratio and rotational speed parameter. This means higher pressures require larger and more complex turbines as well as increased turbine speeds.

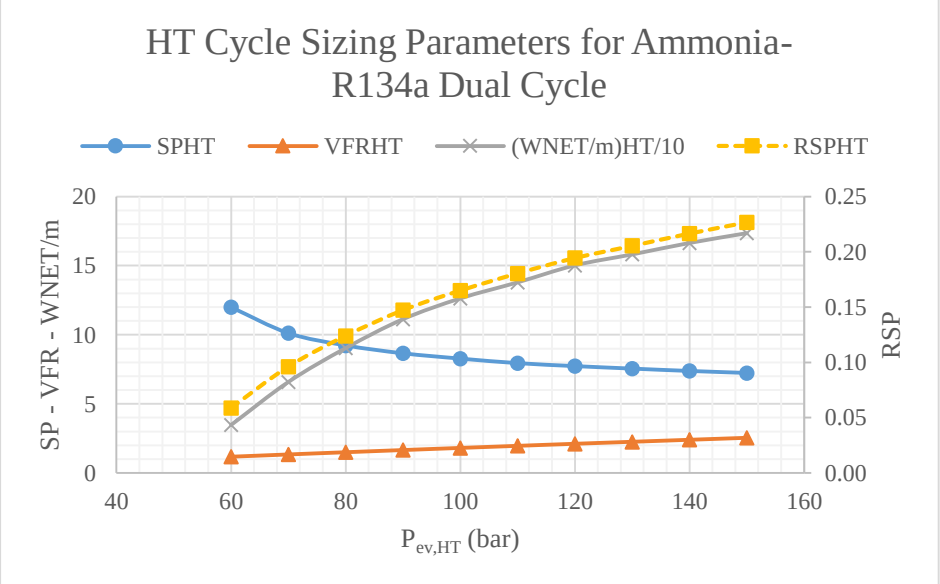

Figure 8.10: HT Cycle Sizing Parameters for Ammonia-134a Dual Cycle

8.2.3 R245fa-R134a Dual Cycle

The saturation pressure for R-245fa at the studied condensation temperature is 9.7 bar so the evaporation pressure must be higher than the same value.

The power output and efficiency of the R245fa-R134a dual cycle follows a similar trend to that shown by the Ammonia-R134a cycle.

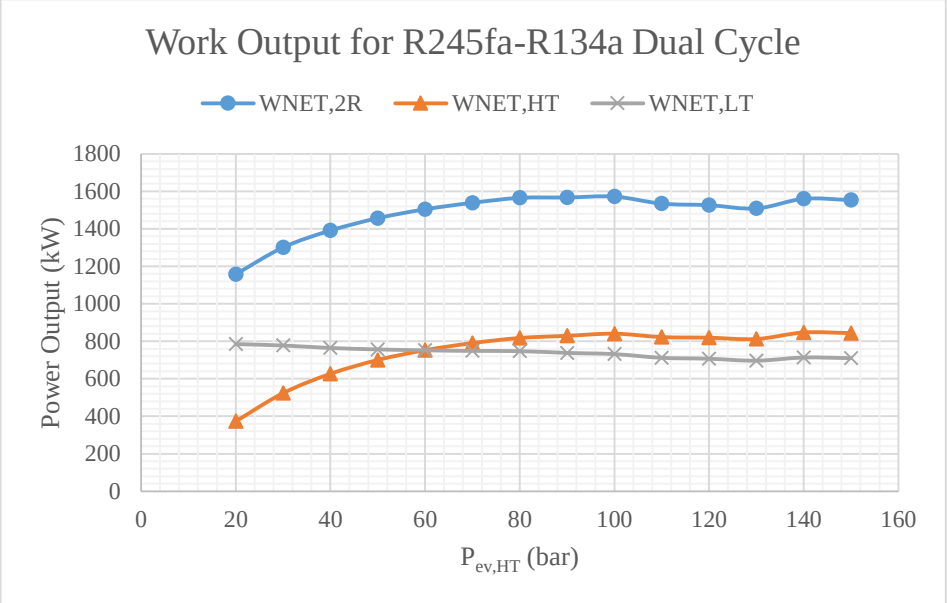

Figure 8.11: Power Output for R245fa-R134a Dual Cycle

Power output for the HT cycle and dual cycle as well as the thermal efficiency are steadily increased with rising pressure, while the output for the low temperature cycle and the heat recovery efficiency fall slightly. Again the recovery of the engine LT cooling water heat is not possible.

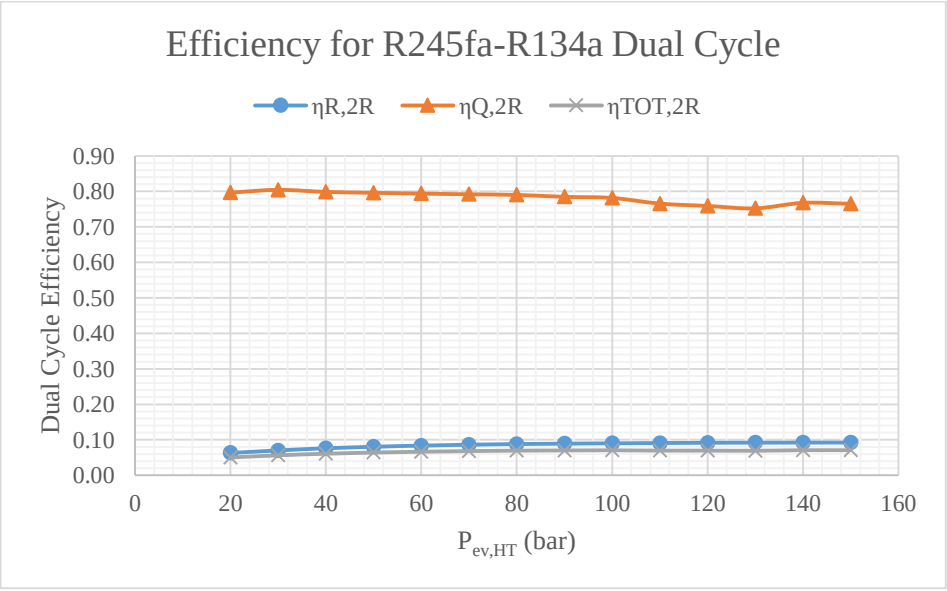

Figure 8.12: Efficiency for R245fa -R134a Dual Cycle

The independent variables do not vary too widely with the mass flows and LT evaporation pressure being slightly decreased for increased HT evaporation pressure and the degree of superheating being increased. A significant change in the superheating and

HT fluid mass flow is noted only near the critical pressure (36.5 bar). Again the pressure in the HT cycle is the decisive parameter.

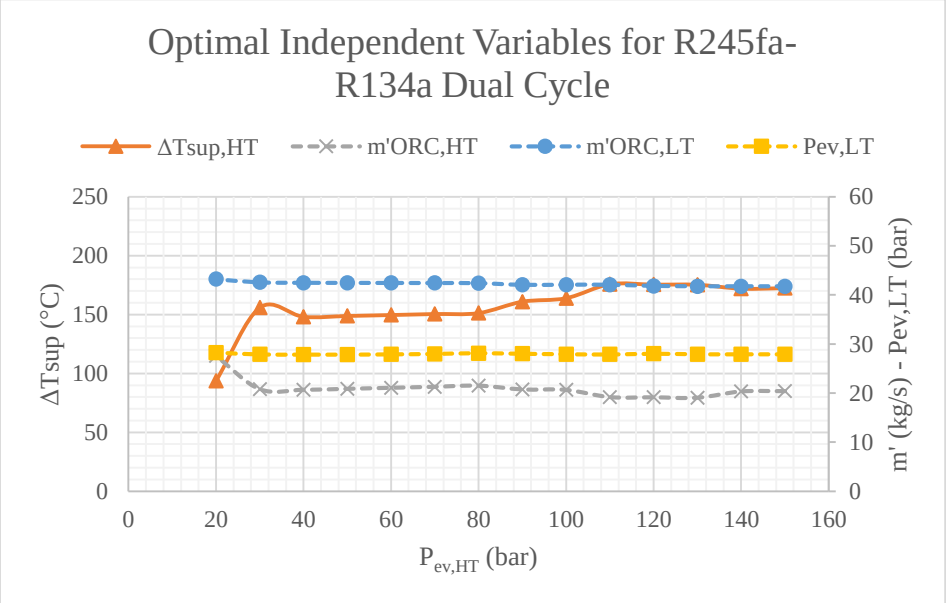

Figure 8.13: Optimal Independent Variables for R245fa-R134a Dual Cycle

Once again, a trade-off can be seen between high pressure and power output and turbine complexity and speed with high pressures being accompanied by high VFR and RSP values.

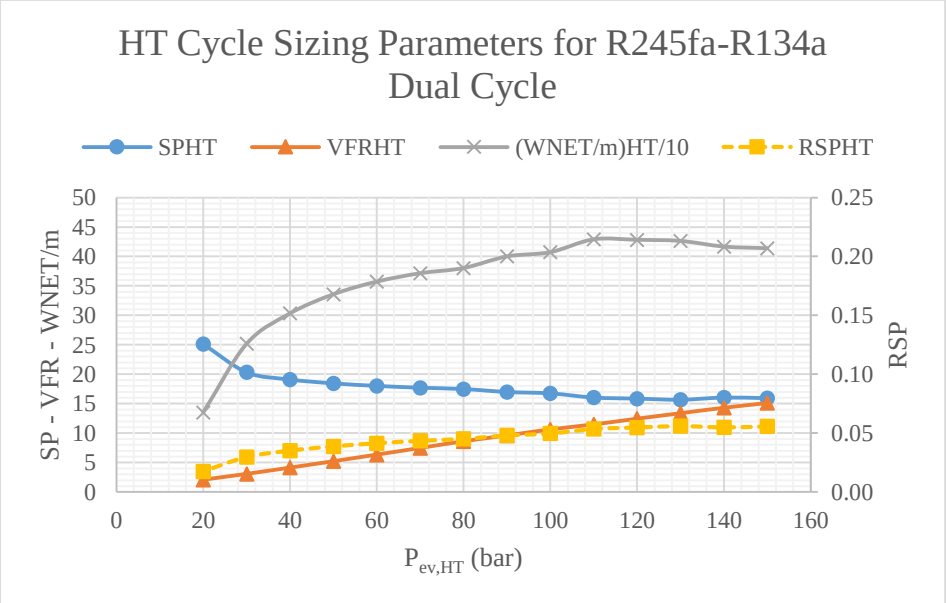

Figure 8.14: HT Cycle Sizing Parameters for R245fa –R134a Dual Cycle

8.2.4 Water-R134a Dual Cycle

For water as a working fluid, the maximum feasible evaporation pressure for the HT cycle is much lower than that allowed for the other fluids. The limitation is the maximum allowed wetness which is exceeded for high pressures as explained in Section 2.1.2.

Nevertheless, it is at a fairly low evaporation pressure that this cycle is able to achieve the best performance with the optimum evaporation pressure occurring at 10 bar as can be seen in Figure 8.15. At higher pressures, the dryness at the turbine outlet falls below the value of 1.

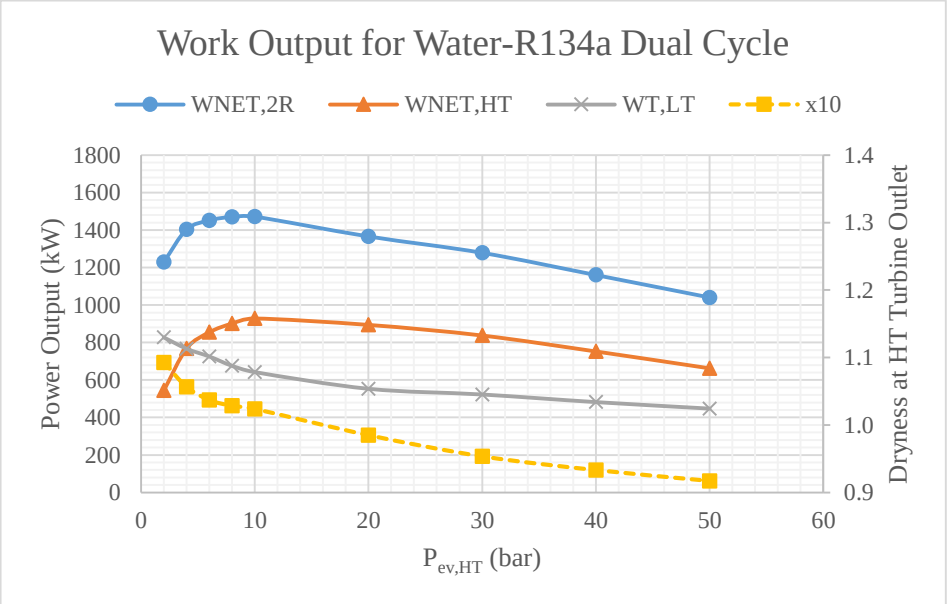

Figure 8.15: Power Output and Turbine Outlet Dryness for Water-R134a Dual Cycle

For HT evaporation pressures below the optimum, the power output of the HT and LT cycles vary conversely: as the power output of the HT cycle increases, the power output of the LT cycle decreases. This is related to the cooling load on the condenser, as in other cycles. However in addition to the reduced dryness or superheating at the turbine outlet as was the case for the other fluid combinations, here this effect is also related to the mass flow in the HT cycle, which is significantly increased for low evaporation pressures as can be seen in Figure 8.16.

Firstly, for HT evaporation pressures below the optimum, the degree of superheating is high so that HT fluid at the outlet of the turbine is a superheated vapor, as can be seen in Figure 8.15. At higher pressures, the feasible superheating is limited by the pinch point, which for higher pressures occurs at the outlet of the evaporator. As a result, the fluid at the outlet of the HT turbine is a steam-water mixture. The higher the HT evaporation pressure, the lower the dryness of the fluid at the turbine outlet, x_{10}, limiting the cooling load on the HT condenser. As a result, the heat input to the LT cycle and corresponding power output is reduced.

Furthermore, the higher mass flow for low evaporation pressures means that there is more fluid to be cooled, increasing the load on the HT cycle condenser. The heat rejected from the HT cycle is absorbed by the LT cycle, increasing its power output.

As can be seen from Figure 8.17, at the optimum point in terms of power output, the thermal efficiency is not maximized with higher thermal efficiencies occurring, predictably, at higher pressures. Nevertheless the heat recovery efficiency is high leading to an increased overall efficiency. This stresses the importance of considering both efficiencies for this type of application. Again for this fluid combination the recovery of the engine LT cooling water heat is not possible.

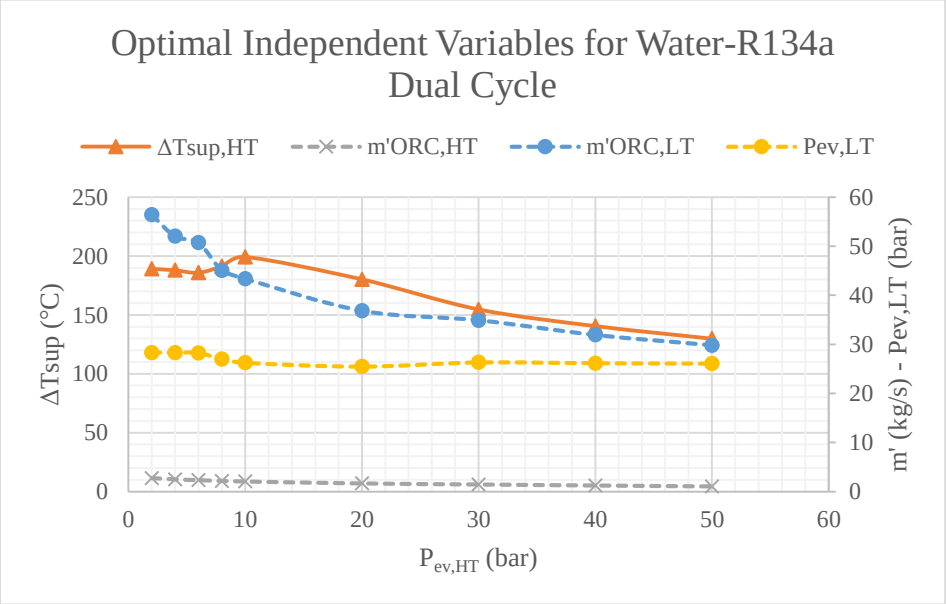

Figure 8.16: Optimal Independent Variables for Water-R134a Dual Cycle

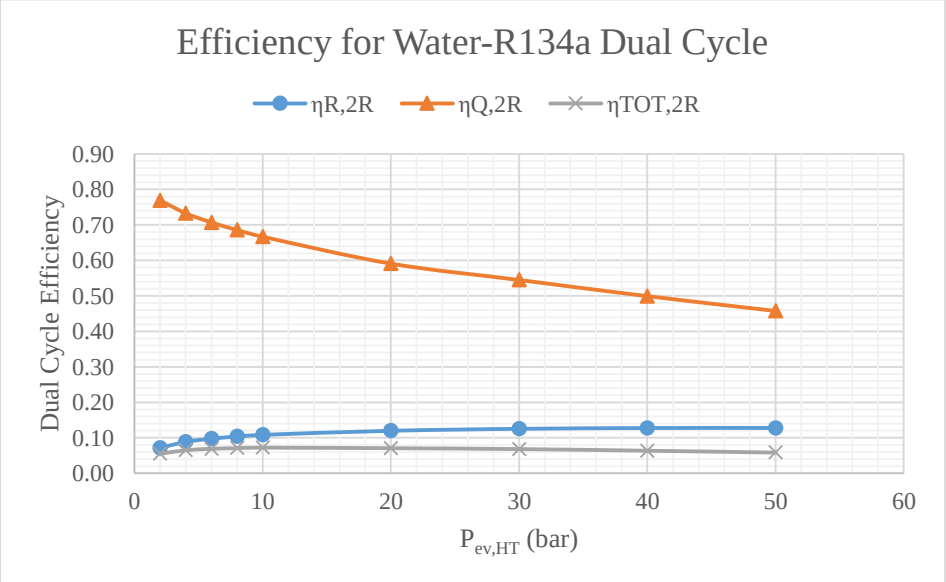

Figure 8.17: Efficiency for Water-R134a Dual Cycle

The sizing parameters for the Water-R134a dual cycle show similar behavior to that seen for the other fluid combinations as can be seen in Figure 8.18.

It is worth noting that at the chosen condensation temperature for the HT system, water is below its atmospheric boiling point meaning a vacuum will be needed to condense

it. As has been mentioned in the literature review, this is acceptable for water since, contrary to organic fluids, water is sufficiently chemically stable not to be in danger from infiltration.

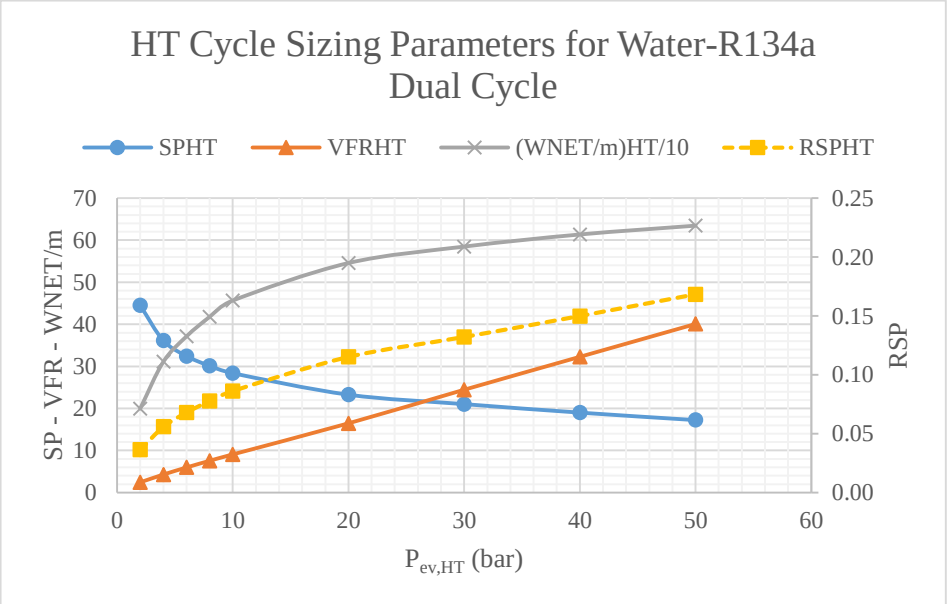

Figure 8.18: HT Cycle Sizing Parameters for Water-R134a Dual Cycle

8.3 Final System Selection and Performance over the Vessel Operating Profile

In the Section 8.1, it was determined that the most promising arrangements for the proposed application are the Water-R134a and R245fa-R134a dual cycles. For the selected cycles, the potential of the system at other speeds will be calculated. The following assumptions are made:

(1) Parameters which are considered to be constant are as follows:

a. The condensation temperature of the HT cycle is set to the maximum expected value for the HT CW at point HT9 in Figure 5.12.

b. The maximum HT evaporation pressure for the water cycle is set to 10.04 bar, maintaining the optimum pump and turbine pressure ratio from above. The HT evaporation pressure for the R245fa cycle is set to 50 bar.

c. The pump and turbine pressure ratio for the LT cycle is set constant to a value which allows feasible results for all engine load levels respecting the pinch point in the condenser and heater for all speeds. For the water-R134a cycle this is 2.3. For the R245fa-R134a cycle this is 1.9.

The value is lower for the latter cycle because, due to the higher mass flow required for the R245fa-R134a cycle, the load on the condenser is higher. This means that the seawater responsible for cooling the LT ORC fluid is heated to a higher temperature at the condenser outlet. In order to respect the pinch point restriction at this point, the LT ORC fluid minimum temperature must be increased.

At the same time, LT cycle maximum pressure is limited by the pinch point restriction in the common heat exchanger joining the HT and LT cycles. As a result, the feasible pressure ratio is reduced.

It is considered that the above listed parameters should be kept constant, especially the pressure ratios, because pumps and turbines are designed to work at or near a particular ratio with high efficiency.

(2) The following parameters are left to be optimized for each vessel speed:

a. Mass flow for the fluids: $\dot{m}_{ORC,HT}$, $\dot{m}_{ORC,LT}$

b. Superheating of HT fluid: $\Delta T_{sup,HT}$

These parameters can be fairly easily altered in an existing system by using partial recirculation of the relevant fluid.

(3) The change in efficiency for cycle components, specifically pumps and turbines, due to operation at off-design points is not considered.

Once the ORC system is put into use, it is clear that the total load on the engines will fall, while the load factor of each engine may decrease or increase depending on whether the same number of engines or fewer engines are required. As a result, the waste heat loads will change and the net power production of the dual cycle will change with them. This process will continue until an equilibrium is reached. The process can be modelled using an iterative method as shown for an example speed of 18 knots in ballast condition. This

speed presents particular interest, because the use of the dual cycle systems allows one less MGE to be run.

Table 8.13: Example of Finding the Equilibrium Point of Water-R134a Dual Cycle and Engines							
Voyage mode			Ballast				
Speed (kn)			18				
Power Required (kW)			22395.56				
Iteration	***No. of Engines***	***Engine Load***	***Engine Power***	***Dual Cycle Power***	***Total Power***	***Req. Total Power***	***Excess Power***
0	4	63.8050%	22396	1987.9	24383.5	22395.6	1987.9
1	3	77.5219%	20408	1573.3	21981.0	22395.6	-414.6
2	3	79.0968%	20822	1590.1	22412.4	22395.6	16.8
3	3	79.0328%	20805	1592.7	22398.2	22395.6	2.6
4	3	79.0229%	20803	1592.7	22395.5	22395.6	-0.1
5	3	79.0233%	20803	1592.7	22395.6	22395.6	0.0

8.3.1 Water-R134a Dual Cycle Performance over Vessel Operating Profile

The results of the iterative equilibrium process for each speed are given in Table 8.14 and Table 8.15, which show the final cycle parameters and operating point in laden and ballast mode, respectively.

Table 8.14: Water-R134a Dual Cycle Operating Point - Laden						
Speed (kn)	MGE Power (kW)	Dual Cycle Power (kW)	$\dot{m}_{ORC,HT}$ (kg/s)	$\dot{m}_{ORC,LT}$ (kg/s)	$\Delta T_{sup,HT}$ (°C)	$T_{max,HT}$ (°C)
14	11838.0	708.3	1.13	23.91	111.16	292.89
15	13800.7	841.7	1.32	30.05	112.72	294.45
16	15722.9	1241.6	1.81	39.91	200.88	382.60
17	18090.3	1431.1	2.09	46.98	193.54	375.26
18	20713.9	1608.8	2.30	54.98	200.04	381.77
19	23323.0	2054.7	3.05	68.63	189.35	371.07
20	28385.3	2271.0	3.35	77.33	188.18	369.91
21	29319.1	2442.9	3.53	87.33	184.48	366.21

Table 8.15: Water-R134a Dual Cycle Operating Point - Ballast						
Speed (kn)	MGE Power (kW)	Dual Cycle Power (kW)	$\dot{m}_{ORC,HT}$ (kg/s)	$\dot{m}_{ORC,LT}$ (kg/s)	$\Delta T_{sup,HT}$ (°C)	$T_{max,HT}$ (°C)
13	10471.8	762.0	1.00	35.26	105.46	287.18
14	12149.3	909.0	1.18	41.15	110.02	291.75
15	14017.0	1062.4	1.33	49.41	112.62	294.35
16	16022.0	1282.9	1.90	42.56	193.70	375.43
17	18300.6	1440.5	2.12	49.23	190.73	372.46
18	20802.9	1592.7	2.33	58.87	188.73	370.46
19	23230.6	2044.3	3.05	68.52	185.88	367.60
20	26136.8	2248.6	3.33	76.67	184.39	366.12
21	29319.2	2414.5	3.52	86.01	180.93	362.66

The dual cycle operating point with the maximum net power output is considered to be the sizing case based on which the cycle components will be dimensioned. For this point, relevant parameters are given in Table 8.16.

Table 8.16:Water-R134a Dual Cycle Sizing Case							
Speed (kn)				21			
Voyage Mode				Laden			
HT Cycle				***LT Cycle***			
Components Power	$\dot{W}_{NET}$	1579.52	kW	Components Power	$\dot{W}_{NET}$	863.42	kW
	$\dot{W}_P$	5.7	kW		$\dot{W}_P$	190.7	kW
	$\dot{Q}_H$	9946.6	kW		$\dot{Q}_H$	14654.4	kW
	$\dot{W}_T$	1585.2	kW		$\dot{W}_T$	1054.1	kW
	$\dot{Q}_C$	8190.4	kW		$\dot{Q}_C$	13654.8	kW
HT Heater	HT Fluid	Exhaust	-	LT Heater 1	HT Fluid	MGE HT CW	-
	LT Fluid	Water	-		LT Fluid	R134a	-
	$\dot{Q}$	9946.6	kW		$\dot{Q}$	6464.1	kW
	$\dot{m}_H$	48.0	kg/s		$\dot{m}_H$	137.6	kg/s
	c_{pH}	1.18	kJ/kgK		c_{pH}	4.19	kJ/kgK
	$T_{H,in}$	404.0	°C		$T_{H,in}$	89.2	°C
	$T_{H,out}$	228.38	°C		$T_{H,out}$	63.73	°C
	$T_{C,in}$	89.68	°C		$T_{C,in}$	47.58	°C
	$T_{C,out}$	366.21	°C		$T_{C,out}$	81.83	°C
	ΔT_{lm}	77.60	K		ΔT_{lm}	11.17	K
HT Cooler / LT Heater 2	HT Fluid	Water	-	LT Cooler	HT Fluid	R134a	-
	LT Fluid	R134a	-		LT Fluid	Seawater	-
	$\dot{Q}$	8190.4	kW		$\dot{Q}$	13654.8	kW
	$T_{H,in}$	106.66	°C		$T_{H,in}$	46.00	°C
	$T_{H,out}$	89.52	°C		$T_{H,out}$	46.00	°C
	$T_{C,in}$	81.83	°C		$T_{C,in}$	25.00	°C
	$T_{C,out}$	85.24	°C		$T_{C,out}$	39.90	°C
	ΔT_{lm}	13.40	K		ΔT_{lm}	12.05	K
Cycle Flow	$\dot{m}_{HT,ORC}$	3.53	kg/s	Cycle Flow	$\dot{m}_{LT,ORC}$	87.33	kg/s
	$\dot{V}_{P,in}$	13.17	m^3/hr		$\dot{V}_{P,in}$	280.57	m^3/hr
	$\dot{V}_{T,in}$	3537.18	m^3/hr		$\dot{V}_{T,in}$	2039.98	m^3/hr
	$\dot{V}_{T,out}$	32044.88	m^3/hr		$\dot{V}_{T,out}$	5299.48	m^3/hr

8.3.2 R245fa-R134a Performance over Vessel Operating Profile

The results of the iterative equilibrium process for each speed are given in Table 8.17 and Table 8.18 which show the final cycle parameters for each speed in laden and ballast mode respectively.

Table 8.17: R245fa-R134a Dual Cycle Operating Point - Laden

Speed (kn)	MGE Power (kW)	Dual Cycle Power (kW)	$\dot{m}_{ORC,HT}$ (kg/s)	$\dot{m}_{ORC,LT}$ (kg/s)	$\Delta T_{sup,HT}$ (°C)	$T_{max,HT}$ (°C)
14	11838.0	713.7	15.71	25.61	90.14	244.15
15	13800.7	833.8	17.92	30.77	91.07	245.08
16	15722.9	1144.1	25.35	43.46	89.81	243.82
17	18090.3	1289.3	28.72	46.57	86.45	240.46
18	20713.9	1447.9	32.10	53.54	84.37	238.38
19	23323.0	1801.2	40.49	65.05	84.83	238.84
20	28385.3	1989.0	44.37	72.83	84.39	238.40
21	29319.1	2181.3	47.91	81.85	83.65	237.66

Table 8.18: R245fa-R134a Dual Cycle Operating Point - Ballast

Speed (kn)	MGE Power (kW)	Dual Cycle Power (kW)	$\dot{m}_{ORC,HT}$ (kg/s)	$\dot{m}_{ORC,LT}$ (kg/s)	$\Delta T_{sup,HT}$ (°C)	$T_{max,HT}$ (°C)
13	10471.8	759.4	14.19	34.71	88.63	242.64
14	12149.3	880.2	16.35	43.36	87.57	241.58
15	14017.0	1021.9	18.03	49.17	92.46	246.47
16	16022.0	1162.6	25.24	41.56	93.67	247.68
17	18300.6	1301.3	28.65	47.13	88.67	242.68
18	20802.9	1450.9	31.56	53.74	88.04	242.05
19	23230.6	1794.8	39.98	64.83	86.71	240.72
20	26136.8	1971.6	43.97	72.00	84.75	238.76
21	29319.2	2152.6	47.10	80.53	84.90	238.91

The dual cycle operating point with the maximum net power output is considered to be the sizing case based on which the cycle components will be dimensioned. For this point, relevant parameters are given in Table 8.19.

Table 8.19: R245fa-R134a Dual Cycle Sizing Case							
Speed (kn)				21			
Voyage Mode				Laden			
HT Cycle				***LT Cycle***			
Components Power	$\dot{W}_{NET}$	1226.92	kW	Components Power	$\dot{W}_{NET}$	954.39	kW
	$\dot{W}_P$	265.7	kW		$\dot{W}_P$	137.3	kW
	$\dot{Q}_H$	13687.9	kW		$\dot{Q}_H$	18819.2	kW
	$\dot{W}_T$	1492.6	kW		$\dot{W}_T$	1091.7	kW
	$\dot{Q}_C$	12268.6	kW		$\dot{Q}_C$	17729.7	kW
HT Heater	HT Fluid	Exhaust	-	LT Heater 1	HT Fluid	MGE HT CW	-
	LT Fluid	R245fa	-		LT Fluid	R134a	-
	$\dot{Q}$	13687.9	kW		$\dot{Q}$	6550.6	kW
	$\dot{m}_H$	48.4	kg/s		$\dot{m}_H$	139.3	kg/s
	c_{pH}	1.18	kJ/kgK		c_{pH}	4.19	kJ/kgK
	$T_{H,in}$	402.9	°C		$T_{H,in}$	89.2	°C
	$T_{H,out}$	162.41	°C		$T_{H,out}$	56.90	°C
	$T_{C,in}$	93.27	°C		$T_{C,in}$	50.76	°C
	$T_{C,out}$	237.66	°C		$T_{C,out}$	77.07	°C
	ΔT_{lm}	110.31	K		ΔT_{lm}	8.80	K
HT Cooler / LT Heater 2	HT Fluid	R245fa	-	LT Cooler	HT Fluid	R134a	-
	LT Fluid	R134a	-		LT Fluid	Seawater	-
	$\dot{Q}$	12268.6	kW		$\dot{Q}$	17729.7	kW
	$T_{H,in}$	184.57	°C		$T_{H,in}$	107.24	°C
	$T_{H,out}$	89.52	°C		$T_{H,out}$	49.50	°C
	$T_{C,in}$	77.07	°C		$T_{C,in}$	25.00	°C
	$T_{C,out}$	131.64	°C		$T_{C,out}$	44.34	°C
	ΔT_{lm}	27.97	K		ΔT_{lm}	40.73	K
Cycle Flow	$\dot{m}_{HT,ORC}$	47.91	kg/s	Cycle Flow	$\dot{m}_{LT,ORC}$	81.85	kg/s
	$\dot{V}_{P,in}$	151.93	m^3/hr		$\dot{V}_{P,in}$	266.74	m^3/hr
	$\dot{V}_{T,in}$	818.23	m^3/hr		$\dot{V}_{T,in}$	3224.06	m^3/hr
	$\dot{V}_{T,out}$	4565.44	m^3/hr		$\dot{V}_{T,out}$	6208.33	m^3/hr

9 Thermo-economic and Environmental Analysis

In order to calculate the benefit of the dual cycle system and to compare the two proposed systems, the annual energy savings as well as the costs incurred to achieve them must be defined and translated into financial terms.

9.1 Energy Savings

As mentioned in previous sections, an important characteristic of LNG carriers is that, due to imperfect insulation, a part of their cargo is constantly and unavoidably boiling off and can be used as fuel.

Up to a certain speed, the fuel energy content of the naturally boiling gas is sufficient to cover the ship energy needs. Above this speed, forced vaporization must be used. The characteristic speed at which all of the vessel's energy requirements (both for propulsion and other loads) are met but not exceeded by the natural boil-off gas is called the natural boil-off speed. It is clear that for speeds below the NBOG speed, an energy saving device does not provide any benefit, because the available energy from the boiling cargo is already more than enough and there is no reliquefaction equipment installed on this vessel.

The NBOG speed can be calculated from the following set of equations:

$$\dot{E}_{NBOG} = \nabla_{CARGO} \cdot BOR \cdot LHV_{NBOG} \tag{9.1}$$

$$\dot{H}_{f,tot}(V_S) = \dot{E}_{NBOG} \tag{9.2}$$

where

- $\dot{E}_{NBOG}$ the thermal energy released by burning of natural boil-off gas per day.
- ∇_{CARGO} the cargo capacity in cubic meters
- BOR the vessel natural boil-off rate expressed as a fraction of the cargo capacity per day
- LHV_{NBOG} the lower heating value of natural gas expressed in kJ/m^3
- V_S the ship speed
- $\dot{H}_{f,tot}(V_S)$ the fuel energy required by the vessel to maintain an average speed of V_S and cover the corresponding accommodation loads for one day.

The determination of each of these components is described below.

(1) Available energy from NBOG

From Equation (9.1) it can be seen that the available energy is a function of the cargo capacity, BOR and heating value of the cargo.

The first of the three quantities, cargo capacity, is easily found as 98.5% of the cargo tank volume. This is a common filling restriction placed by the International Code for the Construction and Equipment of Ships Carrying Liquefied Gases in Bulk (IGC Code) and subsequently increased as allowed by relevant ship Administrations [70].

The latter quantities, BOR and LHV_{NBOG}, are less obvious and are closely intertwined.

Each LNGC is characterized by a nominal natural boil-off rate, which is dependent on the cargo containment system design and which is guaranteed by the system designer. The actual boil-off rate is more difficult to determine, as it is the result of many factors including the voyage leg, atmospheric conditions, sea state, cargo composition as well as the destination terminal's pressure and temperature requirements for cargo on arrival. For this reason, the boil-off rate is not constant, even throughout the course of a single voyage.

At the same time, the lower heating value (LHV) of the fuel will vary greatly depending on the nitrogen content. Even for a known composition, as a result of the varying volatility of the main components of LNG, the thermal characteristics of the resulting NBOG will change throughout the voyage.

Dimopoulos and Frangopoulos in [71] developed a dynamic model to predict the amount and composition of NBOG during an LNG carrier voyage. They found that the change in NBOG production, composition and as a result LHV varies greatly, so much so that the commonly applied assumption of constant boil-off rate and pure methane LHV is not accurate [71].

The volatile components which comprise the boil-off for cold cargo at the beginning of the voyage, i.e. methane and nitrogen, have a low molecular weight, 16 g/mol and 28 g/mol respectively, compared to heavier ethane (30 g/mol), butane (44 g/mol) and propane (58 g/mol). As a result, the molecular weight and therefore mass flow of the NBOG mixture is correspondingly reduced.

Of all the components in LNG, nitrogen is the most volatile (having the lowest boiling point) and so will evaporate quickly from the beginning of the voyage. The corresponding heat content of the NBOG will be low since incombustible nitrogen does not contribute to the energy release of the fuel.

These two effects can be seen in Figure 9.1.

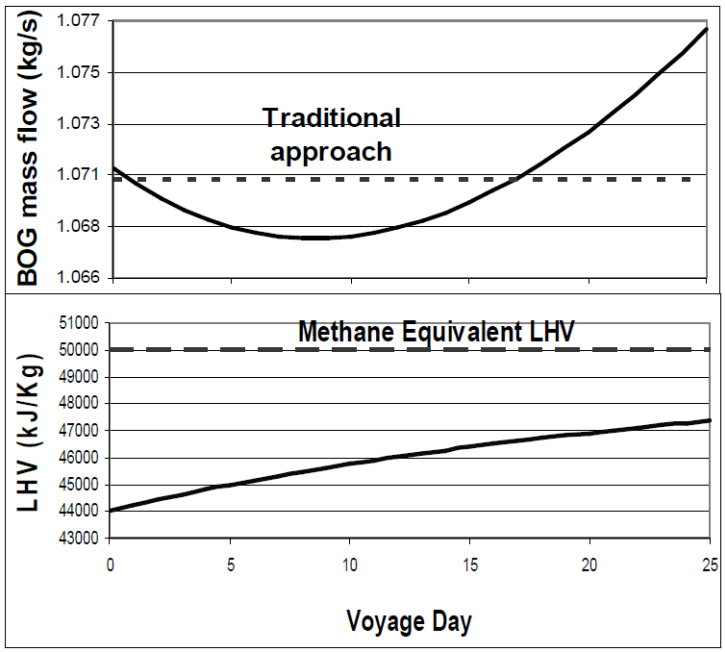

Figure 9.1: Change in BOG mass flow and LHV through a voyage [71]

Nevertheless, a detailed analysis of the changing BOR and LHV goes beyond the scope of the present study. Therefore, the following assumptions will be made:

(1) For the laden passage, the BOR will be assumed to be equal to a nominal value, given as a percentage of the cargo capacity. The effect of a varying nominal BOR will be examined by testing the results using varied figures for BOR.

(2) For the ballast passage, the BOR will be assumed to be equal to 45% of the nominal BOR for the laden passage. This is the practice assumed by the maker of the cargo containment system.

(3) The differing compositions of NBOG and FBOG will be taken into account as applicable.

The boil-off rate for the studied vessel is 0.125% of the total cargo volume per day. Some other nominal boil-off rates of the most widely-used, existing and planned membrane-type cargo containment systems will be investigated for comparison. The chosen rates are given in Table 9.1 for laden and corresponding ballast legs.

Table 9.1: Natural Boil-off Rates

Laden	***Ballast***
(%V_{CARGO}/day)	(%V_{CARGO}/day)
0.090	0.041
0.100	0.045
0.108	0.049
0.125	0.056
0.150	0.068

The initial LNG composition which will be examined, is taken from the capacity calculation for the vessel cargo handling equipment. Relevant properties are in Table 9.2.

Table 9.2: Relevant LNG properties

	Gas Composition - Mole fraction (%)	
	LNG	***NBOG***
Methane	93.16	92.56
Ethane	6.24	0.03
Propane	0.18	0.00
Butane	0.10	0.00
Nitrogen	0.32	7.41
	LNG Heating Value	
LHV (MJ/kg)	49.45	43.90
LHV (MJ/m^3)[11]	21957.6	19489.8
LNG Liquid Density	ρ (kg/m^3)	444

[11] It is important to note that while FBOG and NBOG are in gaseous form, the BOR as a percentage of the cargo capacity refers to liquid volume. For example, for a BOR of 0.125% and a cargo volume of 100,000 m^3, the cargo volume lost as boil-off each day will be 125 m^3 of liquid natural gas. The corresponding volume of gaseous natural gas which will be consumed is approximately 600 times larger. Therefore, the calculation of the LHV in MJ/m^3 using the LHV in MJ/kg and the liquid density is valid.

Knowing the cargo capacity, BOR and LHV of the NBOG, the energy provided by the NBOG can be calculated as in Table 9.3.

Table 9.3: NBOG energy release as a function of nominal BOR			
BOR		***Daily fuel energy release $\dot{E}_{NBOG}$***	
Laden	Ballast	Laden	Ballast
(%V_{CARGO}/day)	(m^3/day)	(kW)	(kW)
0.090	0.041	31965.2	14384.3
0.100	0.045	35516.9	15982.6
0.108	0.049	38358.2	17261.2
0.125	0.056	44396.1	19978.2
0.150	0.068	53275.3	23973.9

(2) Required Energy

The required energy in Equation (9.2), $\dot{H}_{f,tot}(V_S)$, is already known from Table 5.8 and Table 5.9 as a function of speed for each voyage mode, laden and ballast respectively.

(3) NBOG Speed

Knowing both the available energy as a function of BOR and the required energy as a function of speed, the NBOG speed for each nominal BOR can be calculated. A summary is given in Table 9.4.

Table 9.4: Calculated NBOG Speed			
BOR		***NBOG Speed***	
Laden	Ballast	Laden	Ballast
(%V_{CARGO}/day)	(m^3/day)	(kn)	(kn)
0.090	0.041	14.62	9.27
0.100	0.045	15.37	9.90
0.108	0.049	15.94	10.37
0.125	0.056	17.07	11.27
0.150	0.068	18.58	12.45

The same results can be seen graphically in Figure 9.2 and Figure 9.3.

For speeds below the NBOG speed, the available energy from the naturally boiling gas exceeds the power requirements of the vessel. In this case, any waste heat recovery system designed to produce additional power is not of use because there is no equipment on the particular vessel to re-liquefy the excess natural gas. However, for speeds above the NBOG speed, a waste heat recovery system can be used to produce power that would otherwise be provided by fuel oil or forced boil-off gas.

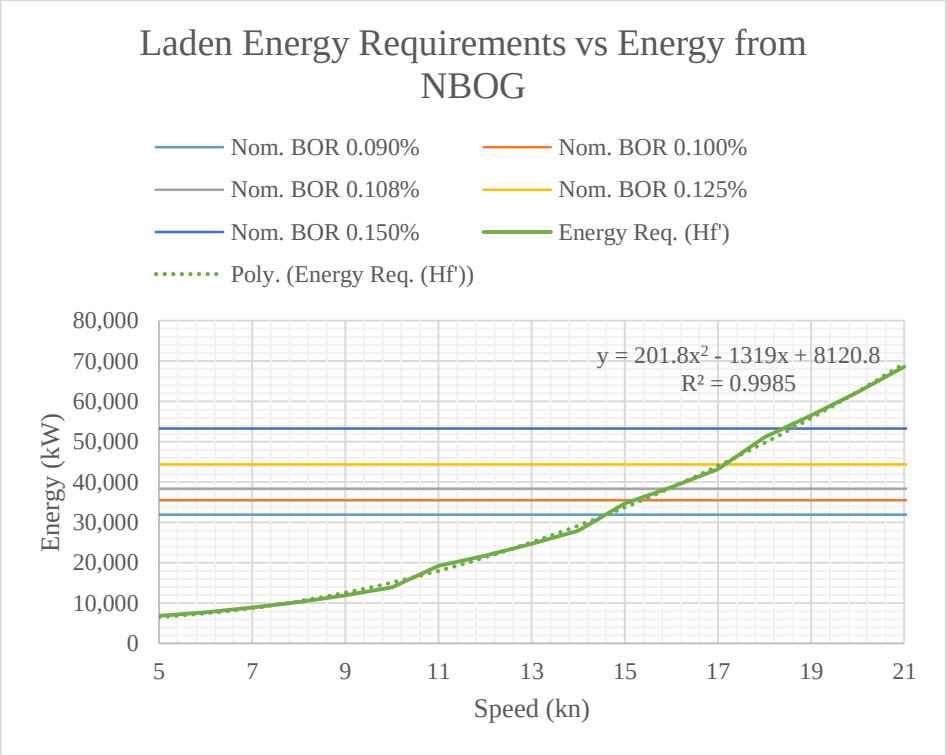

Figure 9.2: Graphical method of finding NBOG speed for laden voyage

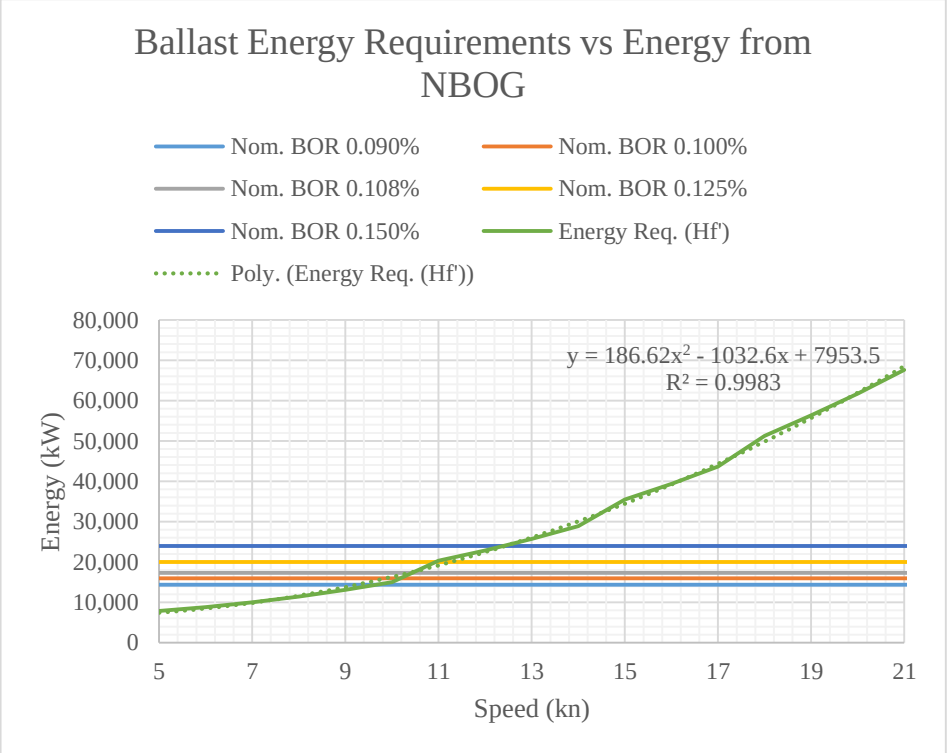

Figure 9.3: Graphical method of finding NBOG speed for ballast voyage

The preceding analysis can be used to determine when the dual cycle system will be in use. When the system is not in use, all required power must be covered by the main generator engines. The required mechanical and fuel power without the ORC system are given in Table 5.7 and Table 5.8.

When the system is in use, the power production required from the engines is known from the iterative process for equilibrium described in Section 0. Based on the reduced engine power needed with the dual cycle system in use, the new number of engines needed, n_{MGE}, and their new load factor, f_L, can be calculated. Then, using the specific fuel energy consumption (SFEC) of the engines, $\dot{q}_f$, as a function of the load factor, f_L, which is known from the engine maker, the new fuel energy needed by the engines can be deduced.

$$\dot{H}_{f,Tot} = \dot{q}_{f,j} \cdot \dot{W}_{m,MCR} \cdot f_L \cdot n_{MGE} \tag{9.3}$$

This calculation is shown for the Water-R134a dual cycle in Table 9.5 and Table 9.6, and for the R245fa-R134a cycle in Table 9.7 and Table 9.8.

Table 9.5: Power Production with Water-R134a Dual Cycle - Laden Voyage

Speed	***% Time at Spd***	***DC Power***	***MGE Power***	***Engines***		***SFEC***	***Fuel Power***	***Plant Effic.***
(kn)	(-)	(kW)	(kW)	Number	Load	(kW/kW)	(kW)	(-)
15	4.0%	842	13801	2	78.6%	2.17	29944	48.90%
16	4.8%	1241	15723	3	59.7%	2.34	36798	46.10%
17	4.5%	1431	18090	3	68.7%	2.25	40658	48.01%
18	5.0%	1609	20714	3	78.7%	2.17	44937	49.67%
19	4.4%	2054	23323	4	66.4%	2.27	52922	47.95%
20	1.8%	2271	28385	4	80.9%	2.16	61206	46.88%
21	0.7%	2443	29319	4	83.5%	2.14	62809	51.39%

Table 9.6: Power Production with Water-R134a Dual Cycle - Ballast Voyage

Speed	***% Time at Spd***	***DC Power***	***MGE Power***	***Engines***		***SFEC***	***Fuel Power***	***Plant Effic.***
(kn)	(-)	(kW)	(kW)	Number	Load	(kW/kW)	(kW)	(-)
13	1.7%	762	10472	2	59.7%	2.34	24515	45.82%
14	2.6%	909	12149	2	69.2%	2.24	27249	47.92%
15	1.7%	1062	14017	2	79.9%	2.16	30306	49.76%
16	5.0%	1283	16022	3	60.9%	2.33	37293	46.40%
17	3.6%	1441	18301	3	69.5%	2.24	40997	48.15%
18	2.8%	1593	20803	3	79.0%	2.17	45086	49.67%
19	4.2%	2044	23231	4	66.2%	2.27	52772	47.89%
20	2.9%	2249	26137	4	74.5%	2.20	57475	49.39%
21	0.8%	2415	29319	4	83.5%	2.14	62809	50.52%

Table 9.7: Power Production with R245fa- R134a Dual Cycle - Laden Voyage								
Speed	***% Time at Spd***	***DC Power***	***MGE Power***	***Engines***		***SFEC***	***Fuel Power***	***Plant Effic.***
(kn)	(-)	(kW)	(kW)	Number	Load	(kW/kW)	(kW)	(-)
15	4.0%	714	11833	2	67.4%	2.26	26737	46.92%
16	4.8%	834	13809	2	78.7%	2.17	29957	48.88%
17	4.5%	1144	15820	3	60.1%	2.34	36960	45.90%
18	5.0%	1289	18232	3	69.3%	2.24	40886	47.75%
19	4.4%	1448	20875	3	79.3%	2.17	45206	49.38%
20	1.8%	1801	23576	4	67.2%	2.26	53331	47.58%
21	0.7%	1989	28385	4	80.9%	2.16	61206	46.88%

Table 9.8: Power Production with R245fa -R134a Dual Cycle - Ballast Voyage								
Speed	***% Time at Spd***	***DC Power***	***MGE Power***	***Engines***		***SFEC***	***Fuel Power***	***Plant Effic.***
(kn)	(-)	(kW)	(kW)	Number	Load	(kW/kW)	(kW)	(-)
13	1.7%	759	10474	2	59.7%	2.34	24519	45.82%
14	2.6%	880	12178	2	69.4%	2.24	27295	47.84%
15	1.7%	1022	14058	2	80.1%	2.16	30375	49.64%
16	5.0%	1163	16142	3	61.3%	2.32	37491	46.16%
17	3.6%	1301	18440	3	70.0%	2.24	41222	47.89%
18	2.8%	1451	20945	3	79.6%	2.16	45324	49.41%
19	4.2%	1801	23576	4	67.2%	2.26	53331	47.58%
20	2.9%	1971	26414	4	75.3%	2.19	57929	49.00%
21	0.8%	2153	29581	4	84.3%	2.14	63267	50.16%

Based on the above, the potential efficiency improvements and energy savings when using the dual Rankine cycle system are given in Table 9.9 for Water-R134a and in Table 9.10 for R245fa-R134a.

Table 9.9: Potential Performance Improvements with Water-R134a Dual Cycle						
Speed	***Laden***			***Ballast***		
	Efficiency Increase	***Reduction in Fuel Power Consumption***		***Efficiency Increase***	***Reduction in Fuel Power Consumption***	
(kn)	**(-)**	(kW)	(-)	**(-)**	(kW)	(-)
13	-	-	-	2.1%	1195.0	4.6%
14	2.1%	1257.9	4.5%	2.7%	1649.9	5.7%
15	2.7%	1722.7	5.4%	7.2%	5165.0	14.6%
16	2.3%	1966.5	5.1%	2.4%	2066.5	5.3%
17	2.9%	2575.2	6.0%	2.9%	2619.7	6.0%
18	6.0%	6230.9	12.2%	6.0%	6209.7	12.1%
19	3.0%	3583.6	6.3%	3.0%	3554.4	6.3%
20	0.8%	1093.8	1.8%	3.4%	4286.5	6.9%
21	4.3%	5757.8	8.4%	3.6%	4802.9	7.1%

Table 9.10: Potential Performance Improvements with R245fa-R134a Dual Cycle						
Speed	***Laden***			***Ballast***		
	Efficiency Increase	***Reduction in Fuel Power Consumption***		***Efficiency Increase***	***Reduction in Fuel Power Consumption***	
(kn)	**(-)**	(kW)	(-)	**(-)**	(kW)	(-)
13	-	-	-	2.1%	1191.1	4.6%
14	2.1%	1266.7	4.5%	2.7%	1603.4	5.5%
15	2.6%	1709.7	5.4%	7.1%	5096.7	14.4%
16	2.1%	1805.1	4.7%	2.2%	1868.5	4.7%
17	2.6%	2346.4	5.4%	2.6%	2394.9	5.5%
18	5.8%	5962.0	11.7%	5.8%	5972.0	11.6%
19	2.7%	3174.7	5.6%	2.7%	3151.0	5.6%
20	0.8%	1093.8	1.8%	3.0%	3833.3	6.2%
21	3.9%	5300.5	7.7%	3.2%	4345.9	6.4%

The above results can be seen graphically in Figure 9.4 to Figure 9.7. One important observation from the above is that, when using either Rankine system, a speed of 21 knots can be maintained without exceeding the vessels NCR (85% of MCR), something which was not possible without the use of the system.

The system efficiency can be significantly improved especially in cases where the use of the Rankine system allows for the use of one less engine without exceeding the NCR (for example at a laden speed of 18 knots). These cases show a particular benefit, since not only is the power requirement lower and one less engine running, meaning a lower overall consumption, but also the remaining engines are running at a higher load factor and as a result higher efficiency.

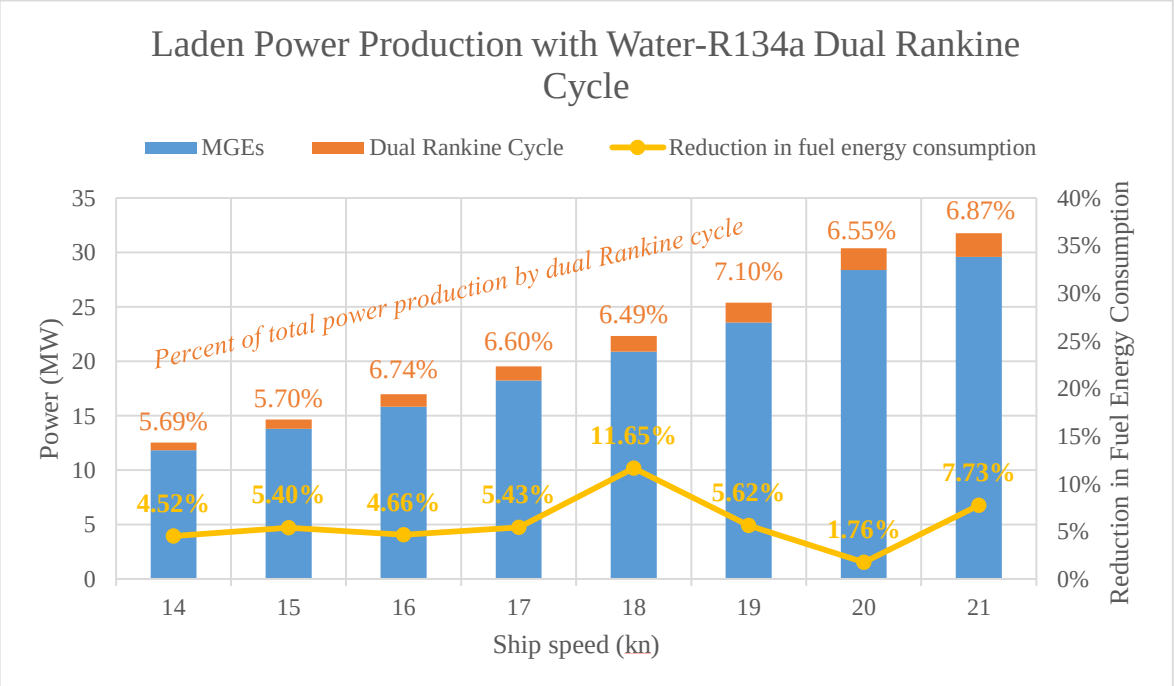

Figure 9.4: Laden Power Production with Water-R134a Dual Rankine Cycle

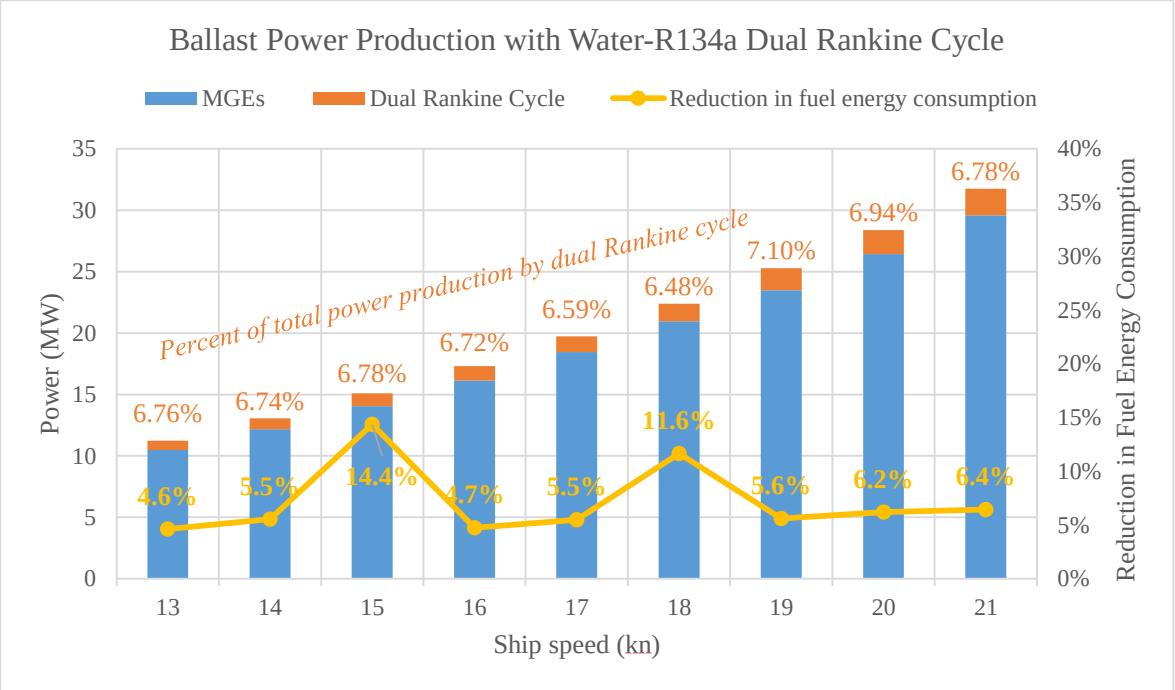

Figure 9.5: Ballast Power Production with Water-R134a Dual Rankine Cycle

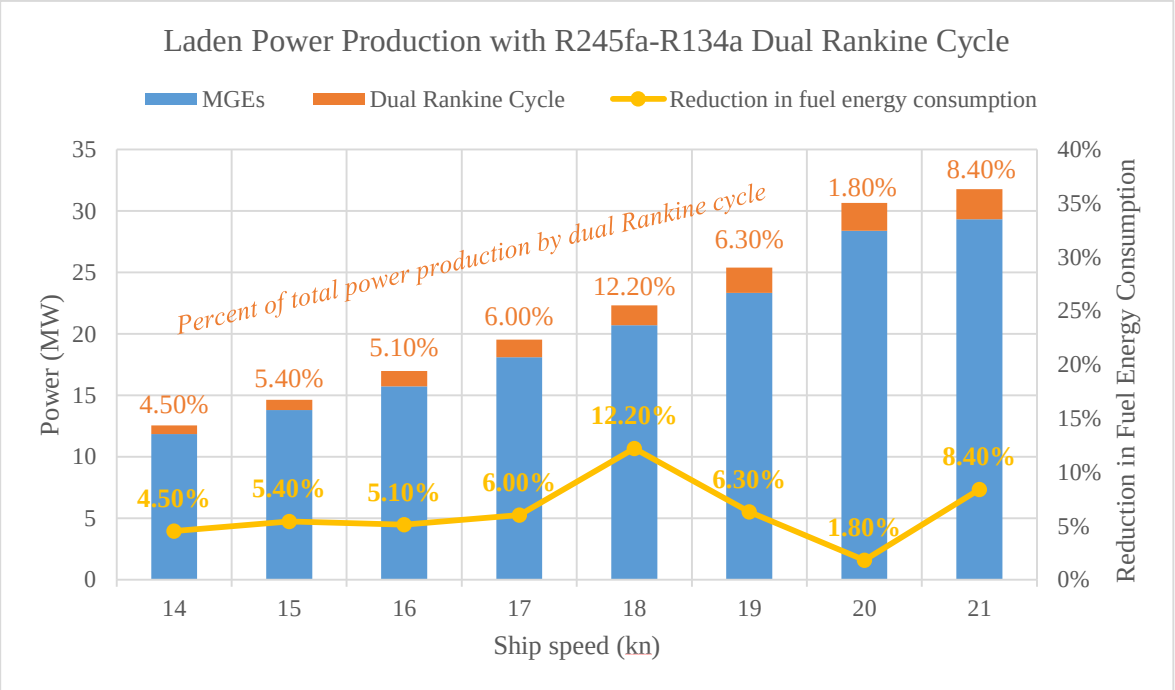

Figure 9.6: Laden Power Production with R245fa-R134a Dual Rankine Cycle

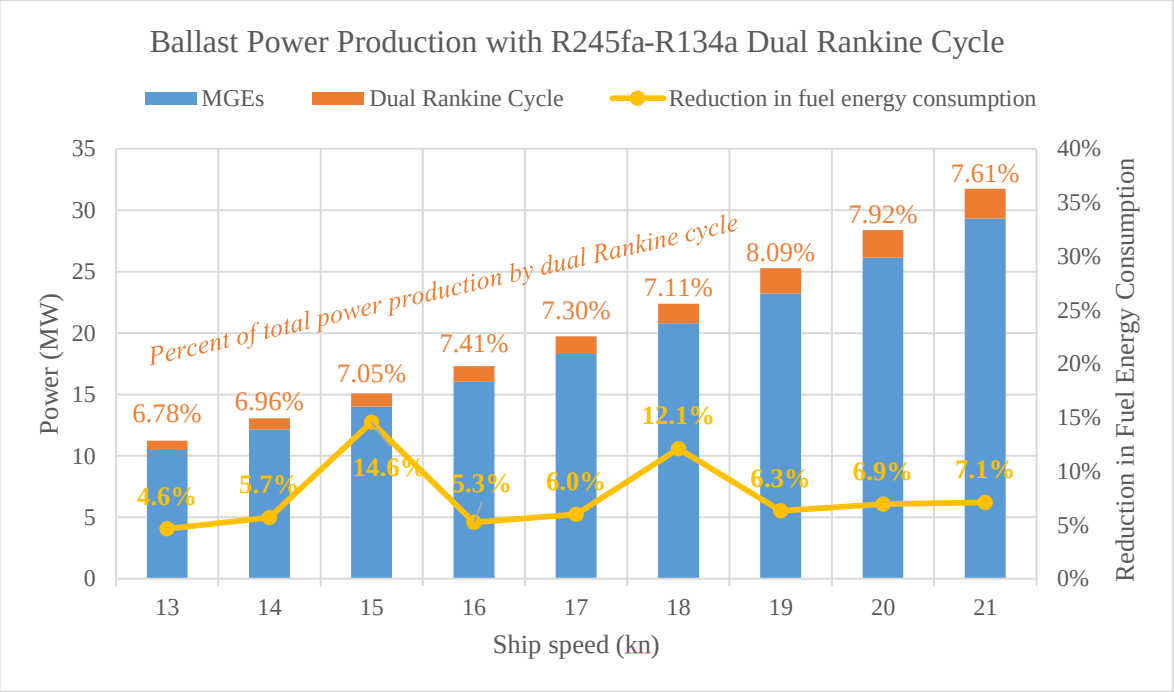

Figure 9.7: Ballast Power Production with R245fa-R134a Dual Rankine Cycle

However, the potential improvements in efficiency and fuel consumption will not be fully realized as the dual cycle system will not always be in use. In fact, it is assumed that the system will only be activated when the net fuel energy required while using the system is higher than the energy available from natural boil off, i.e. when the following inequality is true:

$$\dot{H}_{f,Tot} \geq \dot{E}_{NBOG}(BOR) \tag{9.4}$$

where

BOR the natural boil-off rate for the voyage mode and ship design and

$\dot{E}_{NBOG}(BOR)$ the energy released by the natural boil off as a function of the design BOR, as given in Table 9.3.

Therefore, the energy savings for the speed, also a function of the BOR, are:

$$\dot{E}_S(V_S, BOR) = \begin{cases} \dot{W}_{NET,2R}(V_S) \; if \; \dot{H}_{f,Tot} \geq \dot{E}_{NBOG}(BOR) \\ 0 \; if \; \dot{H}_{f,Tot} \leq \dot{E}_{NBOG}(BOR) \end{cases} \tag{9.5}$$

With the known percentage of time spent at each speed, $\tau(V_S)$, the total energy savings for the studied time frame T can be calculated as:

$$E_S(BOR) = \sum_i \dot{E}_{Si}(V_{Si}, BOR) \cdot \tau_i(V_{Si}) \cdot T \tag{9.6}$$

The resulting energy savings with the studied system are given in Table 9.11, Table 9.12 and Table 9.13 for Water-R134a and in Table 9.14, Table 9.15 and Table 9.16 for R245fa-R134a.

Table 9.11: Energy Saved per Year with Water-R134a Dual Cycle - Laden Voyage

Speed	***% Time at Speed***	***BOR 0.09%***	***BOR 0.10%***	***BOR 0.11%***	***BOR 0.125%***	***BOR 0.15%***
(kn)	(-)	(MWh)				
15	4.0%					
16	4.8%	834.28	834.28			
17	4.5%	1007.15	1007.15	1007.15		
18	5.0%	2709.53	2709.53	2709.53	2709.53	
19	4.4%	1376.12	1376.12	1376.12	1376.12	
20	1.8%	173.37	173.37	173.37	173.37	173.37
21	0.7%	361.30	361.30	361.30	361.30	361.30
Total (MWh)		***6461.75***	***6461.75***	***5627.47***	***4620.32***	***534.68***

Table 9.12: Energy Saved per Year with Water-R134a Dual Cycle - Ballast Voyage

Speed	**% Time at Speed**	***BOR 0.09%***	***BOR 0.10%***	***BOR 0.11%***	***BOR 0.125%***	***BOR 0.15%***
(kn)	**(-)**	(MWh)				
11	1.9%					
12	1.9%					
13	1.7%	173.28	173.28	173.28	173.28	173.28
14	2.6%	373.11	373.11	373.11	373.11	373.11
15	1.7%	761.07	761.07	761.07	761.07	761.07
16	5.0%	897.88	897.88	897.88	897.88	897.88
17	3.6%	825.20	825.20	825.20	825.20	825.20
18	2.8%	1549.32	1549.32	1549.32	1549.32	1549.32
19	4.2%	1321.36	1321.36	1321.36	1321.36	1321.36
20	2.9%	1103.77	1103.77	1103.77	1103.77	1103.77
21	0.8%	348.21	348.21	348.21	348.21	348.21
Total (MWh)		7353.20	7353.20	7353.20	7353.20	7353.20

Table 9.13: Energy Saved per Year with Water-R134a Dual Cycle – Overall (MWh)

BOR 0.09%	***BOR 0.10%***	***BOR 0.11%***	***BOR 0.125%***	***BOR 0.15%***
13814.95	12980.66	11973.52	7887.87	13814.95

Table 9.14: Energy Saved per Year with R245fa-R134a Dual Cycle - Laden Voyage						
Speed	***% Time at Speed***	***BOR 0.09%***	***BOR 0.10%***	***BOR 0.11%***	***BOR 0.125%***	***BOR 0.15%***
(kn)	(-)	(MWh)				
15	4.0%					
16	4.8%	765.82	765.82			
17	4.5%	917.68	917.68	917.68		
18	5.0%	2592.57	2592.57	2592.57	2592.57	
19	4.4%	1219.09	1219.09	1219.09	1219.09	1219.09
20	1.8%	173.37	173.37	173.37	173.37	173.37
21	0.7%	332.61	332.61	332.61	332.61	332.61
Total (MWh)		***6001.14***	***6001.14***	***5235.32***	***4317.64***	***1725.07***

Table 9.15: Energy Saved per Year with R245fa-R134a Dual Cycle - Ballast Voyage						
Speed	**% Time at Speed**	***BOR 0.09%***	***BOR 0.10%***	***BOR 0.11%***	***BOR 0.125%***	***BOR 0.15%***
(kn)	**(-)**	(MWh)				
11	1.9%					
12	1.9%					
13	1.7%	172.71	172.71	172.71	172.71	172.71
14	2.6%	362.62	362.62	362.62	362.62	362.62
15	1.7%	751.00	751.00	751.00	751.00	751.00
16	5.0%	811.86	811.86	811.86	811.86	811.86
17	3.6%	754.40	754.40	754.40	754.40	754.40
18	2.8%	1490.02	1490.02	1490.02	1490.02	1490.02
19	4.2%	1171.38	1171.38	1171.38	1171.38	1171.38
20	2.9%	987.08	987.08	987.08	987.08	987.08
21	0.8%	315.08	315.08	315.08	315.08	315.08
Total (MWh)		***5501.77***	***6816.15***	***6816.15***	***6816.15***	***6816.15***

Table 9.16: Energy Saved per Year with R245fa-R134a Dual Cycle – Overall (MWh)				
BOR 0.09%	***BOR 0.10%***	***BOR 0.11%***	***BOR 0.125%***	***BOR 0.15%***
12817.30	12817.30	12051.48	11133.79	8541.23

Knowing the heat content of the fuel, the energy savings can be converted into fuel savings. Because the fuel which is not burned due to the use of the ORC is FBOG, the heat content of FBOG will be used. The results for the two proposed systems are shown in Table 9.17 and Table 9.18.

Table 9.17: Fuel Saved per Year with Water-R134a Dual Cycle – Overall (Metric Tonnes)				
BOR 0.09%	***BOR 0.10%***	***BOR 0.11%***	***BOR 0.125%***	***BOR 0.15%***
1005.66	1005.66	944.93	871.61	574.20

Table 9.18: Fuel Saved per Year with R245fa-R134a Dual Cycle – Overall (Metric Tonnes)				
BOR 0.09%	***BOR 0.10%***	***BOR 0.11%***	***BOR 0.125%***	***BOR 0.15%***
933.03	933.03	877.29	810.48	621.76

It is noted that, for each different BOR, the energy requirements remain the same. What changes, aside from the available NBOG energy, of course, is the required steam for forcing vaporization. For lower nominal boil-off rates, more steam will be needed at higher speeds. Keeping in mind that only two of the four identical engines on the studied ship are fitted with EGBs, the engines selected for use at each speed depend directly on the steam requirement. In the above calculations, it is assumed that the minimum number of engines with EGBs are used in order to cover the steam needs of the ship.

As a result, for the same hull at a certain speed but with a different nominal BOR, a different engine configuration may be used in order to produce the steam needed. As a result, the profile of the exhaust gas and corresponding Rankine power production would be slightly different. This effect is not taken into account in the present work.

9.2 Economic Analysis

Knowing the energy savings associated with each dual cycle installation, the system can then be analyzed using well known economic indices. Three common such indices which will be applied here are the Net Present Value (NPV), Dynamic Payback Period (DPP) and Internal Rate of Return (IRR) of the investment. These are analyzed further below.

9.2.1 Savings from ORC System

LNG is generally priced in USD per mmBTU, so that the conversion from energy saved to money saved would seem quite straightforward. However, the heat content of the fuel burned will depend on many factors (including whether it is the product of forcing or natural boil off, the fuel composition and the time elapsed since port) so that the heat content (and therefore price) of one ton of cargo is not the same as the heat content (and therefore price) of one ton of gas burned as fuel.

For example, when burning natural boil-off which is high in methane and nitrogen, the heat content (and therefore theoretical selling price) of the fuel is less than that of the cargo which will be discharged. Nevertheless, a detailed analysis of this effect goes beyond the scope of the present work. For simplicity, it is assumed here that the cost of the natural gas mixture burned is the same as the cost of the LNG to be discharged. As a wide range of LNG costs will be reviewed when calculating the economic benefit of this system, it is considered that this simplification is acceptable.

Therefore, assuming a price of LNG at c_{LNG} (USD/kJ) ,the annual fuel savings from the use of the Rankine system are:

$$C_{fs,i} = c_{LNG,i} \cdot E_{S,i} \tag{9.7}$$

where the subscript i denotes that both the cost of LNG and the energy savings (as a function of the voyage profile) may change from year to year.

9.2.2 Spending for ORC System

The trade-off for the fuel savings of the Rankine system, is the initial capital cost and cost of additional operation and maintenance of the system.

9.2.2.1 *Capital costs*

To estimate the capital cost, an analysis is needed of the main components to be used. The method and costs introduced in [25] followed in [6] are applied assuming an exchange rate of 1.12 USD to Euros.

Pump

The cost of the pump is a direct function of its power output:

$$C_P = c_p \left(\frac{\dot{W}_P}{300} \right)^{0.25} \tag{9.8}$$

Turbine

The cost of the expander depends directly on its type which in turn is a function of the system power output. Since both cycle loops have power outputs in the range of 500 to 2000 kW, it can be assumed as per the analysis in [40] that a screw type turbine will be used for these cases.

For a screw type turbine, the cost can be approximated with the following relationship:

$$C_{T,b} = c_{Tb,1} \dot{W}_T^2 + c_{Tb,2} \dot{W}_T + c_{Tb,3} \tag{9.9}$$

Heat exchangers

The investment required for the heat exchangers depends directly on their size as quantified by the heat exchanger area, which can be calculated as:

$$A = \frac{\dot{Q}}{k \Delta T_{lm}} \tag{9.10}$$

where

$\dot{Q}$ the heat flow rate exchanged in kW

k the overall heat transfer coefficient in $\frac{kW}{m^2 K}$

ΔT_{lm} the logarithmic mean temperature difference:

$$\Delta T_{LM} = \frac{\left(T_{H,in} - T_{C,out}\right) - \left(T_{H,out} - T_{C,in}\right)}{\ln\left(\frac{T_{H,in} - T_{C,out}}{T_{H,out} - T_{C,in}}\right)} \tag{9.11}$$

where the subscripts H and C refer to the hot and cold stream, respectively.

In the present work the heat exchangers fall under the types listed in Table 9.19, where, for each case, the heat transfer coefficient is estimated based on relevant literature [72].

Table 9.19: Assumed heat transfer coefficients	
Type of heat exchanger	***k (W/Km^2)***
Evaporator with organic fluid and flue gases	500
Condenser/evaporator of organic fluid with organic fluid	1000
Condenser/evaporator of water with organic fluid	1000

It is noted that a final economic analysis would need to include a more detailed design of the heat exchangers and subsequently a closer approximation of the heat transfer coefficients as a function of the thermodynamic properties of the fluid (i.e. the density, viscosity, thermal conductivity and resulting Prandtl number), the exchanger design (i.e. the plate size and thickness and hydraulic diameter of flow area) and finally the corresponding flow characteristics (i.e. Reynold's number, friction coefficient).

For simplicity, here the area will be approximated using Equation (9.10) and the values in Table 9.19. The resulting cost estimate is:

$$C_{HEx} = c_{HEx,1} + Ac_{HEx,2} \tag{9.12}$$

An exception to the above method is made for the evaporator for the HT cycle of the Water-R134a cycle. For this particular case, the cost of the exhaust gas boiler will be approximated using the following relationship, as proposed in [73] with coefficients as modified in [74] and [75]:

$$C_{EGB} = c_{EGB,1}\left[\left(\frac{\dot{Q}_{ec}}{\Delta T_{lm,ec}}\right)^{0.8} + \left(\frac{\dot{Q}_{ev}}{\Delta T_{lm,ev}}\right)^{0.8} + \left(\frac{\dot{Q}_{sup}}{\Delta T_{lm,sup}}\right)^{0.8}\right] + c_{EGB,2}\dot{m}_s + c_{EGB,3}\dot{m}_g^{1.2} \tag{9.13}$$

where

$\dot{Q}$ the heat transfer in each component
ΔT_{lm} the logarithmic mean temperature difference in each component
$\dot{m}_s$ the water/steam mass flow rate
$\dot{m}_g$ the exhaust gas flow rate
ec refers to the economizer
ev refers to the evaporator
sup refers to the superheater

Furthermore, it has been assumed in the model that the existing spare freshwater cooler will be used as the condenser for the low temperature cycle with some modification. As such the cost of this component is not included, while the cost of modification is included in the labor costs and other costs as described below.

Pipes

The cost of piping depends on the length and diameter of the pipes used. The former can be estimated based on available literature for on shore systems, as given in Table 9.20. The latter must be approximated based on the normal allowed fluid speeds within the system piping as given in Table 9.20. The relevant equation for the diameter is:

$$u = \frac{\dot{V}}{\frac{\pi d_i^2}{4}} \rightarrow d_i = \sqrt{\frac{4\dot{V}}{\pi u}}$$

where

$\dot{V}$ is the volumetric flow for the examined piping and

d_i the relevant diameter

Table 9.20: Normal speed of fluid within piping and length of piping in ORC system		
	Length (m)	***Speed (m/s)***
Between condenser and pump	1.5	0.6
Between evaporator and expander	3	10
Between expander and condenser	1.5	12

The cost can then be calculated as:

$$C_{Pipes} = \sum_i \left(c_{Pipes,1} + c_{Pipes,2} d_i\right) L_i \tag{9.14}$$

where

d_i the pipe diameter

L_i the pipe length.

Working fluid

The cost of the working fluid is

$$C_{WF} = \dot{m} c_{WF} \tag{9.15}$$

The cost of water is considered very conservatively to be 20% of the organic fluid cost while a comparison to the price of water for domestic use suggest it may be much less [76].

Control system

The cost of the automatic control system is considered fixed:

$$C_{CS} = 1904\ USD\ for\ combined\ cycle \tag{9.16}$$

Other costs

$$C_{Other} = 1120\ USD \tag{9.17}$$

Labor

$$C_{Labor} = 0.3 \cdot TCC\ USD$$

where TCC the sum of the previously described capital costs.

Based on the above, the total cost of the dual cycle can be calculated as:

$$C = \left(\left(C_P + C_T + C_{Hex,evap} + C_{Hex,cond} + \sum_i C_{Pipes,i} + C_{WF} \right)_{HT} + \left(C_P + C_T + C_{Hex,evap} + C_{Hex,cond} + \sum_i C_{Pipes,i} + C_{WF} \right)_{LT} + C_{CS} + C_{Other} \right) \cdot 1.3 \quad (9.18)$$

where the constant values for the cost calculations are taken as in Table 9.21.

Table 9.21: Constant values for components cost estimation

Constant	***Value***	***Unit***
c_P	3740.8	\$/kW$^{0.25}$
$c_{Tb,1}$	-0.00157	\$/kW^2
$c_{Tb,2}$	16.24672	\$/kW
$c_{Tb,3}$	71637.44	\$
$c_{HEx,1}$	1680	\$
$c_{HEx,2}$	2447.2	\$/m^2
$c_{EGB,1}$	9650	\$
$c_{EGB,2}$	11820	\$/(kg/s)
$c_{EGB,3}$	658	\$/(kg/s)$^{1.2}$
c_{WF}	112 for water 560 for organic fluids	\$/kg/s
$c_{Pipes,1}$	3.752	\$/m
$c_{Pipes,2}$	0.8736	\$/m^2

It can be seen from the results of the capital cost analysis in Table 9.22 that the water-R134a cycle is cheaper than the R245fa-R134a system. Savings come from the pump in the HT cycle (due to the much lower mass flow of the water cycle), the HT evaporator and of course the fluid itself. The much lower mass flow of water compared to R245fa seems to be a decisive factor.

Table 9.22: Comparison of Capital Costs for Proposed Systems					
Water-R134a Dual Cycle Cost			R245fa-R134a Dual Cycle Cost		
	Component	***Cost (USD)***		***Component***	***Cost (USD)***
HT Cycle	Pump	7,795	HT Cycle	Pump	20,407
	Turbine	93,451		Turbine	92,394
	Heater	110,264		Heater	608,985
	Pipes	25		Pipes	24
	Fluid	396		Fluid	26,827
LT Cycle	Pump	18,782	LT Cycle	Pump	17,302
	Turbine	87,021		Turbine	87,505
	LT Heater 1	1,417,475		LT Heater 1	1,824,215
	Pipes	24		Pipes	24
	Fluid	45,835		Fluid	45,835
Common	HT Heater - LT Cooler	1,497,504	Common	HT Heater - LT Cooler	1,075,117
	Control system	1,904		Control system	1,904
	Other	1,120		Other	1,120
Totals	Total materials	3,281,596	Totals	Total materials	3,801,659
	Total work	984,479		Total work	1,140,498
	Total	4,266,075		Total	4,942,156

.

9.2.2.1 *Operational costs*

In addition to the investment cost, yearly operational costs will be incurred for the use of the dual cycle system. This cost includes the operation and maintenance costs of the new system ($C_{OM,ORC}$), a burden which will be at least partially offset by the decreased costs of operation and maintenance of the generator engines ($\Delta C_{OM,GE}$), so that the net operation and maintenance costs related to the ORC system can be derived as:

$$\Delta C_{OM,i} = C_{OM,ORC,i} - \Delta C_{OM,GE,i} \tag{9.19}$$

Based on the analysis in [17], which studied a similar propulsion arrangement, this will be assumed to be $\Delta C_{OM,i} = 3\ USD/MWh$.

9.2.3 Economic Indices

From the savings and spending determined in the previous sections, the annual cash flow related to the ORC system can finally be calculated as:

$$F_i = \begin{cases} -C, for\ i = 0 \\ C_{fs,i} - \Delta C_{OM,i}, for\ i \geq 1 \end{cases} \tag{9.20}$$

Based on the known cash flow, the first economic index, Net Present Value, can be derived:

$$NPV = \sum_{i=0}^{N} \frac{F_i}{(1+d_i)^i} \tag{9.21}$$

where

N the number of years for which the investment will be analyzed

d_t the market discount rate.

In the present calculation, the assumption will be made that the voyage profile and therefore yearly energy savings, the cost of LNG and the market discount rate will remain constant for the duration of the period examined. Furthermore, fuel cost and general inflation will be ignored. Finally the salvage cost of the installation will be assumed to be zero. As such, Equation (9.21) can be modified as follows:

$$NPV = F_0 + F_1 \left(\frac{1-(1+d)^{-N}}{d} \right) \tag{9.22}$$

The Net Present Value is an indication of the worth that the investment could have. However, an equally important consideration is how much time is needed until the gains from the system cover the cost of the initial investment and upkeep. The Dynamic Payback Period quantifies this time and is the number of years which are required so that the net present value equals zero. Under the same assumptions as mentioned for Equation (9.22), the dynamic payback period can be calculated as follows:

$$DPB = -\frac{\ln\left(1+d\left(\frac{F_0}{F_1}\right)\right)}{\ln(1+d)} \tag{9.23}$$

If $1 + d\left(\frac{F_0}{F_1}\right) < 0, DPB \to \infty$. This means that the investment will never pay for itself and is not economically tenable.

Finally, a useful economic metric is the Internal Rate of Return. The IRR is the market discount rate for which the NPV equals zero. Generally, the higher the IRR, the better the investment.

Here, based on the analysis in [17], which studies an ORC system for a similar propulsion plant, the following constants will be assumed for the economic analysis:

Assumptions for Economic Analysis			
Analysis years	N	30	years
Market discount rate	d	8	%

A range of fuel costs will be examined based on the historic price of LNG over the past fifteen years. As can be seen in Figure 9.8, the price of LNG can vary widely based on the location of export/import and the year.

Figure 9.8: Historic LNG prices in USD/mmBTU since 1997 in different areas [77]

From the results which follow, it can be seen that the water-R134a dual cycle is techno-economically superior. It is an economically viable option (having positive NPV and IRR and finite DPP) for unit fuel costs above 10 USD/mmBTU. For the R245fa-R134a case, the unit fuel costs must be above 20 USD/mmBTU for economic viability, except for the very lowest BOR.

As can be clearly noted from Figure 9.9 to Figure 9.14, the potential benefit of both dual cycle systems is increased as the vessels nominal BOR is decreased. This is because there is less "free" energy from the boil off, and more opportunity for a fuel saving device to be used. As the trend in LNG carrier design is to constantly push for lower BORs, the economic performance of the proposed system would improve.

For the current price of LNG as detailed in Figure 9.8, the investment cost is justified for the water-R134a cycle if the BOR is less than 0.150%, especially if the vessel's trading route is in Europe or Japan where the price of LNG is relatively high.

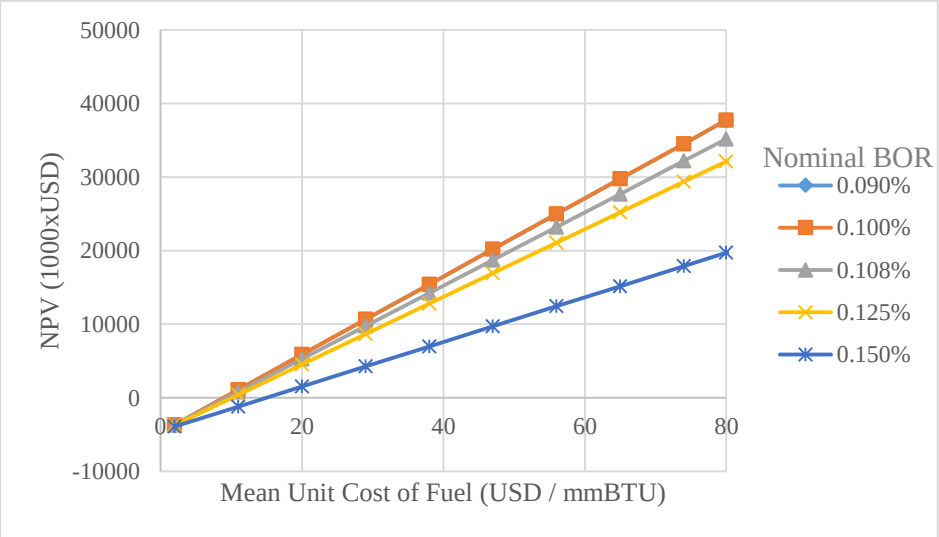

Figure 9.9: NPV for Water-R134a Dual Cycle

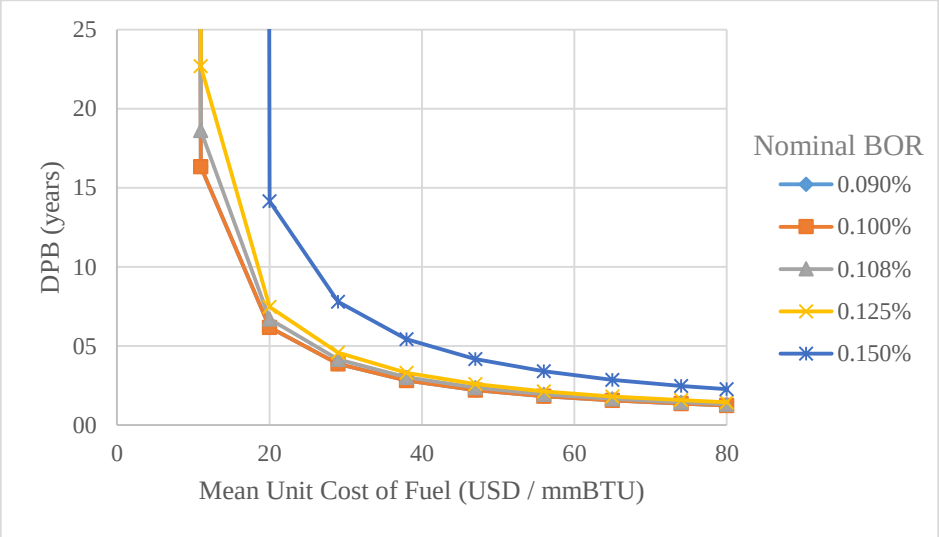

Figure 9.10: DPB for Water-R134a Dual Cycle

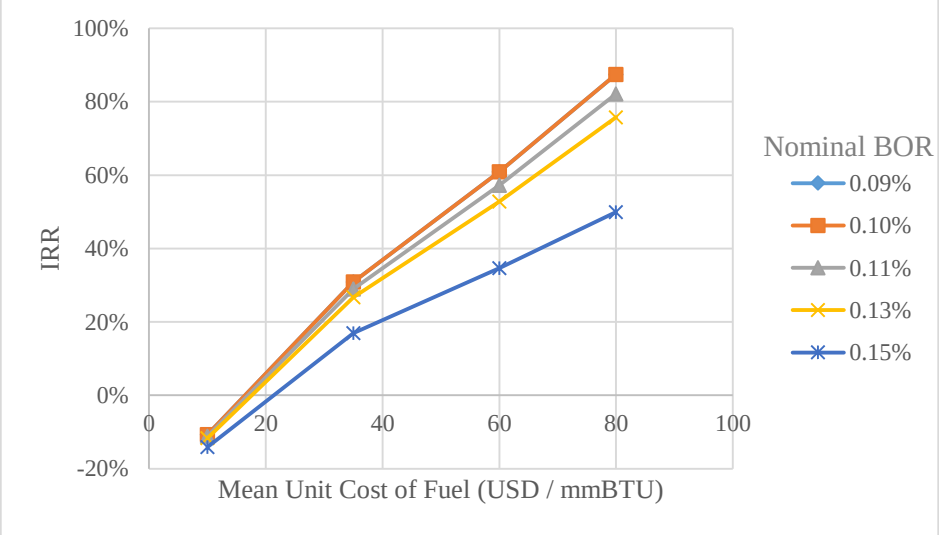

Figure 9.11: IRR for Water-R134a Dual Cycle

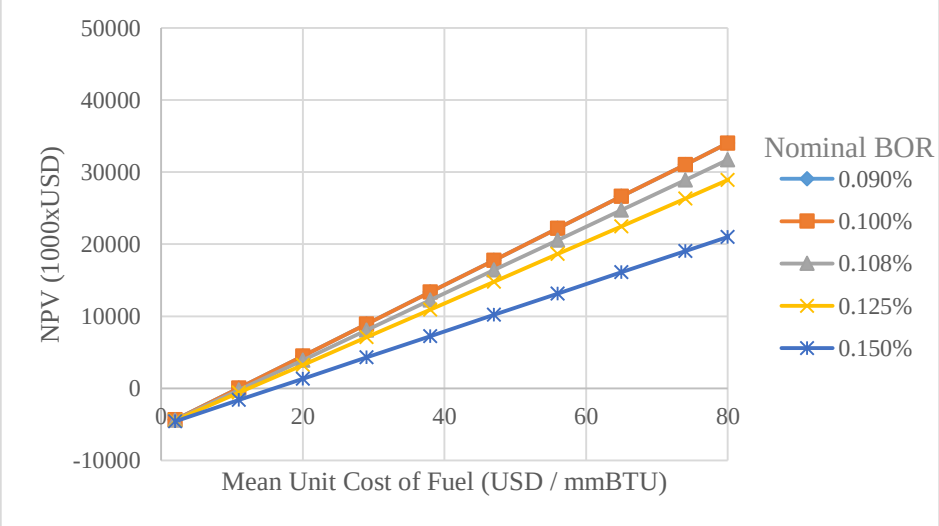

Figure 9.12: NPV for R245fa-R134a Dual Cycle

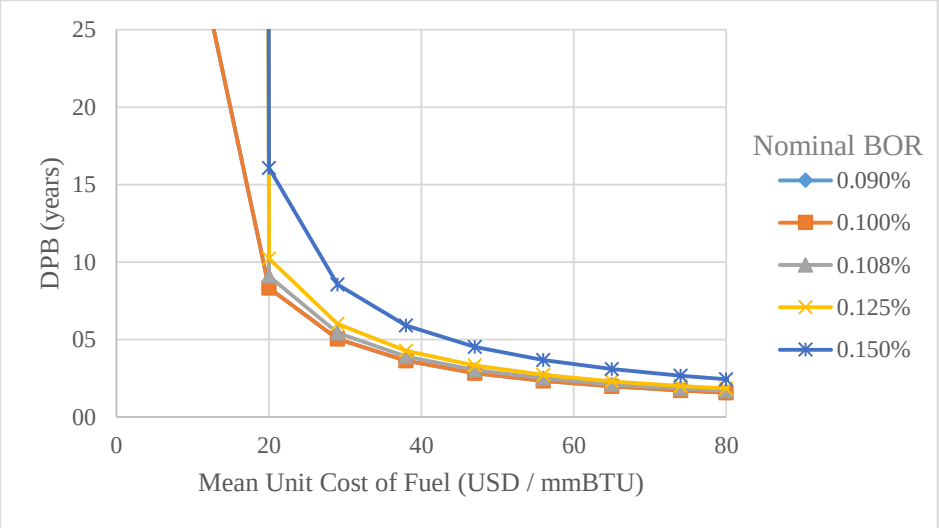

Figure 9.13: DPB for R245fa-R134a Dual Cycle

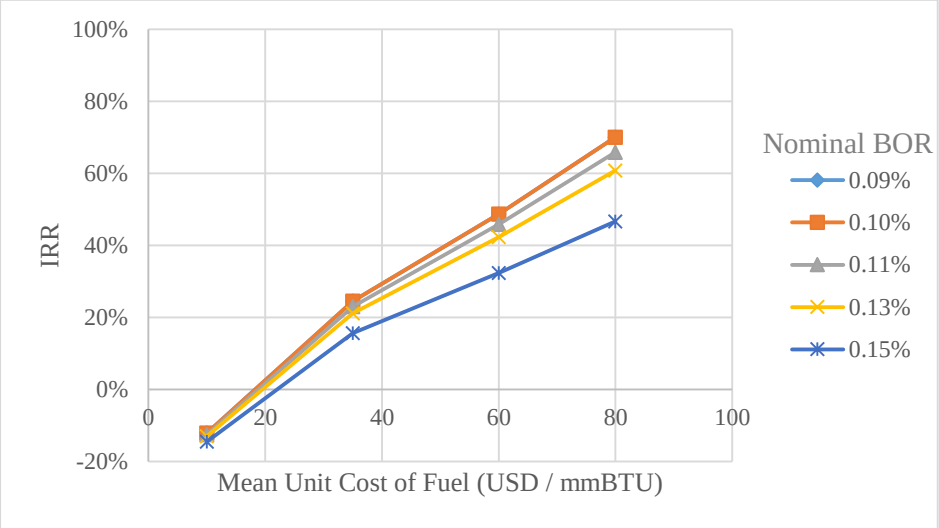

Figure 9.14: IRR for R245fa-R134a Dual Cycle

9.3 Environmental Analysis

The reduction in fuel burned due to the use of the ORC system provides not only financial gains, but also environmental benefits in the form of reduced emissions.

The average engine emissions are known from the product guide of the studied engine being around 1.8 g/kWh for NO_X and 430 g/kWh for CO_2. Since the reduction in engine MWh per year as a result of using the ORC system is known, the corresponding reduction in emissions can be calculated. The savings as a function of the vessel design BOR are given in Table 9.23 and Table 9.24.

Table 9.23: Emissions reductions in Metric Tonnes for Water-R134a Dual Cycle

	BOR 0.09%	***BOR 0.10%***	***BOR 0.11%***	***BOR 0.125%***	***BOR 0.15%***
NO_X	24.87	24.87	23.37	21.55	14.20
CO_2	6078.58	6078.58	5711.49	5268.35	3470.66

Table 9.24: Emissions reductions in Metric Tonnes for R245fa-R134a Dual Cycle					
	BOR 0.09%	***BOR 0.10%***	***BOR 0.11%***	***BOR 0.125%***	***BOR 0.15%***
NO_X	23.07	23.07	21.69	20.04	15.37
CO_2	5639.61	5639.61	5302.65	4898.87	3758.14

10 Conclusions and Suggestions for Further Study

The present study examined the potential for waste heat recovery onboard an LNG carrier with a tri-fuel diesel electric propulsion system. Sources of waste heat which have been exploited are the engines exhaust gas streams and HT cooling water. The proposed system is a dual loop Rankine cycle system with the top loop utilizing the exhaust gas waste heat and the bottom loop utilizing the top loop condensation heat as well as the engine cooling water heat.

Initially four fluid combinations were examined at a design point: R416a-R134a, Ammonia-R134a, R245fa-R134a and Water-R134a, and it was found that the best potential performance in terms of power output was shown by the ammonia and water-topped cycles. However, with the exception of water, all HT fluids showed their best power output performance for high evaporation pressures. As a result, when the evaporation pressure was limited to 50 bar, the water-topped cycle showed the best performance followed closely by the R245fa-R134a combination.

These final two arrangements were further examined across the vessel operating profile for potential power output at all speeds. An iterative process was used to determine the operating point for both the main generator engines and the dual Rankine cycle system for each speed. The potential energy savings as a function of the vessel BOR were found. It was seen that the propulsion system efficiency could be improved by 2-7%, depending on the speed, while the fuel energy consumption could be reduced by 5-14.5%, respectively. Also the vessel maximum service speed with NCR power was increased.

Finally, the cost of installing and maintaining the proposed systems was examined and the two proposals were compared from a techno-economic standpoint. The economic criteria applied were the net present value, dynamic payback period and internal rate of return. The water-R134a cycle proved to be superior showing not only better performance in terms of energy savings but also a lower investment cost and a better economic performance overall. This system is economically viable for current LNG prices for ships trading in Europe and the Far East. Its potential will improve further as improvements of cargo containment system technology drives the BOR down even more.

Certain modifications could be made to the proposed design with the potential for improving the system performance even further. It can be seen in Table 8.11 and Table 8.12 that the outlet temperature of the exhaust gas from the HT evaporator is around 192^{0}C for the R245fa-R134a cycle and 255^{0}C for the Water-R134a cycle. This would suggest that further heat recovery from the exhaust gas is possible, considering that the minimum allowable exhaust temperature was assumed to be 120°C. As a result, the partially cooled exhaust gas could be used as an additional heating medium in the low temperature cycle, similar to the arrangement proposed in [62]. A more detailed study of the minimum allowable temperature in the cycle would be merited in this case. Furthermore, a techno-economic evaluation would be required as this modification would add further complexity to the system.

Indeed, the main drawback of the proposed system is the complexity and therefore installation cost, so that further studies on the system should also examine how to reduce this cost. In the present study, the optimal working fluid combination turned out to be topped by water. It would be worth examining if the existing EGBs could be used as

evaporators for the topping cycle with some modification or enlargement. Furthermore, a single loop cycle which may have a lower power output but also a lower cost than the dual cycle could be examined.

The detailed design of cycle components was not attempted in this study. This item is especially important because a more developed design could lead to a more accurate cost estimate. Furthermore, the performance of the studied cycle components at off-design points was not considered, which is another potential improvement by a future work.

The present work only intervened in the engine waste heat streams at two points because of the difficulty of modifying the existing complex, but also compact system at more positions. A complete redesign of the cooling arrangements in order to make use of higher temperature heat sources such as the charge air would be worth investigating.

It is clear from the above that the overall performance of the studied system reveals it to be a viable technology. Nevertheless, continued research is merited to explore the full potential of this technology onboard.

Appendix: Calculation of the power production profile

The power required as a function of speed can be found from statistical data gathered from the vessel's voyages. From the vessel's noon reports, the following data is available:

(1) Average speed
(2) Shaft power measured with strain gauges
(3) Running hours and electric energy in MWh for each gen-set

From item (3), the average total produced power measured at the generator terminals can be calculated as:

$$\dot{W}_{e,tot} = \sum_{j=1}^{4} \frac{W_j}{T_j} \tag{A.1}$$

where:

W_j the electric energy produced by generator j in one day.

T_j the running hours of engine j in one day.

The electric power required to produce the measured shaft power $\dot{W}_{ep}$ can be calculated using the assumed efficiencies for the various propulsion components:

$$\dot{W}_{ep} = \frac{\dot{W}_p}{\eta_{GB} \cdot \eta_{EPM} \cdot \eta_{FC} \cdot \eta_{TF} \cdot \eta_{SB}} \tag{A.2}$$

The difference between the produced power $\dot{W}_{e,tot}$ and the electric power required for propulsion $\dot{W}_{ep}$ is symbolized $\dot{W}_e$. This includes power used by any consumers other than the main propulsion (such as hotel load).

$$\dot{W}_e = \dot{W}_{e,tot} - \dot{W}_{ep} \tag{A.3}$$

The measured powers $\dot{W}_{e,tot}$, $\dot{W}_{ep}$ and $\dot{W}_e$ as a function of speed are given in Figure A.1, Figure A.2 and Figure A.3.

For the purposes of creating a model, a formula will need to be developed in order to predict each of these powers as a function of speed. A regression formula will be used.

For shaft power vs. speed, as can be expected from the theory of the propeller curve, the relationship is approximately cubic. Therefore, an exponential regression line is used for the model. The remaining power shows a great deal of dispersion and a regression formula is not able to be developed with sufficient accuracy. An increasing linear relationship is used which fits the most consistent data well as can be seen in Figure A.3.

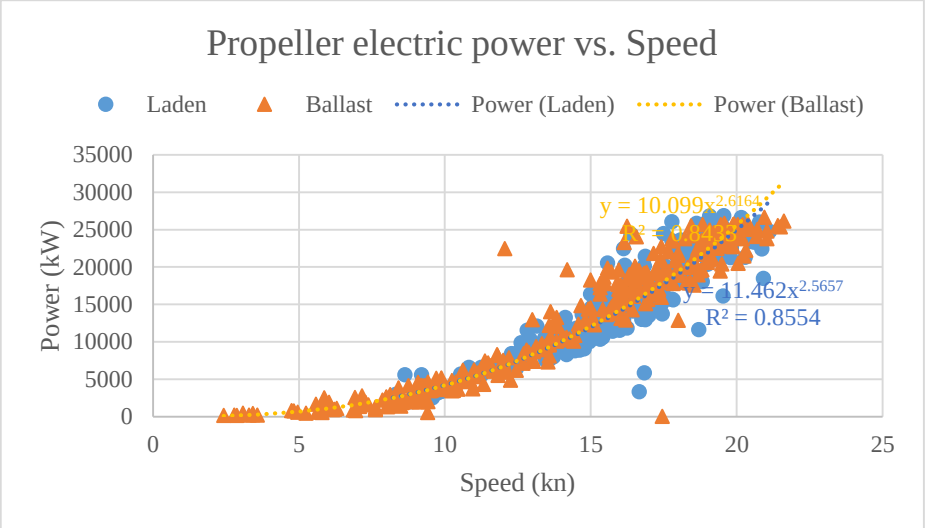

Figure A.1: Measured data for electric power for propulsion

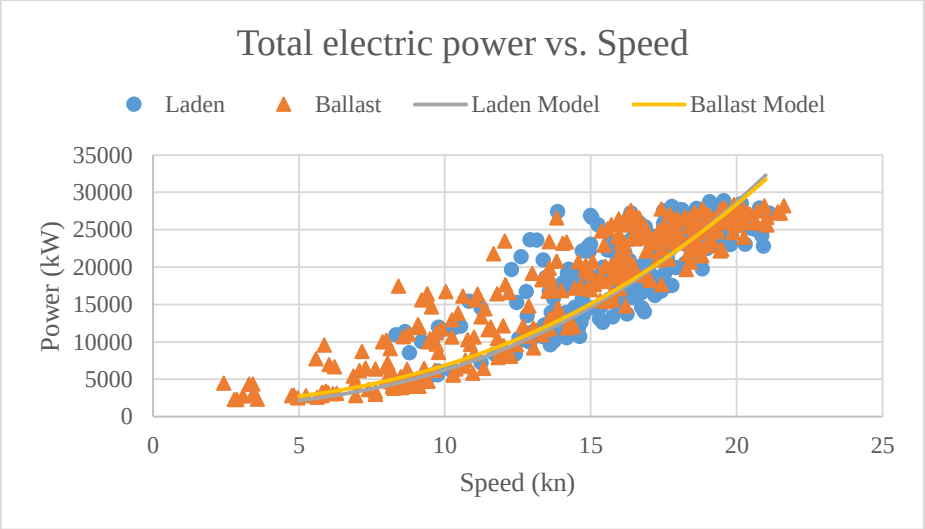

Figure A.2: Measured data for total electric power produced

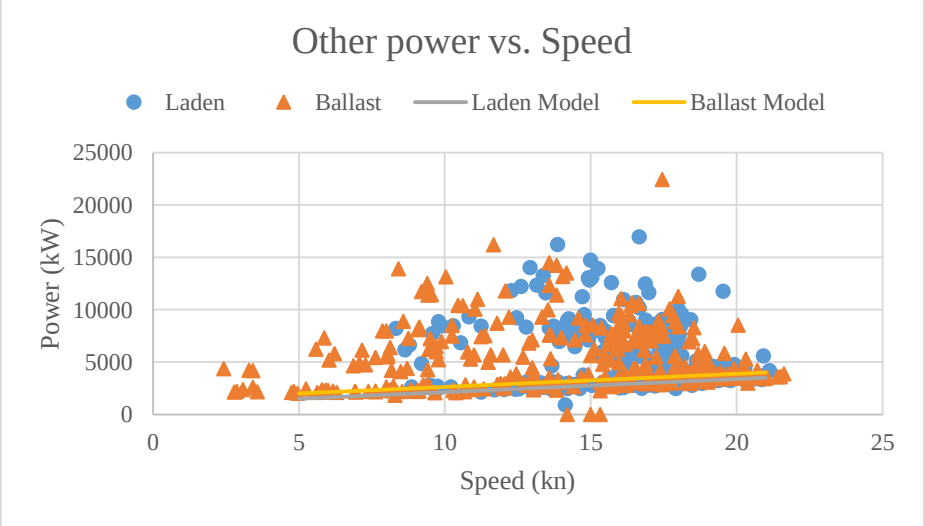

Figure A.3: Calculated data for remaining electric power as

$$\dot{W}_e = \dot{W}_{e,tot} - \dot{W}_{ep}$$

It is notable that at medium speeds, the required power for the laden draft is actually lower than the required power for the ballast draft. (For a clearer comparison, see Table 5.8Table 5.9.)This is consistent with the results of the model tests and sea trials for the studied vessel and is considered to be a design decision at the time of the hull design.

In this model, speeds below 5 knots are not considered, as this is the maneuvering speed of the vessel and therefore the lowest expected speed during the steaming time. Furthermore, the collected data shows that a negligible amount of time is spent below this speed.

Calculation of the consumption profile

After determining the required mechanical power for each speed as:

$$\dot{W}_m = \dot{W}_e/\eta_{gen} \tag{A.4}$$

we can find the chemical energy (fuel consumption) which is required to produce it. Since the actual load factor of each engine is known, the total energy consumption is:

$$\dot{H}_{f,Tot} = \sum_{j=1}^{4} \dot{q}_{f,j} \cdot \dot{W}_{m,MCR} \cdot f_L \tag{A.5}$$

where the specific energy consumption $\dot{q}_{f,j}$ is known from the engine maker as a function of the specific load factor f_L.

For the sake of creating a model, an assumption will have to be made about the number of engines used to produce the necessary power. One method, followed in [17], is to assume that for each speed, the minimum number of engines is used with an equal load on each engine. However, the engine load is not allowed to exceed 85%.

The result of this approach is shown in Figure 5.8 and Figure 5.9 while actual statistical data for the number of engines used is shown in Figure A.4. It suggests that this approach is a fairly realistic, though not exact, approximation of the operators working philosophy, particularly for the ballast passage.

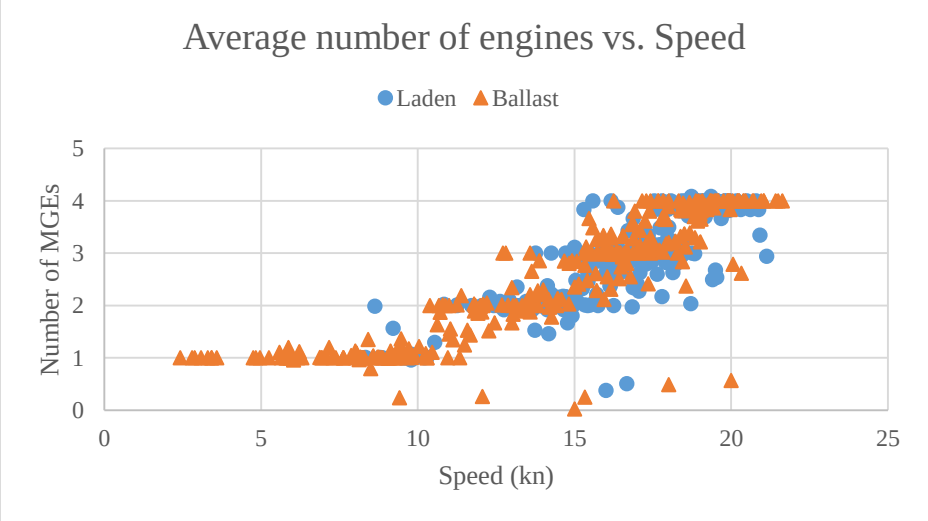

Figure A.4: Actual number of engines used vs. speed

Bibliography

[1] Wallenius Shipping, "M/V Figaro," [Online]. Available: http://www.walleniuslines.com/PageFiles/1814/Figaro_NB4459.pdf. [Accessed 6 January 2015].

[2] Opcon Marine, "Commissioning and testing of first reference installation of Opcon technology for ships," [Online]. Available: http://www.opcon.se/web/First_installation_1_1.aspx. [Accessed 4 January 2015].

[3] Pagini J., "Ramping up Engine Performance by Exploiting Lower Temperature Heat," *Twenty four7 Wartsila Stakeholder Magazine,* pp. 63-64, January 2009.

[4] Φραγκόπουλος Χ., "Ενεργειακά Συστήματα Πλοίου", Τεύχος Β', Αθήνα: Ε.Μ.Π., 2009.

[5] Braimakis K., Preisiger M., Bruggeman D., Karrelas S. and Panopoulos K., "Low grade waste heat recovery with subcritical and supercritical Organic Rankine Cycle based on natural refrigerants and their binary mixtures," *Energy,* Vol. 90, 2015, pp. 1-13.

[6] Καλικατζαράκης Μ., "Εκμετάλλευση Απορριπτόμενης Θερμότητας Χαμηλών Θερμοκρασιών Ναυτικών Κινητήρων Diesel με Χρήση Οργανικού Κύκλου Rankine," Διπλωματική Εργασία, Αθήνα: Ε.Μ.Π., 2013.

[7] Hung T.C., Wang S.K., Kuo C.H., Pei B.S. and Tsai K.F., "A study of organic working fluids on system efficiency of an ORC using low-grade energy sources," *Energy,* Vol. 35, No. 3, pp. 1403-1411, March 2010.

[8] Tsatsaronis G. and Cziesla F., "Exergy Balance and Exergetic Efficiency," in *Exergy, Energy System Analysis and Optimization - Vol.I,* [Ed. C.A. Frangopoulos] from Encyclopedia of Life Support Systems (EOLSS). Developed under the Auspices of the UNESCO. Eolls Publishers, 2004, Oxford, U.K. http://www.eolss.net.

[9] Chen H., Goswami D.Y. and Stefanakos E.K., "A review of thermodynamic cycles and working fluids for the conversion of low-grade heat," *Renewable and Sustainable Energy Reviews,* Vol. 14, No. 9, pp. 3059-3067, 2010.

[10] Karellas S. and Schuster A., "Supercritical Fluid Parameters in Organic Rankine Cycle Applications," *International Journal of Thermodynamics,* Vol. 11, No. 3, pp. 101-108, 2008.

[11] Pan L., Wang H. and Shi W., "Performance analysis in near-critical conditions of

organic Rankine cycle," *Energy*, Vol. 37, pp. 281-286, 2012.

[12] Bao J. and Zhao L., "A review of working fluid and expander selections for organic Rankine cycle," *Renewable and Sustainable Energy Reviews*, Vol. 24, pp. 325-342, August 2013.

[13] Wolverine Tube, Inc., "Thermodynamics of Refrigerant Mixtures and Refrigerant-Oil Mixtures," *Engineering Data Book III* [Online]. Available: http://www.wlv.com/products2/databook/db3/data/db3ch15.pdf

[14] Lecompte S., Van Den Broek M. and De Pape M., "Exergy analysis of zeotropic mixtures as working fluids in Organic Rankin Cycles," *Energy Conversion and Management*, Vol. 85, pp. 727-739, 2014.

[15] Le V.L., Kheiri A., Feidth M. and Pelloux-Prayer S., "Thermodynamic and economic optimizations of a waste heat to power plant driven by subcritical ORC (Organic Rankine Cycle) using pure or zeotropic working fluid," *Energy*, Vol. 78, pp. 622-638, 2014.

[16] Zhao L. and Bao J., "Thermodynamic analysis of organic Rankine cycle using zeotropic mixtures," *Applied Energy*, Vol. 130, pp. 748-756, 2014.

[17] Soffiato M., "Design and Performance Evaluation of an Organic Rankine Cycle System Exploiting the Low Grade Waste Heat of the Main Engines in a LNG Carrier", M.Sc. Thesis, Padova: Universita Degli Studi di Padova, 2014.

[18] Vlaskos I., Feulner P. and Michos C., *Waste Heat Recovery in Marine Propulsion Systems*, SNAME Greek Section Technical Meeting Presentation, February 20, 2014.

[19] International Maritime Organization, Revised MARPOL Annex VI, Regulation 12 - Ozone Depleting Substances, 2008.

[20] Turboden, Pratt & Witney, "Turboden ORC plants for Industrial Heat Recovery," 3 September 2012. [Online]. Available: http://www.turboden.eu/.

[21] Kuo C.R., Hsu S.W., Chang K.H. and Wang C.C., "Analysis of a 50 kW organic Rankine cycle system", *Energy*, Vol. 36, pp. 5877-5885, 2011.

[22] Liu B.T., Chien K.H. and Wang C.C., "Effect of working fluids on organic Rankine cycle for waste heat recovery," *Energy*, Vol. 29, No. 8, pp. 1207-1217, June 2004.

[23] Quoilin S., "Sustainable Energy Conversion Through the Use of Organic Rankine Cycles for Waste Heat Recovery and Solar Applications", Doctoral Thesis, University of Liege, 2011.

[24] Burel F., Taccani R. and Zuliani N., "Improving sustainability of maritime transport through utilization of Liquefied Natural Gas (LNG) for propulsion," *Energy,* Vol. 57, pp. 412-420, 1 August 2013.

[25] Quoilin S., Sebastien D., Tchanche B. and Lemort V., "Thermo-economic optimization of waste heat recovery Organic Rankine Cycles," *Applied Thermal Engineering,* Vol. 31, pp. 2885-2893, 2011.

[26] Brasz L.J. and Bilbow W.M., "Ranking of Working Fluids for Organic Rankine Cycle Applications," in *International Refridgeration and Air Conditioning Conference,* Purdue University, July 12-15, 2004.

[27] Mancini S., "Design and Performance Evaluation of an ORC System Exploiting the Waste Heat of the Main Engine of a Tanker", M.Sc. Thesis, Padova: Universita Degli Studi di Padova, 2013.

[28] Papadopoulos A., Stijepovic M. and Linke P., "On the systematic design and selection of optimal working fluids for Organic Rankine Cycles," *Applied Thermal Engineering,* Vol. 30, No. 6-7, pp. 760-769, 2010.

[29] Myhre G. et al, "8SM: Anthropogenic and Natural Radiative Forcing Supplementary Material," in *Climate Change 2013: The Physical Science Basis,* Intergovernmental Panel on Climate Change, 2013.

[30] Myhre G. et al., "Chapter 8: Anthropogenic and Radiative Forcing," in *Climate Change 2013: The Physical Science Basis,* Intergovernmental Panel on Climate Change, 2013.

[31] Air Conditioning and Refrigeration Industry Board, "2014 F-Gas Regulation and GWP Values," May 2015. [Online]. Available: http://www.acrib.org.uk. [Accessed 06 June 2015].

[32] United States Environmental Protection Agency EPA, "Overview of Greenhouse Gases," [Online]. Available: http://www.epa.gov/climatechange/ghgemissions/gases.html. [Accessed 19 June 2015].

[33] Gschrey B. and Zeiger B., "Information for technicians and users of refrigeration, air conditioning and heat pump equipment containing fluorinated greenhouse gases," European Commission, DG Climate Action, 2015.

[34] *Regulation (EU) No 517/2014 of the European Parliament and of the Council of 16 April 2014 on fluorinated greenhouse gases,* 2014.

[35] *The Montreal Protocol on Substances that Deplete the Ozone Layer as either adjusted and/or amended in London 1990, Copenhagen 1992, Vienna 1995,*

Montreal 1997, Beijing 1999, Nairobi: United Nations Environment Programme, 2000.

[36] *Regulation (EC) No 1005/2009 of the European Parliament and of the Council on Substances that Deplete the Ozone Layer,* 2009.

[37] Lloyd's Register, "Guidance notes Revised MARPOL Annex VI Regulation 12 - Ozone Depleting Substances," 2010.

[38] International Institute of Refrigeration, "Classification of Refrigerants," [Online]. Available: www.iifiir.org.

[39] United States Government, "Protection of Stratospheric Ozone: Listing of Substitutes for Ozone-Depleting Substances-Hydrocarbon Refrigerants," *U.S. Government Federal Register,* Vol. 75, No. 8, pp. 25799-25815, 2010.

[40] Quoilin S. and Vincent L., "Technological and Economical Survey of Organic Rankine Cycle Systems," in *5th European Conference Economics and Management of Energy in Industry,* Algarve, Portugal, 2009.

[41] Tchanche B.F., "Low-Grade Heat Conversion into Power Using Small Scale Organic Rankine Cycles," Doctoral Thesis, Athens: Agricultural University of Athens Department of Natural Resources and Agricultural Engineering, 2010.

[42] Marindagen S. and Haraldson L., "Potentialer for verkingsgradsforbattringar," 05 April 2011. [Online]. Available: http://www.marindagen.se/wp-content/uploads/2010/11/Lennart-Haraldsson-W%C3%A4rtsil%C3%A4.pdf. [Accessed 21 December 2014].

[43] Yue G., Dong S., Zheng Q. and Li J., "Design of Marine Diesel Engine Waste Heat Recovery System With Organic Rankine Cycle," *Applied Mechanics and Materials,* Vols. 148-149, pp. 1264-1270, 2012.

[44] Larsen U., Pierobon L., Haglind F. and Gabrielli C., "Design and optimisation of organic Rankine cycles for waste heat recovery in marine applications using the principles of natural selection," *Energy,* Vol. 55, pp. 803-812, 2013.

[45] Opcon Marine, "About Opcon Marine," [Online]. Available: http://www.opcon.se/web/About_opcon_marine.aspx. [Accessed 6 January 2015].

[46] "Organic Rankine Cycle heat recovery technology ready for ships," The Motorship, 10 April 2014. [Online]. Available: http://www.motorship.com/news101/engines-and-propulsion/organic-rankine-cycle-heat-recovery-ready-for-ships?SW_DESIGN_NAME=print&. [Accessed 7 December 2014].

[47] Aldous L. and Smith T., "Speed Optimisation for Liquefied Natural Gas Carriers: A Techno-Economic Model," in *Low Carbon Shipping Conference*, 2012.

[48] *International Maritime Organization, International Code for the Construction and Equipment of Ships Carrying Liquefied Gases in Bulk (IGC Code).*

[49] *Drawings and manuals of studied ship cargo equipment.*

[50] *Vessel Machinery Operating Manual.*

[51] Wärtsilä, *Wärtsilä 50DF Product Guide,* Vaasa, 2012.

[52] Shu G., Liu L., Wei H. and Yu G., "Parametric and working fluid analysis of a dual-loop organic Rankine cycle (DORC) used in engine waste heat recovery," *Applied Energy,* Vol. 113, pp. 1188-1198, 2014.

[53] Angelino G. and Invernizzi C., "Experimental investigation on the thermal stability of some new zero ODP refrigerants," *International Journal of Refrigeration,* Vol. 26, pp. 51-58, 2003.

[54] Calderazzi L. and di Paliano P.C., "Thermal stability of R-134a, R-141b, R-1311, R-7146, R-125 associated with stainless steel as a containing material," *International Journal of Refrigeration,* Vol. 20, No. 6, pp. 281-289, 1997.

[55] Ito M., Dang C. and Hihara E., "Thermal Decomposition of Lower-GWP Refrigerants," in *International Refrigeration and Air Conditioning Conference*, Purdue University, 2014.

[56] Larjola J., "Electricity from industrial waste heat using high-speed organic Rankine cycle," *International Journal of Production Economics,* Vol. 41, pp. 227-235, 1995.

[57] Hossain S. and Bari S., "Waste heat recovery from exhaust of a diesel generator set using organic fluids," *Procedia Engineering,* Vol. 90, pp. 439-444, 2014.

[58] Song S., Zhang H., Lou Z., Yang F., Yang K., Wang H., Bei C., Chang Y. and Yao B., "Performance analysis of exhaust waste heat recovery system for stationary CNG engine based on organic Rankine cycle," *Applied Thermal Engineering,* Vol. 76, pp. 301-309, 2015.

[59] Hanlon M., "BMW unveils the turbosteamer concept," Gizmag, 13 December 2005. [Online]. Available: http://www.gizmag.com/go/4936/. [Accessed 1 September 2015].

[60] Zhang H., Wang E. and Fan B., "A performance analysis of a novel system of a dual loop bottoming organic Rankine cycle (ORC) witha light-duty diesel engine", *Applied Energy,* Vol 102, 2013, pp. 1504-1513.

[61] Song J. and Gu C., "Performace analysis of a dual-loop organic Rankine cycle (ORC) system with wet steam expansion for engine waste heat recovery," *Applied Energy,* Vol. 156, pp. 280-289, 2015.

[62] Zhang C., Shu G., Tian H., Wei H. and Liang X., "Comparative study of alternative ORC-based combined power systems to exploit high temperature waste heat," *Energy Conversion and Management,* Vol. 89, pp. 541-554, 2015.

[63] Choi B. and Kim Y., "Thermodynamic analysis of a dual loop heat recovery system with trilateral cycle applied to exhaust gases of internal combustion engine for propulsion of the 6800 TEU container ship," *Energy,* Vol. 58, pp. 404-416, 2013.

[64] Panesar A., Morgan R., Miche N. and Heikal M., "A Novel Organic Rankine Cycle System with Improved Thermal Stability and Low Global Warming Fluids", 4th International Conference on Production, Energy and Reliability, Kuala Lumpur, May 2014.

[65] Hydro Instruments, "Ammonia Handling Manual," [Online]. Available: www.hydroinstruments.com.

[66] Jarahnejad M., "New Low GWP Synthetic Refrigerants," M.Sc. Thesis, Stockholm: KTH School of Industrial Engineering and Management Division of Applied Thermodynamics and Refrigeration, 2012.

[67] Natural Resources Canada, "Pinch Analysis: For the Efficient Use of Energy, Water & Hydrogen," 2003. [Online]. Available: http://canmetenergy.nrcan.gc.ca. [Accessed 5 July 2015].

[68] Bejan A., Tsatsaronis G. and Moran M., "Thermal Design & Optimization", New York: John Wiley & Sons, Inc., 1996.

[69] Microsoft, "Solver Uses Generalized Reduced Gradient Algorithm," 19 September 2011. [Online]. Available: https://support.microsoft.com/en-us/kb/82890. [Accessed 17 September 2015].

[70] *Guidelines for Automatic Cargo Tank Overfill Protection Aboard Gas Carriers,* Society of International Gas Tanker & Terminal Operators Ltd., 1993.

[71] Dimopoulos G.G. and Frangopoulos C.A., "A Dynamic Model for Liquefied Natural Gas Evaporation During Marine Transportation," *International Journal of Thermodynamics,* Vol. 11, No. 3, pp. 123-131, September 2008.

[72] Kakac S. and Hongtan L., "Heat Exhangers: Selection, Rating, and Thermal Design," Boca Raton: CRC Press, 2002.

[73] Foster-Pegg R.W., "Capital Cost of gas-turbine heat recovery boilers," *Chemical Engineering,* Vol. 93, No. 14, pp. 73-78, 1986.

[74] Frangopoulos C.A., "Application of the Thermoeconomic Functional Approach to the CGAM Problem," *Energy,* Vol. 19, No. 3, pp. 323-342, 1994.

[75] Dimopoulos G.G., "Synthesis, Design and Operation Optimization of Marine Energy Systems," Ph.D. Thesis, National Technical University of Athens, School of Naval Architecture and Marine Engineering, 2009.

[76] US Environmental Protection Agency, "Water Facts," June 2004. [Online]. Available: http://water.epa.gov/. [Accessed 13 October 2015].

[77] British Petroleum, "BP Statistical Review of World Energy 64th Edition," June 2015. [Online]. Available: http://www.bp.com/content/dam/bp/pdf/Energy-economics/statistical-review-2015/bp-statistical-review-of-world-energy-2015-full-report.pdf. [Accessed 14 September 2015].

[78] "Web MIT," 10 January 2015. [Online]. Available: http://web.mit.edu/16.unified/www/FALL/thermodynamics/notes/node65.html.

[79] United States Environmental Protection Agency, "Ozone Layer Protection Glossary," 16 December 2010. [Online]. Available: http://www.epa.gov/Ozone/defns.html.

[80] *Regulation (EU) No 517/2014 of the European Parliament and of the Council of 16 April 2014 on fluorinated greenhouse gases*, 2014.

[81] Chandler D.L., "MIT News Office," Online Article, 10 March 2010. [Online]. Available: http://newsoffice.mit.edu/2010/explained-radforce-0309. [Accessed 04 June 2015].

[82] Chen H., Goswami D.Y., Rahman M.M. and Stefanakos E.K., "Energetic and exergetic analysis of CO2- and R32-based transcritical Rankine cycles for low-grade heat conversion," *Applied Energy,* Vol. 88, pp. 2802-2808, 2011.

[83] Dimopoulos G.G. and Frangopoulos C.A., "Thermoeconomic Simulation of Marine Energy Systems for a Liquefied Natural Gas Carrier," *International Journal of Thermodynamics,* Vol. 11, No. 4, pp. 195-201, December 2008.

[84] Radulovic J. and Beleno Castaneda N., "On the potential of zeotropic mixtures in ORC powered by geothermal energy source," *Energy Conversion and Management,* Vol. 88, pp. 365-371, 2014.

[85] Smolen S., "Simulation and Thermodynamic Analysis of a Two-Stage Organic Rankine Cycle for Utilistion of Waste Heat at Medium and Low Temperature Levels," *Energy Science and Technology,* Vol. 1, No. 1, pp. 64-78, 2011.

[86] Vidhi R., Goswami D.Y. and Stefanakos K., "Parametric study of supercritical Rankine cycle and earth-air-heat exchanger for low temperature power generation" *Proceedings of the SolarPACES 2013 International Conference*, Vol.49, 2014, pp 1228–1237.

[87] Yang K., Zhang H., Wang Z., Yang F., Wang E. and Yao B., "Study of zeotropic mixtures of ORC (organic Rankine cycle) under engine various operating conditions," *Energy,* Vols. 494-510, p. 58, 2013.

[88] Zhao L. and Bao J., "The influence of composition shift on organic Rankine cycle (ORC) with zeotropic mixtures," *Energy Conversion and Management,* Vol. 83, pp. 203-211, 2014.

[89] The Chemical Engineer's Resource Page, "Pinch Technology: Basics for Beginners," [Online]. Available: www.cheresources.com.

[90] Sprouse C. and Depcik C., "Review of organic Rankine cycles for internal combustion engine exhaust waste heat recovery," *Applied Thermal Engineering,* Vol. 51, pp. 711-722, 2013.

[91] Chen Y., "Thermodynamic Cycles using Carbon Dioxide as Working Fluid (CO_2 transcritical power cycle study)," Doctoral Study, Stockholm: KTH Industrial Engineering and Management , 2011.

[92] Kim Y., Kim C. and Favrat D., "Transcritical or supercritical CO2 cycles using both low- and high-temperature heat sources," *Energy,* Vol. 43, pp. 402-415, 2012.

[93] Κακατσιος Ξ., "Αρχές Μεταφοράς Θερμότητας και Μάζης," Αθήνα: Εκδόσεις Συμεών, 2006.

[94] Πασπαλάς Κ., "Μετάδοση Θερμότητας," Θεσαλλονίκη: Εκδόσης Δημητρίου Κ. Σαλονικίδη, 1993.

[95] BDH, "Material Safety Data Sheet Toluene," 21 December 2005. [Online]. Available: http://kni.caltech.edu/facilities/msds/toluene.pdf. [Accessed 3 October 2015].